

Time-Delay Cosmography: Measuring the Hubble Constant and other cosmological parameters with strong gravitational lensing

S. Birrer^{1,2,†}, M. Millon^{2,3}, D. Sluse⁴, A. J. Shajib^{5,6}, F. Courbin³, L. V. E. Koopmans⁷,
S. H. Suyu^{8,9,10}, T. Treu¹¹

Received: date / Accepted: date

Abstract Multiply lensed sources experience a relative time delay in the arrival of photons. This effect can be used to measure absolute distances and the Hubble constant (H_0) and is known as time-delay cosmography. The methodology is independent of the local distance ladder and early-universe physics and provides a precise and competitive measurement of H_0 . With upcoming observatories, time-delay cosmography can provide a 1% precision measurement of H_0 and can decisively shed light on the current reported ‘Hubble tension’. This paper presents the theoretical background and the current techniques applied for time-delay cosmographic studies and the measurement of the Hubble constant. The paper describes the challenges and systemat-

ics in the different components of the analysis and strategies to mitigate them. The current measurements are discussed in context and the opportunities with the anticipated data sets in the future are laid out.

Contents

1	Introduction	1
2	Time delays and the time-delay distance	2
3	Overview of analysis ingredients	6
4	Measuring time delays	6
5	Determining lensing potential	10
6	Estimating line-of-sight contributions	15
7	Cosmographic inference	19
8	Future constraints from galaxy clusters	21
9	Current status and results	21
10	Outlook in the (near) future	22

† E-mail: simon.birrer@stonybrook.edu

¹ Kavli Institute for Particle Astrophysics and Cosmology and Department of Physics, Stanford University, Stanford, CA 94305, USA

² Department of Physics and Astronomy, Stony Brook University, Stony Brook, NY 11794, USA

³ Institute of Physics, Laboratory of Astrophysics, Ecole Polytechnique Fédérale de Lausanne (EPFL), Observatoire de Sauverny, 1290 Versoix, Switzerland

⁴ STAR Institute, Quartier Agora - Allée du six Août, 19c B-4000 Liège, Belgium

⁵ Department of Astronomy and Astrophysics, University of Chicago, Chicago, IL 60637, USA

⁶ Kavli Institute for Cosmological Physics, University of Chicago, Chicago, IL 60637, USA

⁷ Kapteyn Astronomical Institute, University of Groningen, P.O.Box 800, 9700AV Groningen, the Netherlands

⁸ Max-Planck-Institut für Astrophysik, Karl-Schwarzschild-Str. 1, 85748 Garching, Germany

⁹ Technical University of Munich, TUM School of Natural Sciences, Physics Department, James-Frank-Straße 1, 85748 Garching, Germany

¹⁰ Academia Sinica Institute of Astronomy and Astrophysics (ASIAA), 11F of ASMA, No.1, Section 4, Roosevelt Road, Taipei 10617, Taiwan

¹¹ Department of Physics and Astronomy, University of California, Los Angeles CA 90095

1 Introduction

The relative arrival times of multiply lensed sources can be used to measure an absolute distance of the Universe. The method, known to date as time-delay cosmography, was originally proposed over half a century ago, prior to the discovery of the first extragalactic gravitational lens, by Refsdal (1964). Time-delay cosmography provides a one-step measurement of the Hubble constant (H_0), independent of the local distance ladder or probes anchored with sound horizon physics, such as the cosmic microwave background (CMB).

Almost a century after its first measurement, the Hubble constant H_0 still remains arguably the most debated number in cosmology. In the past few years, a tension has emerged between a number of local measurements, and inferences from early-Universe probes such as the cosmic microwave background (CMB) and Big Bang Nucleosynthesis, under the assumption of flat Λ cold dark matter (Λ CDM) cosmology (see, e.g., Verde et al., 2019; Shah et al., 2021, for recent

summaries). If this tension is real, and not due to unknown systematic uncertainties in multiple measurements and their analyses, it implies that the standard Λ CDM model is not sufficient and new physical ingredients beyond this model are required. From a theoretical standpoint, a number of possible solutions – for example, involving early dark energy – have been proposed (e.g., Knox and Millea, 2020; Di Valentino et al., 2021; Schöneberg et al., 2021, and references therein), often requiring fine-tuning of free parameters not to violate other observational constraints. From an observational standpoint, besides improving the precision of the measurements, significant attention has turned to the systematic investigation of unknown systematic uncertainties (e.g., Riess et al., 2019; Freedman et al., 2019, 2020; Riess et al., 2021; Mortsell et al., 2021).

This manuscript details the general methodology developed over the past decades in time-delay cosmography, discusses recent advances and results, and, foremost, provides a foundation and outlook for the next decade in providing accurate and ever more precise measurements with increased sample size and improved observational techniques. This manuscript will be submitted as a chapter of a Space Science Reviews, Topical Collection "Strong Gravitational Lensing", eds. J. Wambsganss et al. We will refer throughout this manuscript to other forthcoming chapters of the same collection covering a wide range of strong lensing theory and applications (e.g., Saha et al. (in preparation), Shajib et al. (in preparation), Suyu et al. (in preparation), Vernardos et al. (in preparation), McMahon et al. (in preparation)). We refer to, e.g., Treu and Marshall (2016); Suyu et al. (2018) to provide more in-depth historical perspectives on the early years of the field, Treu, Suyu & Marshall, 2022, submitted, to a broader and less technical perspective on the opportunities of time-delay cosmography in this decade, and Moresco et al. (2022) for a compact overview embedded within other cosmological probes.

We discuss the methodology around lensed quasars as source objects to perform time-delay measurements because quasars are currently the most established sources with the most relevant current results. We refer to Oguri (2019) and Suyu et al. (in preparation) using, for example, lensed supernovae or other transient phenomena that can be utilized to perform time-delay cosmographic measurements.

This manuscript is organized as follows: In Section 2 we provide the general concept and physics to turn relative time delays between multiple images of the same source into distance measurements. Section 3 provides an overview of the required analysis ingredients for individual lenses. Subsequent sections go into the details of these ingredients, the time-delay measurement (Section 4), determination of the lensing potential (Section 5), and the study of the line of sight (LOS) of the lenses (Section 6). Section 7 describes the cosmographic inferences and how to utilize a sample of

lenses to perform an H_0 inference. We summarize the current status and results obtained in Section 9. Lastly, in Section 10, we look in the future and discuss the potential and challenges lying ahead for the community.

2 Time delays and the time-delay distance

The deflection of light due to mass over- or under-density in the Universe can be captured in the lens equation (see Saha et al. (in preparation) for the detailed theory, including that this formula is only valid for small angles)

$$\beta = \theta - \alpha(\theta), \quad (1)$$

where β is the angular position of the source without the lensing effect, θ is the corresponding angular coordinate on the sky as seen when lensed, and α is the deflection angle that maps the image position to the source position in angular coordinates as seen from the observer. There exists a scalar potential, the lensing potential ϕ , such that the gradients correspond to the deflection field

$$\nabla\phi(\theta) = \alpha(\theta). \quad (2)$$

The convergence of the potential ϕ , κ , is half the Laplacian

$$\kappa(\theta) = \frac{1}{2} \nabla^2 \phi(\theta) \quad (3)$$

and is given in the thin lens approximation for small angles as

$$\kappa(\theta) = \frac{\Sigma(\theta)}{\Sigma_{\text{crit}}} \quad (4)$$

with $\Sigma(\theta)$ as the projected mass over- or under-density with respect to the mean background density and Σ_{crit} the critical surface density¹

$$\Sigma_{\text{crit}} = \frac{c^2 D_s}{4\pi G D_{\text{ds}} D_d}, \quad (5)$$

where c is the speed of light and G the gravitational constant. D_d is the angular diameter distance to the lens, D_s is the angular diameter distance to the source, and D_{ds} is the angular diameter distance between the lens and the source, respectively.

When the intensity of a strongly lensed background source varies over time, such as an active galactic nucleus (AGN), the variability pattern manifests in each of the multiple images and is delayed in time due to the different light paths of the different images (see Figure 1). The relative arrival time

¹ not to be confused with the critical density of the universe

between two images θ_A and θ_B , Δt_{AB} , originated from the same source β is

$$\Delta t_{AB} = \frac{D_{\Delta t}}{c} [\tau(\theta_A, \beta) - \tau(\theta_B, \beta)], \quad (6)$$

where

$$\tau(\theta, \beta) \equiv \left[\frac{(\theta - \beta)^2}{2} - \phi(\theta) \right] \quad (7)$$

is the Fermat potential (Schneider, 1985; Blandford and Narayan, 1986), and

$$D_{\Delta t} \equiv (1 + z_d) \frac{D_d D_s}{D_{ds}} \quad (8)$$

is the time-delay distance (Refsdal, 1964; Schneider et al., 1992; Suyu et al., 2010). The Fermat potential (Eqn. 7) consists of two terms, a geometric term reflecting the geometric path difference, and a potential term, capturing the difference in the local spacetime dilation, known as the Shapiro delay. The optical terms stated (such as the Fermat potential) are only valid under small-angle and thin-lens assumptions. We refer to Saha et al. (in preparation) for these assumptions and the more general multi-plane formalism.

The angular diameter distance between two redshifts z_1 and z_2 in an Friedmann–Lemaître–Robertson–Walker (FLRW) metric is

$$D(z_1, z_2) = \frac{1}{1 + z_2} f_K[\chi(z_1, z_2)] \quad (9)$$

where

$$\chi(z_1, z_2) = \frac{c}{H_0} \int_{z_1}^{z_2} \frac{dz'}{E(z')} \quad (10)$$

is the comoving distance with $E(z) \equiv H(z)/H_0$ as the dimensionless Friedman equation and

$$f_K(\chi) = \begin{cases} K^{-1/2} \sin(K^{1/2} \chi) & \text{for } K > 0 \\ \chi & \text{for } K = 0 \\ (-K)^{-1/2} \sinh[(-K)^{1/2} \chi] & \text{for } K < 0 \end{cases} \quad (11)$$

is the spatial curvature of the background metric.

In the Λ CDM cosmology with density parameters Ω_m for matter, Ω_k for spatial curvature, and Ω_Λ for dark energy described by the cosmological constant Λ , the dimensionless Friedman equation ($E(z)$, Eqn. 10) is given by

$$E(z) = \left(\Omega_m(1+z)^3 + \Omega_k(1+z)^2 + \Omega_\Lambda \right)^{1/2} \quad (12)$$

and the spatial curvature is $K = -\Omega_k H_0^2 / c^2$.

Constraints on the Fermat potential difference $\Delta \tau_{AB}$ and a measured relative time delay Δt_{AB} between to images of the same source can be turned into constraints of the time-delay distance $D_{\Delta t}$. $D_{\Delta t}$ is an absolute physical distance and

anchors the scale of the Universe within the lensing configuration. The Hubble constant, the local expansion rate of the cosmological background metric, sets the locally linear relationship between relative recess velocities and physical separation of two objects. For a fixed relative velocity or redshift, the Hubble constant is inversely proportional to the absolute physical distance. The Hubble constant is inversely proportional to the absolute scales of objects in the Universe for which redshifts are measured (see e.g., Eqn. 10) and thus scales with $D_{\Delta t}$ as

$$H_0 \propto D_{\Delta t}^{-1}, \quad (13)$$

mildly dependent on the relative expansion history from current time ($z = 0$) to the redshift of the deflector and the source (dependance on $E(z)$ in Eqn. 12). Time-delay cosmography is primarily an *absolute* distance anchor and at the heart of the current tension in cosmology. The mild dependency on other cosmological parameters beyond H_0 can be compensated with other cosmological probes that are sensitive to the *relative* expansion history (such as SNIa luminosity distances, e.g., Taubenberger et al. 2019; Arendse et al. 2019; Liao et al. 2019, 2020), or with a large set of gravitational lenses at different lens and source redshifts.

The time delay between to images Δt_{AB} can be measured from light curves and is hence a direct observable (see Section 4). The relative Fermat potential $\Delta \tau_{AB}$, however, is not a direct observable. The primary observations used to infer $\Delta \tau_{AB}$ are positional constraints of multiple imaged sources and their extended distortions in the lensed arcs from the lensing effect. However, there are degeneracies inherent in gravitational lensing that limit the amount of information accessible by positional and distortion effects as observed in imaging data (e.g., Falco et al., 1985; Gorenstein et al., 1988; Kochanek, 2002; Saha and Williams, 2006; Schneider and Sluse, 2013, 2014; Birrer et al., 2016; Unruh et al., 2017; Birrer, 2021) and Saha et al. (in preparation).

The mass-sheet degeneracy (MSD; Falco et al., 1985) is the most prominent lensing degeneracy impacting the prediction of the Fermat potential and hence time-delay cosmography. The MSD is formally a multiplicative transform of the lens equation (Eq. 1) which preserves image positions under a linear source displacement $\beta \rightarrow \lambda\beta$ combined with a transformation of the convergence field

$$\kappa_\lambda(\theta) = \lambda\kappa(\theta) + (1 - \lambda). \quad (14)$$

Eq. 14 above is a *mathematical transformation* where the term $(1 - \lambda) \equiv \kappa_{\text{mst}}$ is equivalent to an infinite sheet of convergence mass, and hence the name mass sheet transform. κ_{mst} can be positive and negative, since it is defined relative to another density profile and also relative to the average density in the universe. The MSD, by means of preserving image positions and being linear, also preserves any higher order relative differentials of the lens equation. Only

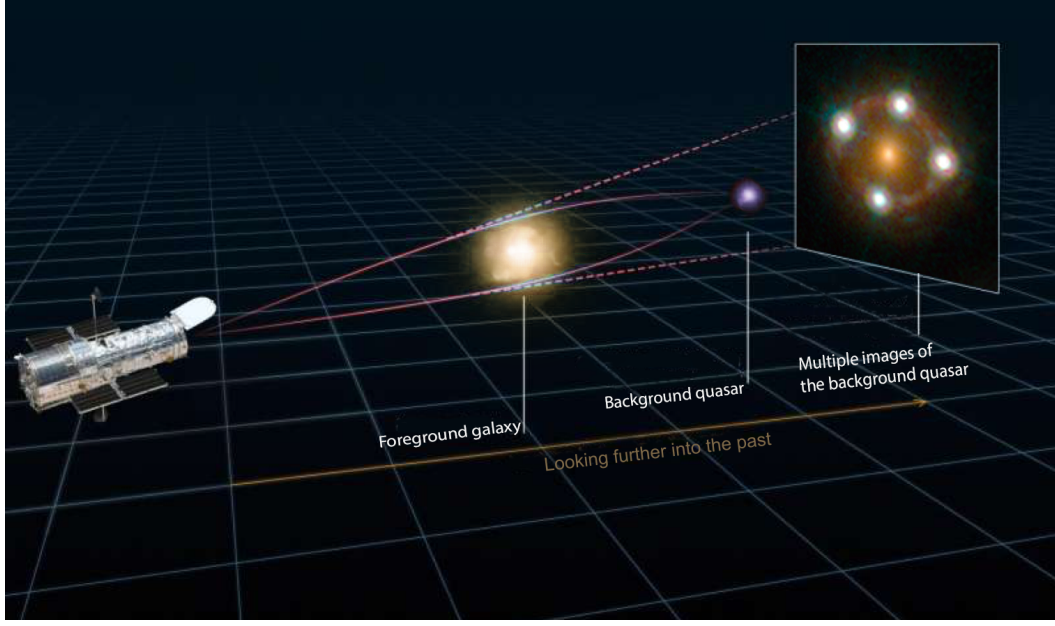


Fig. 1 Illustration of the light path of the quadruply imaged lensed quasar HE0435-1223. The different light paths result in different arrival times. The relative time delays between the images is directly proportional to the overall physical distances from the observer to the lens and source. Measuring the time delays and reconstructing the lensing effect allow one to measure an absolute scale in the universe. Graphics from: Martin Millon, Image from Hubble Space Telescope (Wong et al., 2017).

observables related to either the unlensed apparent source size (β vs. $\lambda\beta$), such as the unlensed apparent brightness, or the lensing potential are able to break the MSD. For example, the same relative lensing observables can be predicted if the mass profile is scaled by the factor λ with the addition of a sheet of convergence (or mass) of $\kappa_{\text{mst}}(\theta) = (1 - \lambda)$ and re-sizing of the source by a factor λ .

The Fermat potential difference between a pair of images A & B (Eq. 7) scales with λ as

$$\Delta\tau_{AB,\lambda} = \lambda\Delta\tau_{AB}, \quad (15)$$

and so does the relative time delay as

$$\Delta t_{AB,\lambda} = \lambda\Delta t_{AB}. \quad (16)$$

When transforming a lens model with an MST, the inference of the time-delay distance (Eqn. 8) from a measured time delay and previously inferred Fermat potential transforms as

$$D_{At,\lambda} = \lambda^{-1}D_{At}. \quad (17)$$

In turn, the Hubble constant, when inferred from the time-delay distance D_{At} , transforms as (from Eqn. 13)

$$H_{0,\lambda} = \lambda H_0. \quad (18)$$

An MSD effect relative to a specified deflector model might be associated with the mass distribution of the main deflector, referred as *internal* MSD with λ_{int} , or with inhomogeneities along the line of sight (LOS) of the strong lens system, referred as *external* MSD.

Mass over- or under-densities relative to the mean background density along the LOS of the strong lensing system cause, to first order, shear and convergence lensing perturbations. Reduced shear distortions do have a measurable imprint on the azimuthal structure of the strong lensing arcs (see e.g., Birrer, 2021; Hogg et al., 2022) while the convergence component of the LOS, denoted as κ_{ext} , describes the focusing or de-focusing of the light rays and is equivalent to an MST, $\kappa_{\text{ext}} \equiv (1 - \lambda)$, and hence not directly measurable from imaging data.

Equivalent to describing the (de-) focusing along specific line-of-sights by convergence terms, we can alter the specific angular diameter distance relative to the homogeneous background metric. In our notation, we define D^{lens} as the angular diameter distance along a specific line of sight, such as a lens being impacted by LOS structure and we specifically note the angular diameter distance from the homogeneous background metric without any perturbative contributions as D^{bkg} . The relation between D^{lens} and D^{bkg} are given by the convergence terms as

$$\begin{aligned} D_d^{\text{lens}} &= (1 - \kappa_d)D_d^{\text{bkg}} \\ D_s^{\text{lens}} &= (1 - \kappa_s)D_s^{\text{bkg}} \\ D_{ds}^{\text{lens}} &= (1 - \kappa_{ds})D_{ds}^{\text{bkg}}, \end{aligned} \quad (19)$$

where κ_d is the external convergence from the observer to the deflector, κ_s from the observer to the source, and κ_{ds} from the deflector to the source, respectively (Birrer et al., 2020). The

individual convergence terms can be calculated in the Born approximation along undeflected light paths independent of the strong lensing deflector.

The notation of perturbed angular diameter distances allow us also to directly calculate the impact of line-of-sight structure on the cosmographic inference, and in particular the measurement of the Hubble constant. The time delay can be described as the product of three different angular diameter distances entering $D_{\Delta t}$ in Equation 8 (Birrer et al., 2020; Fleury et al., 2021a), and hence the effective external convergence κ_{ext} impacting the time delay and time-delay distance is

$$1 - \kappa_{\text{ext}} = \frac{(1 - \kappa_d)(1 - \kappa_s)}{1 - \kappa_{\text{ds}}}. \quad (20)$$

We note that, also directly visible from the equation above, the lensing efficiency (see Saha et al. (in preparation)) impacting the linear distortions for both shear and κ_{ext} is different from the standard weak lensing efficiency in the absence of a strong lensing deflector (McCully et al., 2014, 2017; Birrer et al., 2017, 2020; Fleury et al., 2021b).

Uncertainties or biases related to the MSD may also arise in regards to assumptions made in the radial density profile of the main deflector galaxy (see e.g. Kochanek, 2002; Saha and Williams, 2006; Read et al., 2007; Schneider and Sluse, 2013; Coles et al., 2014; Xu et al., 2016; Birrer et al., 2016; Unruh et al., 2017; Sonnenfeld, 2018; Kochanek, 2020; Blum et al., 2020; Birrer et al., 2020; Kochanek, 2021).

The main aspect of this internal mass profile degeneracy can be approximated to first order with an internal MSD and its parameter λ_{int} relative to an assumed mass profile. We will further discuss this aspect in Section 5.2.

The total MST, the relevant transform to constrain for an accurate Fermat potential determination and H_0 measurement, is the product of the internal and external MST (e.g., Schneider and Sluse, 2013; Birrer et al., 2016, 2020)

$$\lambda = (1 - \kappa_{\text{ext}}) \times \lambda_{\text{int}}. \quad (21)$$

To summarize, the prediction of the time delay (Equation 6 can be generalized to

$$\Delta t_{\text{AB}} = (1 - \kappa_{\text{ext}}) \lambda_{\text{int}} \frac{D_{\Delta t}}{c} \Delta \tau_{\text{AB}}. \quad (22)$$

The MST and its generalizations imply that one has to rely either on non-lensing information or assumptions about its functional form to constrain the radial mass density profile with a sufficient level of precision for time-delay cosmography.

The line-of-sight lensing contribution, κ_{ext} , can be estimated by tracers of the large-scale structure using galaxy number counts (e.g., Greene et al., 2013; Rusu et al., 2017) or weak-lensing measurements (Tihhonova et al., 2018, 2020). Galaxy number counts, paired with a cosmological model

including a galaxy-halo connection, are able to constrain the probability distribution of κ_{ext} to a few per cent per sight line. The main uncertainty in this approach arise from the uncertainties of luminous matter traces the more dominant dark matter structure.

To break the total MSD λ with observations, we require observations that are sensitive to the total MSD. Stellar kinematics is the most prominent and commonly used one to break the total MSD. The collective motion of stars is a direct tracer of the three-dimensional gravitational potential and hence provides an independent mass estimate. Joint lensing+dynamics constraints have been used to provide measurements of galaxy mass profiles (e.g., Grogan and Narayan, 1996; Romanowsky and Kochanek, 1999; Treu and Koopmans, 2002; Koopmans, 2004; Barnabè et al., 2011, 2012). The modelling of the kinematic observables in lensing galaxies range in complexity from spherical Jeans modeling (Binney and Tremaine, 2008) to Schwarzschild (Schwarzschild, 1979) methods.

The prediction of the LOS velocity dispersion σ_v from any model, regardless of the approach, can be decomposed into a cosmology-dependent and cosmology-independent part, as (see e.g., Birrer et al., 2016, 2019)

$$\sigma_v^2 = \frac{1 - \kappa_s}{1 - \kappa_{\text{ds}}} \frac{D_s}{D_{\text{ds}}} c^2 J(\xi_{\text{lens}}, \beta_{\text{ani}}, \lambda_{\text{int}}), \quad (23)$$

where J is a dimensionless quantity dependent on the deflector model parameters (ξ_{lens}), c is the speed of light, and β_{ani} the stellar anisotropy distribution. The dimensionless factor J incorporates also the observational conditions and luminosity-weighting within the aperture of the dispersion measurement being taken (e.g., Binney and Mamon, 1982; Treu and Koopmans, 2004; Suyu et al., 2010). The internal component λ_{int} should be physically interpretable as a three-dimensional mass profile and incorporated into the kinematics modeling term J , in particular when there are multiple aperture measurements available (Teodori et al., 2022). In the approximate case of a very extended sheet-like perturbation, we can approximate

$$J(\xi_{\text{lens}}, \beta_{\text{ani}}, \lambda_{\text{int}}) \approx \lambda_{\text{int}} J(\xi_{\text{lens}}, \beta_{\text{ani}}). \quad (24)$$

Combined lensing+dynamics constraints are sensitive to the combination of terms present in Equation 23. Such an analysis is under-constraint itself and different assumptions about certain terms in Equation 23 lead to constraints on other parameters. For example, when assuming the relative expansion history through the involved angular diameter distance ratio D_s/D_{ds} , and the LOS contributions κ_s and κ_{ds} , an inference on λ_{int} is possible. On the other hand, when assuming λ_{int} and the convergence terms, an inference on the angular diameter distance ratio, and hence the relative expansion history, is possible.

When combining time delays with lensing+dynamics, the observations of the time delay and kinematics need to be simultaneously described by Equation 22 and Equation 23 in addition of the imaging data. These two independent equations can be arbitrarily algebraically combined in two-dimensional angular diameter distance constraints (Birrer et al., 2016, 2019). A convenient transform of those constraints is in the basis of

$$D_{\Delta t} = \frac{1}{(1 - \kappa_{\text{ext}})\lambda_{\text{int}}} \frac{\Delta t_{\text{ABc}}}{\Delta \tau_{\text{AB}}} \quad (25)$$

and

$$D_{\text{d}} = \frac{1}{1 - \kappa_{\text{d}}} \frac{\Delta t_{\text{ABC}}}{\sigma_{\text{v}}^2} \frac{\lambda_{\text{int}}}{J(\xi_{\text{lens}}, \beta_{\text{ani}}, \lambda_{\text{int}})}. \quad (26)$$

When mapped into the $D_{\Delta t}$ – D_{d} plane as outlined above, the projection on constraints in D_{d} is invariant under any pure external MSD parameter κ_{ext} (Paraficz and Hjorth, 2009; Jee et al., 2015; Birrer et al., 2019; Yıldırım et al., 2021)². If the approximation of Equation 24 holds, D_{d} becomes even independent of λ_{int} , and is overall less susceptible to the internal MST.

3 Overview of analysis ingredients

To measure the cosmographic distances, in particular the time-delay distance $D_{\Delta t}$ (Equation 8), or the more general $D_{\Delta t}$ – D_{d} combination, from a strong lensing system with a time-variable source, the following data products are required:

1. discovery of a lens with a time-variable source that is multiply imaged,
2. spectroscopic redshifts of the source, z_{s} , and lens, z_{d} ,
3. measured time delays between at least one multiple image pair,
4. lens mass model to determine the Fermat potential between the multiple images,
5. lens environment studies to constrain external lensing effects.

A complete analysis for an individual lensing system requires the coordination of multiple independent observations. The analysis can be severely limited in its precision and reliability by a single missing ingredient. For example, without measurements of a time delay, no constraints on absolute distances involved can be achieved, and thus, regardless of the approach or external priors chosen, no direct constraints on the Hubble constant can be made.

The spectroscopic redshifts of the quasar sources, z_{s} , are often obtained using the frequent emission lines in quasars. The redshift of the lens, z_{d} , can be challenging to measure since massive elliptical galaxies lack prominent and

sharp absorption or emission lines and the bright quasar images can outshine the lens galaxy. Measuring z_{d} of a lensed quasar systems often require high signal-to-noise ratio spectra taken under good seeing condition, to deblend the lensing galaxy from the quasar. Technically, the redshifts involved in the lensing system are not directly required for the distance measurement. However, for the cosmological interpretation of the obtained distances, the redshifts are of crucial importance.

We describe in the next sections the remaining three ingredients; time delays (Section 4), lensing potential (galaxy scale and cluster) (Section 5), and line-of-sight perturbations (Section 6).

4 Measuring time delays

4.1 Monitoring of lensed quasars

Lensed quasars are variable on short timescale, making the time-delay measurements possible, and sufficiently bright to be observed at cosmological distances. They were hence quickly identified as excellent sources for time-delay cosmography. Lensed quasars are also currently much more common than lensed supernovae as around 300 lensed quasars have been discovered at the time of writing compared to only four lensed supernovae (see Suyu et al. (in preparation)). Lensed quasars are typically found in the redshift range $z_{\text{s}} \sim 1 - 3$, with massive early-type galaxies acting as the lenses located around redshift $z_{\text{d}} \sim 0.2 - 0.8$ (e.g., Lemon et al., 2022, and McMahon et al. (in preparation)). This lensing configuration typically produces multiple images separated by a few arcseconds, which is sufficient to be resolved with small ground-based telescope. The monitoring of lensed quasars and the measurement of their individual brightness fluctuations is thus challenging but possible with 1-m or 2-m class telescopes, provided that a regular and long-term access is guaranteed (see e.g. the COSMOGRAIL collaboration Eigenbrod et al., 2005; Courbin et al., 2011; Tewes et al., 2013a). It is however limited by several astrophysical, observational and instrumental factors, that are listed below.

Photometric accuracy : In the optical, most quasars are variable on a timescale of weeks to years, and the longest variations also have the largest amplitude. This means that either long-duration light curves or high photometric accuracy are required to measure the delay reliably. In one visibility season, variations of the order of 0.2 mag are often observed, which requires a photometric accuracy of a few milli-magnitudes to identify precisely the inflexion points. These inflexions points are essential features in the light curves since it is not possible to measure a time delay if the quasars does not display any variations, or if the first

² D_{d} is still dependent on the LOS between observer and lens, κ_{d} (Eqn. 19).

derivative remains always constant. Reaching a photometric accuracy of only a few milli-magnitude is challenging as the quasar images are often blended with extended sources such as gravitational arcs or the lens galaxy. Consequently, the reconstruction of the Point Spread Function (PSF) and proper treatment of the contaminating light from these extended sources are usually the key to reduce the noise in the light curves.

Monitoring cadence and duration of the monitoring: A fast and precise temporal sampling of the light curve is necessary if one targets the fast variations of small amplitudes of the quasar. The monitoring cadence then needs to be commensurate with the timescale of the targeted variations. The total time span of the monitoring campaign also needs to be sufficient to cover the lensing time delays and to ensure that enough variations of the quasar are recorded for multiple images at relative delayed times. To obtain light curves to such specifications requires continuous access to the telescope for at least one visibility season, which is typically 6 to 8 months.

Windowing effects and correlated noise: Seasonal gaps are often unavoidable in optical light curves since only circumpolar targets are observable all year-long. The fact that data are missing every year can introduce some windowing effects, which should be accounted for when using cross-correlation techniques to measure time delays. The missing data introduces a periodic signal that must be carefully removed or taken into account before attempting to measure the time delays. Additionally, great care should be taken in the presence of correlated noise, which is often present in the light curves due to cross-talk between the quasar images. If no evident variations can be matched unambiguously in both light curves, it is unlikely that any statistical methods will robustly measure a time delay.

Extrinsic variability: Extrinsic variations are often observed in the light curves. They are caused mainly by the microlensing of the quasar images, and also a variety of other astrophysical effects (see e.g. Schechter et al., 2003; Blackburne and Kochanek, 2010; Dexter and Agol, 2011; Sluse and Tewes, 2014, and Vernardos et al. (in preparation)). Microlensing is caused by the stars in the lensing galaxy, which add some extra time-variable "micro-magnification" on top of the static "macro-magnification" produced by the lensing galaxy. As described in Vernardos et al. (in preparation), the modulation of the micro-magnification due to the relative motion between the quasar, the lens and the observer introduces some extrinsic variations on top of the quasar intrinsic variations. For this reason, the light curves, even shifted in time and magnitude, rarely match perfectly. These extrinsic variations can severely bias time-delay measurements if not

appropriately modelled and marginalized over.

In the past two decades, these difficulties have been progressively dealt with. The advances in photometric instrumentation in the late 1990s allowed us to acquire accurate and well-sampled light curves, which yielded the first robust time-delay measurements from optical monitoring (e.g., Kundić et al., 1997a; Schechter et al., 1997; Burud et al., 2000, 2002; Hjorth et al., 2002; Colley et al., 2003; Kochanek et al., 2006) and in radio monitoring (Fassnacht et al., 1999, 2002; Biggs et al., 1999; Koopmans et al., 2000). Although some of these measurements already reached an excellent precision of a few percents, the majority had $\sim 10\text{--}15\%$ errors, hence limiting the measurement of H_0 to the same precision. These first encouraging results led to a systematic attempt to monitor a sample of lensed quasars in both hemispheres by the COSMOGRAIL program, which started in 2003 (Courbin et al., 2005). The observing strategy then was to follow a dozen of lenses at bi-weekly cadence until the time delays can be measured to a few percent precision. This strategy yielded precise measurements for the brightest and most variable objects in about five years (Vuissoz et al., 2007, 2008; Courbin et al., 2011; Tewes et al., 2013b; Eulaers et al., 2013; Rathna Kumar et al., 2013) but required more than a decade of monitoring to obtain the time delays for most of the less variable and fainter targets (Millon et al., 2020a). An example of a light curves acquired by the COSMOGRAIL program over the past 15 years is shown in Figure 2. Thanks to this long-term observing effort and other monitoring campaigns (e.g. Poindexter et al., 2007; Goicoechea and Shalyapin, 2016; Giannini et al., 2017; Shalyapin and Goicoechea, 2019), about 40 lensed quasars have now known time delays, although with variable precision, but the sample starts to be sufficiently large to vastly reduce the random uncertainties and to enable a statistical study of the time-delay lenses.

As time-delay cosmography is now entering a new regime with an increasing number of lensed quasars being discovered every year, the time delays now need to be measured rapidly to turn these newly discovered systems into cosmological constraints. Courbin et al. (2018) demonstrated that it is possible to obtain accurate time-delay measurements in only one monitoring season thanks to the small amplitude variations of the quasars, of the order of 10 to 50 millimag, that happen on a timescale of weeks or months. These variations are faster than the microlensing variability, which varies on a typical timescale of several months or years. If detected at a sufficient signal-to-noise ratio (SNR), these features reduce the need for long light curves as it allows us to disentangle the intrinsic and microlensing variability more easily. However, this change of strategy requires almost a daily cadence to obtain a sufficient sampling of these small features in the light curves. Their amplitude is of the

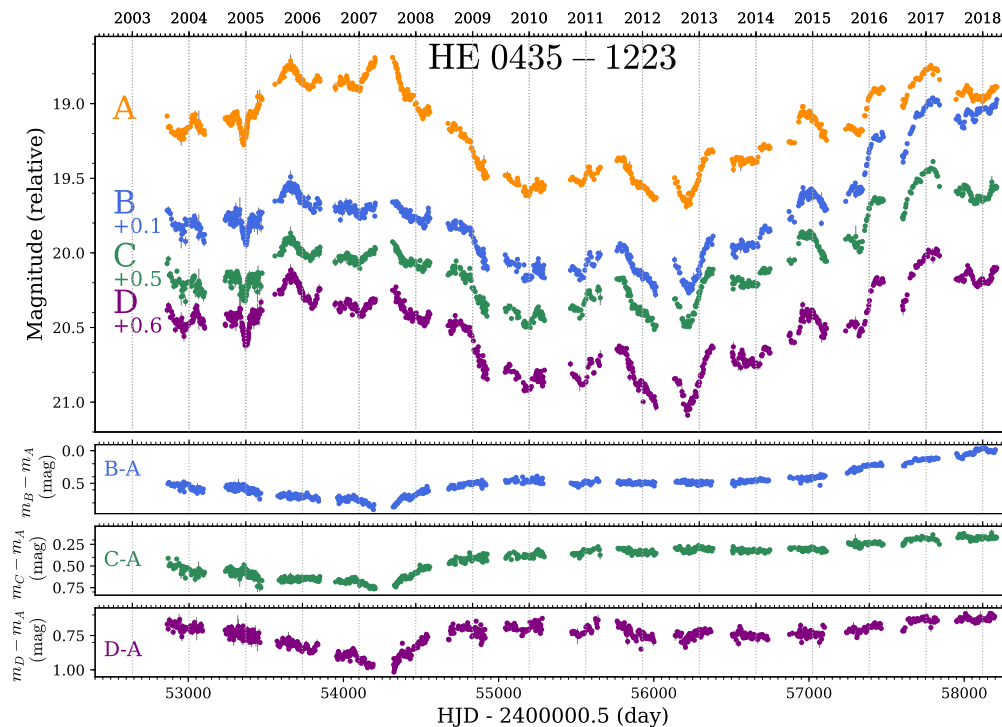


Fig. 2 R-band light curves of the lensed quasar HE0435-1223, obtained by the COSMOGRAIL program from the Euler 1.2m Swiss Telescope, the 1.5m telescope at the Maidanak Observatory, the Mercator 1.2m telescope, and the SMARTS 1.3m telescope. The bottom panels corresponds to the difference between pairs of light curves, corrected by the time delays, highlighting the microlensing variability. Figure reproduced from (Millon et al., 2020a).

order of 10 mmag, which requires 2-m class telescopes to obtain a sufficient SNR in 30 minutes of exposure at magnitude as faint as ~ 20 . This is illustrated in Fig. 3 in the case of the bright quadruple quasar WFI 2033-4723 (Bonvin et al., 2019). The technique has allowed to measure 6 new time delays in 1 single season (Millon et al., 2020c), with more to follow.

In the future, the Vera Rubin Observatory will obtain high-SNR multiband data for all southern lensed quasars, opening the possibility of building a sample of a few hundreds lensed quasars with known time delays. The cadence will however be limited to one point every few days in each band, which might not be sufficient to obtain the time delays at a few percent precision for the most interesting targets. Complementary, observations from 2-m class telescope at a daily cadence might still be useful to refine the time-delay measurements of the most promising objects.

4.2 Time-delay measurements techniques

Once well-sampled light-curves have been acquired, the next step consists of identifying time-variable features that can be matched in all light curves from the individual images. The shifting of the light curve to match the features leads to a measurement of the time delays.

This step is significantly complicated by the presence of extrinsic variations due to microlensing in the light curves on top of the quasar intrinsic variations. The signature of micro-lensing can be seen in most lensed quasar light curves. In some cases, it manifests itself by a sharp rise of the luminosity in one of the multiple images, which happens when the source approaches or crosses a micro-caustic. This probably happened, for example, in 2007 for image A of HE0435-1223. In Figure 2, we show the light curves of HE0435-1223 as well as the differential curves between the images, highlighting the microlensing signal. Caustic crossing events are not the only signature of microlensing visible in the data. Most quasar light curves also exhibit slow variations of the microlensing over several years. An example of this phenomenon is image B of HE0435-1223, which slowly raised by ~ 0.5 mag between 2013 and 2018. It typically happens when the stellar density is high and the quasar is located in regions where the microcaustics overlap. The net effect is a smooth variation of the microlensing magnification as the quasar moves through these crowded regions. The extrinsic variations introduced by microlensing contains valuable information about the quasar accretion disk structure (see Vernardos et al. (in prepration)) but is a real source of nuisance when measuring the time delays.

To deal with this issue, several curve-shifting algorithms have been proposed over the years, which can be classified

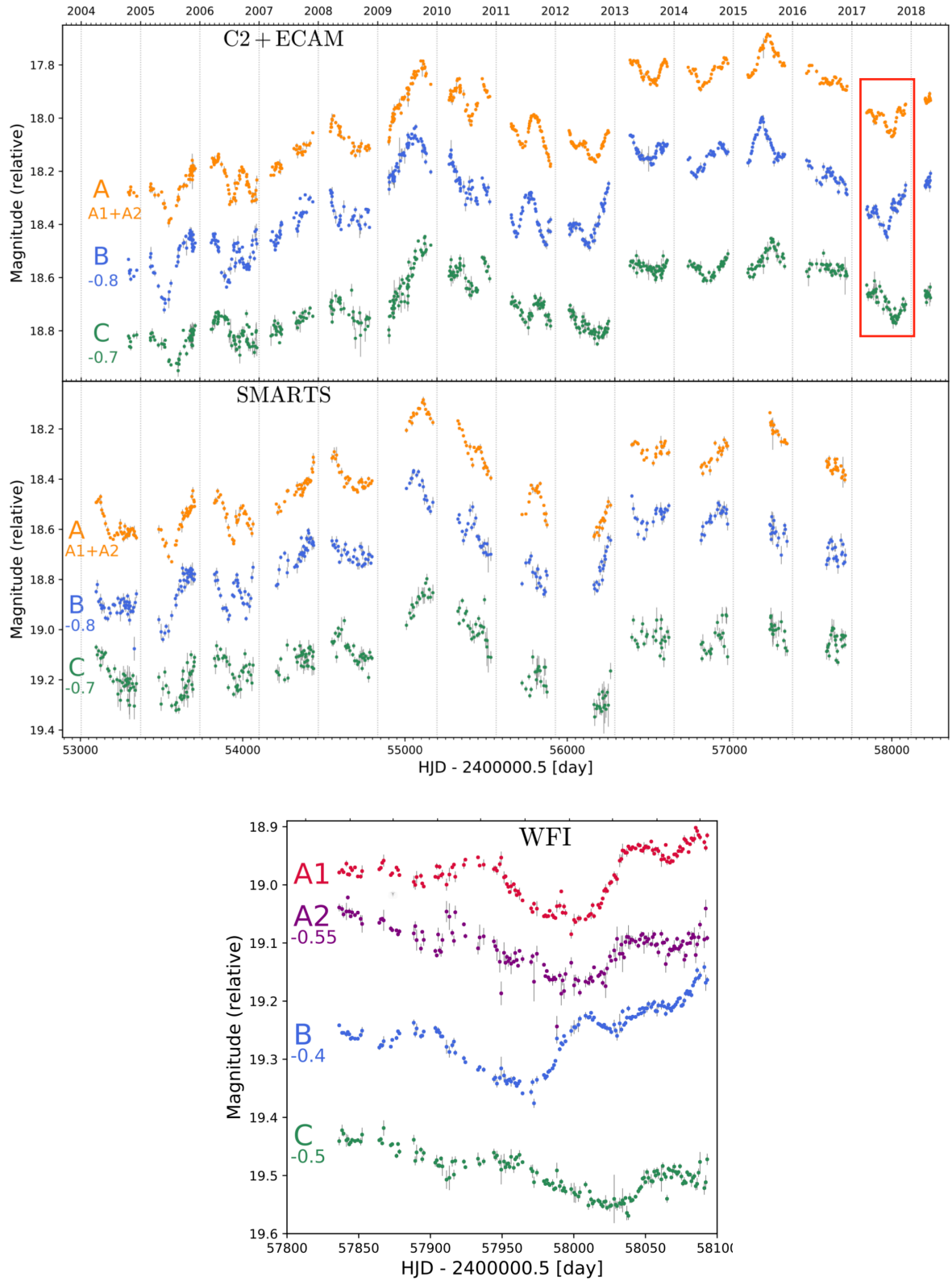


Fig. 3 Comparison of two observing cadences. On the two top panels are shown 14-year-long light curves of WFI 2033-4723, observed with a 4-day cadence at the 1.2m Euler telescope at La Silla and at the SMARTS telescope at Las Campanas. During the season indicated with a red rectangle, the object has also been observed daily with the MPIA 2.2m at La Silla (bottom panel), unveiling exquisite small-scale structures that vary faster than microlensing. Such observations allow to measure time delays in 1 single season, with similar accuracy and precision than the lower cadence data over 14 years (Bonvin et al., 2019; Millon et al., 2020a).

into two categories. On one hand, some methods are based on the light-curve cross-correlations (e.g. Pelt et al., 1996), sometimes without attempting to subtract the microlensing variability (e.g. the smoothing and cross-correlation method by Aghamousa and Shafieloo, 2015). On the other hand, several techniques rely on the analytical modelling of the intrinsic variability of the quasars and/or microlensing variations with, for example, splines (Tewes et al., 2013a) or Gaussian Processes (e.g. Hojjati et al., 2013). When explicitly modelled, the microlensing variations are removed from the light curves before attempting to find the optimal time delays. Due to the broad band nature of the monitored signal, mixing flux arising from multiple emission regions, microlensing is rarely perfectly removed but this is shown to have in general a negligible impact on the delay (Sluse and Tewes, 2014). One can also mention the recent work by Tak et al. (2016), Donnan et al. (2021) and Meyer et al. (2022), aiming to infer the time delays in a Bayesian framework, including an explicit modelling of the microlensing variations.

These methods were tested in the "Time Delay Challenge" (TDC; Dobler et al., 2015), a blind data challenge aiming at assessing the precision and accuracy of the curve shifting algorithm on simulated but realistic data, which includes the microlensing variability. The results and conclusions of the challenge are presented in Liao et al. (2015a) as well as in individual papers (Hojjati and Linder, 2014; Bonvin et al., 2016). The problem is in fact more complicated than it sounds since a large fraction of the participating teams did not meet the requirements in term of precision and accuracy on the first and simplest rung of the challenge. Among the qualified teams to participate to the more advanced rungs of the TDC, the different proposed techniques showed overall good performance given the actual quality of the data. Several teams reached an accuracy of $\lesssim 1\%$ on the most variable light curves. However, it remains to be checked if this level of performance holds if more realistic accretion disk emission mechanisms and source-size effects are included in the simulations.

Among these source-size effects, microlensing time delay, which is described in details in Tie and Kochanek (2018), may be a more subtle manifestation of microlensing acting as a nuisance to measure the time delay. Although it has never been detected so far in lensed quasar light curves directly, this effect may arise when different emission regions of the accretion disc are differentially magnified. A simple model to explain the UV and optical variability of the quasars is the "lamp post" model (e.g. Cackett et al., 2007; Starkey et al., 2017), where the luminosity fluctuations originate close from the supermassive black hole and then illuminate the rest of the disk. This triggers temperature fluctuations in the disk, which result into delayed UV and optical emission due to the light travel time from the center. In the absence of differential magnification caused by microlens-

ing, this time lag cancels out between the multiple images and only the "cosmological" time delay is observed. However, if one of the multiple image is affected by microlensing, the time lag originating from a particular region of the disk might be amplified by microlensing and a net excess of microlensing time delay can add to the "cosmological" time-delay. This effect could reach a few hours to a couple of days, which is negligible for most of the systems with long time delays but it can significantly increase the uncertainties for systems with short time delays. This effect can however be mitigated with multi-band light curves (Chan et al., 2021) or a proper Bayesian treatment of this effect as a source of nuisance (Chen et al., 2018).

Future developments of curve shifting algorithms might also include time-delay measurements from unresolved light curves (e.g. Hirv et al., 2007; Shu et al., 2021; Biggio et al., 2021; Springer and Ofek, 2021), which will open the possibility to monitor small-separation ($< 1''$) lensed quasars. While precise delays from unresolved lightcurves have already been measured in the gamma-ray range (Barnacka et al., 2011; Cheung et al., 2014), they cannot be used for cosmography as the location of the gamma-ray emission w.r.t. the central AGN remains unknown. In the optical range, space-based large sky surveys, such as Euclid, are expected to discover thousands of small-separation systems, which will not be fully resolved from the ground with our current follow-up facilities. Turning this large sample of small-separation lensed quasars into a useful cosmological probe will then require to develop these new techniques.

5 Determining lensing potential

Determining the lensing potential ϕ is a crucial ingredient in time-delay cosmography as it directly enters the time-delay prediction through the Fermat potential (Equation 7). The Fermat potential is generally dominated by a massive elliptical galaxy acting as the main deflector and intervening line-of-sight over- and under-densities. To achieve a precise and accurate cosmographic inference, knowledge of both the line-of-sight structure and the mass distribution within the main deflector need to be known. One of the major limitations in a precise determination of the Fermat potential is the MSD, and the inability with imaging data to constrain the Fermat potential. Thus, either physical assumptions based on what we know from other modelled galaxies, e.g. in the nearby universe, or external data, such as stellar kinematics, is required to constrain the Fermat potential. The measurement of the Hubble constant and constraining the galaxy density profiles are tightly connected and most of the questions asked and techniques being used in Shajib et al. (in preparation) are of the same relevance and applicability for time-delay cosmography.

We discuss observables and inferences from imaging data in Section 5.1. We then discuss assumptions on mass profiles in Section 5.2 and what external information provide necessary constraints in Section 5.3.

5.1 Inference from imaging data

High-resolution imaging of gravitational lenses is able to measure accurate astrometry of multiple images and capture the detailed distorted images of extended source structure. This information is crucial to capture the relative lensing deflection and to achieve a precise determination of the relative Fermat potential between multiple images of the time-variable source. In this section, we discuss the necessary aspects of the mass distribution that imaging data can constrain, apart from the remaining degeneracies.

To derive constraints on the mass of the gravitational lens and its deflection field from imaging data, models of the imaging data with different deflection fields are compared to the data in a Bayesian way on the likelihood level of individual pixels. Besides a description of the deflection field, all light emission components have to be described, containing the light emission of the source and the deflector. All components that affect the imaging data need to be modeled and accounted for, in particular around the region impacted by lensing features. Required modeled components include, but are not limited to, the extended source component of host galaxy of the time-variable source, the image positions of the time-variable source and its resulting approximate point-like flux emission, the surface brightness of the deflector galaxy, differential dust extinction caused by the deflector galaxy on the background source, and any other sources of surface brightness, such as satellite galaxies. In addition, instrument effects, such as the point spread function (PSF), instrumental noise and shot noise, and pixelization, as well as potential data reduction artifacts need to be accurately taken into account in the modeling and comparison with the data.

The lensing effect distorting an extended surface brightness $S(\beta)$, such as from the extended host galaxy, can be computed with a method known as ‘backwards ray-tracing’. Making use of the fact that surface brightness is conserved through lensing, the surface brightness at a position in the image $I(\theta)$ can be computed by the surface brightness in the source plane associated with the corresponding coordinate $\beta(\theta)$ as $I(\theta) = S(\beta(\theta))$, where $\beta(\theta) = \theta - \alpha(\theta)$ is the ‘ray tracing’ term given by the lens equation (Eqn. 1).

For unresolved point-like images, the backwards ray-tracing is numerically inefficient. To guarantee that multiple images precisely come from the same location in the source plane within the astrometric requirements for an accurate time-delay prediction, the lens equation has to be solved for the point source constraints within the astrometric precision,

or alternatively, solutions not satisfying the astrometric requirement (e.g., Birrer and Treu, 2019) need to be discarded.

Given a lens model with parameters ξ_{mass} and surface brightness model with parameters ξ_{light} , a model of the imaging data can be constructed, $\mathbf{d}_{\text{model}}$. The full process of simulating a modeled image can be cast as a consecutive application of operators as follows: starting with the surface brightness operator \mathcal{S} , the lensing operator \mathcal{L} is applied on the lensed source, followed by a PSF convolution operation \mathcal{C} , and finally an operator \mathcal{P} matching the pixel resolution of the data, formally an integral of the convolved surface brightness over the size of a pixel. With this notation and \odot denoting the consecutive application of operators from left to right, we can write the generation of modeled data as

$$\mathbf{d}_{\text{model}} = \mathcal{P} \odot \mathcal{C} \odot [\mathcal{L}(\xi_{\text{lens}}) \odot \mathcal{S}_{\text{source}}(\xi_{\text{light}}) + \mathcal{S}_{\text{lens}}(\xi_{\text{light}})]. \quad (27)$$

The Bayesian analysis to constrain the lens model is performed on the pixel-level likelihood of the imaging data. The likelihood is computed at the individual pixel level accounting for the noise properties from background and other noise properties, such as read-out, as well as the Poisson contribution from the sources. In the Gaussian limit the imaging likelihood is given by

$$p(\mathcal{D}_{\text{img}} | \xi_{\text{mass}}, \xi_{\text{light}}) = \frac{\exp\left[-\frac{1}{2}(\mathbf{d}_{\text{data}} - \mathbf{d}_{\text{model}})^T \Sigma_{\text{pixel}}^{-1}(\mathbf{d}_{\text{data}} - \mathbf{d}_{\text{model}})\right]}{\sqrt{(2\pi)^k \det(\Sigma_{\text{pixel}})}}, \quad (28)$$

where k is the number of pixels used in the likelihood and Σ_{pixel} is the error covariance matrix. We also note that for the flux noise, the error covariance matrix Σ_{pixel} is a function of the brightness of the model $\mathbf{d}_{\text{model}}$ and hence not independent of the model prediction. Current analyses assume uncorrelated noise properties in the individual pixels and the covariance matrix becomes diagonal.

The primary target of an imaging analysis is to retrieve the lens model parameter posteriors marginalized over other model parameters, in particular the surface brightness and regularization parameters as

$$p(\xi_{\text{mass}} | \mathcal{D}_{\text{img}}) = \int p(\mathcal{D}_{\text{img}} | \xi_{\text{mass}}, \xi_{\text{light}}) p(\xi_{\text{mass}}, \xi_{\text{light}}) d\xi_{\text{light}}, \quad (29)$$

where $p(\xi_{\text{mass}}, \xi_{\text{light}})$ denotes the prior on the lens and light model parameters.

To jointly marginalize over an unknown yet possibly complex source morphology, different techniques have been developed. Such techniques include regularized pixelated source reconstruction (e.g., Warren and Dye, 2003; Treu and Koopmans, 2004; Koopmans, 2005; Suyu et al., 2006, 2009), a set

of basis functions, such as shapelets (e.g., Birrer et al., 2015; Birrer and Amara, 2018) or wavelets (Joseph et al., 2019; Galan et al., 2021), or simply parameterized surface brightness profiles, such as Sérsic profiles. The methods mentioned above have in common that their surface brightness amplitude components create all a linear response on the pixel values of the data. The optimization of the often numerous linear coefficient to provide the maximum likelihood of the data given a proposed model for the other parameters (such as surface brightness shape parameters and lensing parameters) can be cast as a linear problem with a solution obtained by a weighted least square minimization. The Gaussian covariance matrix of the linear weighted least square minimization can be used to analytically marginalize over the prior of the linear coefficients (e.g., Suyu et al., 2006; Vegetti and Koopmans, 2009; Birrer et al., 2015)³.

The joint sampling of lens and light model parameters to infer the lens model posterior distribution is then a semi-linear process. While the amplitudes of the light model coefficients can be solved linearly, the remaining parameters, including those pertaining to the lens mass model, and other shape-related surface brightness parameters have to be sampled non-linearly.

Often it is not clear at the beginning of an investigation what the level of complexity in the model is required to describe the data and to guarantee an accurate modeling. Current procedures are to start with a simple model and subsequently increase the complexity in the different model components until a satisfactory fit is achieved. Current criteria for a goodness of fit in use are the Bayesian Information Criteria (BIC) (Birrer et al., 2019) and the Bayesian Evidence (Shajib et al., 2020).

Imaging modeling is primarily performed on high resolution space based *Hubble Space Telescope* (*HST*) or ground-based adaptive optics (AO; Chen et al., 2016, 2019, 2021b) imaging. Figure 4 illustrates, as an example, the imaging data and models for two quadruply imaged lensed quasars, originally presented by Shajib et al. (2020) and Chen et al. (2019). Figure 5 presents the key lens model posteriors from the imaging modeling fit of the lens HE0435–1223 by Chen et al. (2019) for both, *HST* and AO imaging, for a power-law elliptical mass distribution with external shear contribution.

The PSF needs to be characterized very accurately, both to provide a high astrometric precision of the images of the time-variable sources (Birrer and Treu, 2019; Chen et al., 2021a) and for the detailed modeling of the extended source structure without spurious signal of bright quasar images. Current methods to obtain a precise PSF model contain an iterative procedure during the model fitting process to extract improved constraints of the PSF from the data itself (e.g., Chen et al., 2016; Birrer et al., 2016).

³ This is not a statement about the validity of the form of the prior of the linear surface brightness coefficients.

The posteriors are marginalized over a set of systematic effects and modifications in the choice of the source reconstruction and other modeling choices.

5.2 Mass profile assumptions of the main deflector

Resolved multiply imaged structure is an exquisite data product to provide constraints on the relative deflection field (see Section 5.1). Imaging data, in the absence of the knowledge of the unlensed apparent source size or brightness, is not able to break the MST and its generalization, the source position transformation (SPT; Schneider and Sluse, 2014). The MST is particularly impacting the radial constraints of the mass profile. The quantity that is invariant under the MST in the radial direction and hence can be constrained by imaging data is (Kochanek, 2002; Sonnenfeld, 2018; Kochanek, 2020; Birrer, 2021)

$$\xi_{\text{rad}} \equiv \frac{\theta_E \alpha'_E}{1 - \alpha'_E} \propto \frac{\theta_E \alpha''_E}{1 - \kappa_E}, \quad (30)$$

where α'_E is the derivative and α''_E is the second derivative of the deflection angle at the Einstein radius θ_E , respectively, and κ_E is the convergence at θ_E . On azimuthal invariances and observable lensing features, we refer to Birrer (2021) and references therein. Constraining a global mass density profile based on imaging data alone requires assumptions on the radial profile. For example, when imposing the assumption that the mass density profile follows a single power law, the power-law slope γ_{pl} has a direct correspondence to ξ_{rad} (Eqn. 30) with $\xi_{\text{rad}} = \gamma_{\text{pl}} - 2$ and a precise (few percent uncertainty) inference on the Fermat potential is possible. Relaxing the assumption on the shape of the density profile leads to significantly widened constraints. When allowing for a full mass-sheet degree of freedom, the Fermat potential is fully degenerate (i.e. ξ_{rad} remains unchanged by a MST). A pure mass sheet is unphysical as no localized three-dimensional density profile can describe it. However, approximate parameterizations can be found that can be expressed as a three-dimensional density profile and are indistinguishable based on imaging data (Schneider and Sluse, 2013; Blum et al., 2020; Birrer et al., 2020; Yıldırım et al., 2021). Figure 6 illustrates an example of how an approximate MST can be physically interpreted when applied to a composite profile described with a stellar and a dark matter component.

There are also possibilities in deviations in the mass density profiles that do not directly mimic an MST. Any radial mass profile that satisfies the same constraints on ξ_{rad} (Eqn. 30) provides an equally good fit to the data⁴. Azimuthal

⁴ ξ_{rad} is the first-order Taylor expansion term affecting the observed radial distortions. The quantity is well defined for an azimuthally symmetric lens. The generalization of the relevant radial quantity for elliptical mass models needs to be investigated.

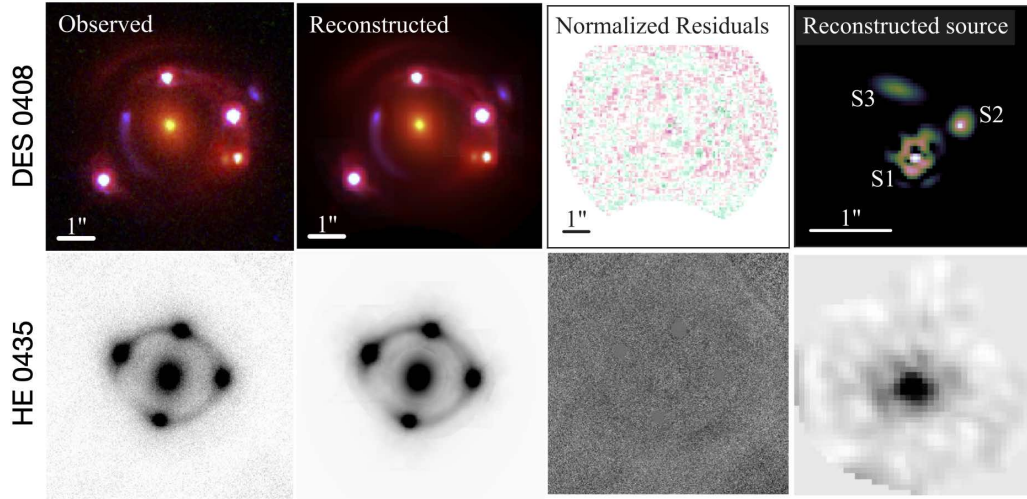


Fig. 4 Illustration of imaging modeling for two lenses. From left to right: Imaging data, the reconstructed model, the reduced residuals ($d_{\text{data}} - d_{\text{model}})/\sigma$, reconstructed source. Top row: HST data and model for DES J0408–5354 in three bands, from Shajib et al. (2020), with shapelet and parameterized source reconstruction using the modeling software LENTRONOMY. Bottom row: Keck adaptive optics imaging and modeling of HE0435–1223, from Chen et al. (2019), with pixelated source reconstruction using the modeling software GLEE.

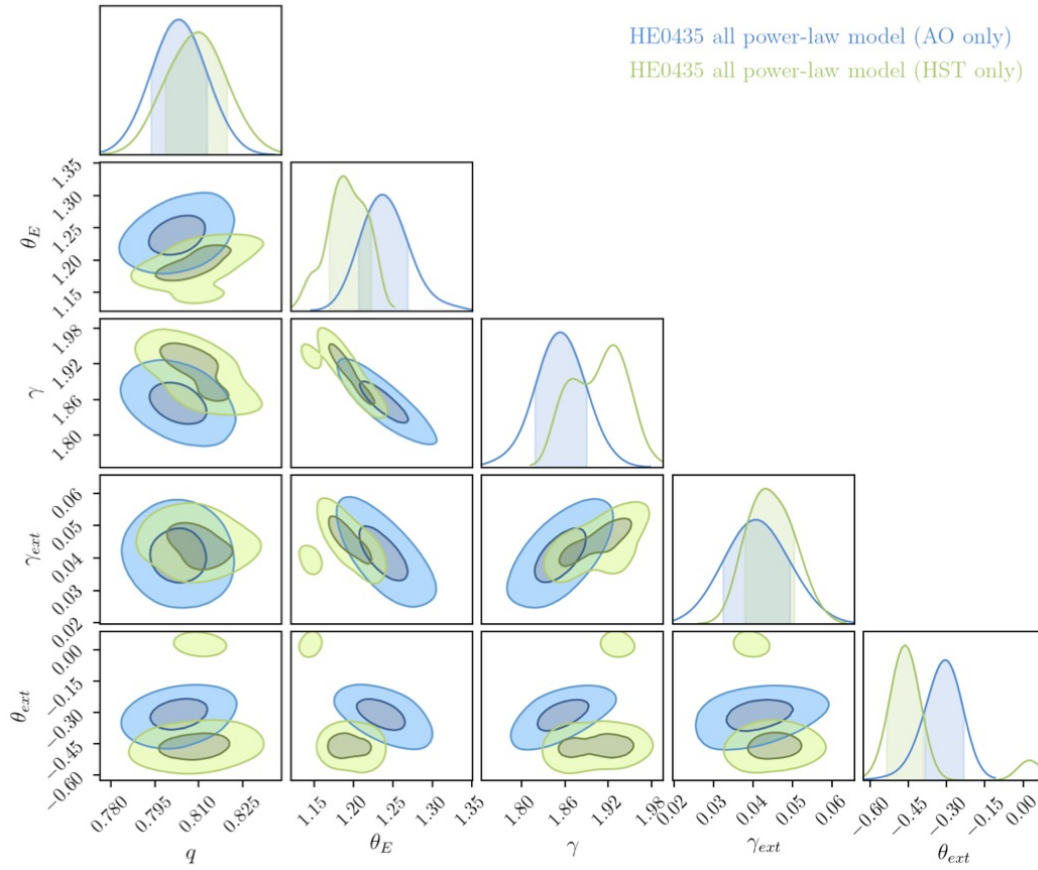


Fig. 5 Key lens model parameter posterior from the fit to imaging data (*HST* and Keck adaptive optics). q is the semi-minor to semi-major axis ratio in the projected mass density profile, θ_E is the Einstein radius, γ the three-dimensional radial power-law density slope, γ_{ext} is the external shear strength, and θ_{ext} is the shear angle. Figure adopted from Chen et al. (2019).

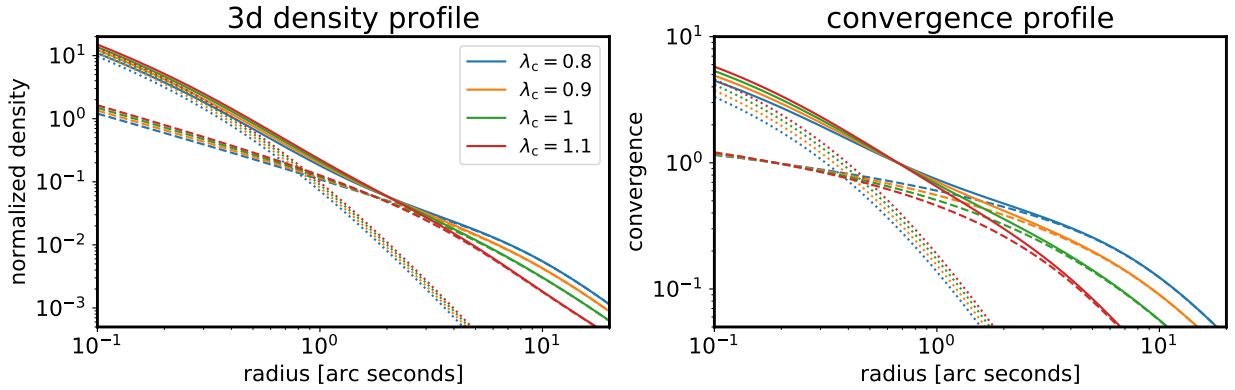


Fig. 6 Illustration of a composite profile consisting of a stellar component (Hernquist profile, dotted lines) and a dark matter component (NFW + cored component with λ_c acting as an approximate MST (from Blum et al., 2020), dashed lines) which transform according to an approximate MST (joint as solid lines). The stellar component gets rescaled by the MST while the cored component transforms the dark matter component. Physically, the profiles of each color differ by a 10% different mass-to-light ratio combined with a slightly more extended or contracted dark matter profile also on the 10% level. **Left:** profile components in three dimensions. **Right:** profile components in projection. Each profile provides a 10% difference in the predicted time delay, and hence H_0 inference. The transforms presented here cannot be distinguished by imaging data alone and require i.e., stellar kinematics constraints. Figure from Birrer et al. (2020).

assumptions of the mass density profile do also matter in the interpretation of the radial components (Birrer, 2021; Kochanek, 2021) and assumptions on diskiness and boxiness, ellipticity gradients and isodensity twists of the density profile may also impact the Fermat potential differences (Van de Vyvere et al., 2022b,a; Gomer and Williams, 2020, 2021).

From a physics point of view, the matter distribution of the main deflector is made of stellar mass, gas, and dark matter, where the stellar mass is dominating the inner-most parts. The dark matter fraction within the Einstein radius is about $\sim 10 - 60\%$ (e.g., Auger et al., 2010; Ferreras et al., 2005). Invisible substructure in the lens and along the LOS can also perturb the Fermat potential (e.g., Oguri, 2007; Keeton and Moustakas, 2009). Gilman et al. (2020) showed that omitting dark substructure does not bias inferences of H_0 . However, perturbations from substructure contribute an additional source of random uncertainty in the inferred value of H_0 ranging from 0.7 - 2.4% depending on the redshift and image configuration. We also highlight that the lensing mass and convergence only accounts for the mass over-density in regard to the cosmological background density.

Different approaches running with different assumptions have been taken in the literature. Among the assumptions being used are single power-law mass profiles, composite models involving a mass-follows-light component with a separate component describing the dark matter profile, free-form pixelated mass profiles (e.g., Saha and Williams, 2004; Coles et al., 2014; Denzel et al., 2021), pixelated lensing potential corrections (e.g., Suyu et al., 2009), or an explicit internal mass profile MST component (Blum et al., 2020; Birrer et al., 2020).

There are multiple considerations in the specific choice of an investigation. On one side, there are physical consider-

ations. What basic assumptions in the modeling deem justified? What priors to choose in the Bayesian modeling? Then there are also practical considerations. What aspects of the model can be constrained by the data? Is it feasible to perform a posterior inference in a finite amount of time with given resources?

Among the simplest models employed is the single power-law profile. It has a one-to-one relation to the radial quantity described in Equation 30 and breaks the MST. A power-law elliptical mass profile is an efficient parameterization to describe the first order radial and azimuthal features in strong lensing imaging data. Composite models do relate to certain physical assumptions of mass follows light and assert a stiffness in the profile that implicitly also break the MST⁵.

An explicit parameterization of the MST in the model denies any prior or assumptions to break the MST and is maximally agnostic to the MST with minimal added parameter degrees.

On the high-complexity end of lens models are free-form methods, such as pixelated mass distributions (Saha and Williams, 2004; Coles et al., 2014). Free-form models come with very few restrictions on the lens mass distribution and offer a different modeling strategy compared to the simply parametrized approaches. The ensemble of models allowed by the data can be interpreted as the model posterior distribution, with the regularization scheme proposing models without data constraints being the prior.

Increased flexibility in the parameterization better guarantees that the underlying truth in the mass distribution, and in particular the prediction of the Fermat potential entering

⁵ The breaking of the MST for composite models is dependent on imposed mass and concentration priors of the dark matter profile, as well as mass-to-light gradients or the absence of it.

the time delays, can be represented by the model. On the other hand, increased flexibility in the model at fixed data constraining power increases the uncertainty in the posterior-predictive model. Less constraining posteriors put inevitably more weight and reliance on the priors applied, whether they are explicitly in a parameterized form, or implicit within an over-parameterized, free-form approach. No matter what choices are being made in the modeling of lenses, mitigating the dependence on the explicit or implicit priors becomes important when combining a set of multiple lenses, as we will discuss in Section 7.2.

We discuss additional data sets that can constrain the lens mass profile in Section 5.3.

5.3 Non-lensing observables

The currently used primary observation to break the MSD is stellar kinematics from the deflector galaxy (Treu and Koopmans, 2002; Koopmans et al., 2003; Koopmans, 2004). The kinematics of stars, in particular their velocity dispersion, is a direct and lensing-independent tracer of the three-dimensional gravitational potential.

The measurement is performed by targeting stellar absorption lines and measuring their width with spectrographs. Figure 7 shows a Keck/LRIS spectrum of HE0435–1223.

The line-of-sight stellar velocity dispersion is an integrated quantity of the radial and tangential components of the velocity dispersion projected along the line of sight. The orbital anisotropy, i.e., the ratio of the radial and tangential velocity dispersion components, is unknown *a priori* and thus introduces a degeneracy in the predicted line-of-sight velocity dispersion corresponding to the same 3D mass profile. This degeneracy is known as the mass–anisotropy degeneracy. Typically, a prior on the anisotropy profile, e.g., isotropic or Osipkov–Merritt (Osipkov, 1979; Merritt, 1985a,b), is assumed. The Osipkov–Merritt profile allows the anisotropy to be isotropic near the center and gradually more radial farther away from the center, which is motivated by the observed properties of the stellar orbits in local elliptical galaxies. The isotropic profile is thus a special case of the Osipkov–Merritt profile. The transition scale radius r_{ani} from isotropic to radial orbits in the Osipkov–Merritt profile is *a priori* unknown, which directly manifests in the mass–anisotropy degeneracy. Thus, the prior on r_{ani} has strong impacts on the kinematics prediction (e.g., Shajib et al., 2018; Birrer et al., 2020). We note that there are many other forms of the radial anisotropy distribution and the specific choice of functional model used might impact the results, as well as what priors are adopted. One way to mitigate this degeneracy is to obtain spatially resolved measurement of the velocity dispersion instead of an unresolved (or, integrated) velocity dispersion (Shajib et al., 2018; Yıldırım et al., 2020, 2021; Birrer and Treu, 2021).

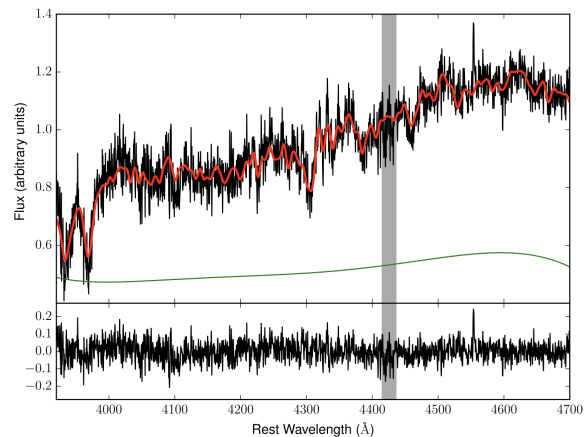


Fig. 7 Top: Keck/LRIS spectrum of HE0435–1223 with the best-fitting model overplotted in red and a polynomial continuum, which accounts for contamination from the lensed QSO images and template mismatch, shown in green. The measurement results in $\sigma_v = 222 \pm 15$ km s^{−1}, including systematic uncertainties due to the templates used, the region of the spectrum that was fitted, and the order of the polynomial continuum. The grey vertical band represents a wavelength range that is excluded from the fit due to the presence of a strong Mg II absorption system. Bottom: Residuals from the best fit. Figure adopted from Wong et al. (2017).

Other proposed observations and analyses methods that can break the MST and provide the necessary constraints on the mass density profile are standardizable magnifications (e.g., Kolatt and Bartelmann, 1998; Oguri and Kawano, 2003; Foxley-Marrable et al., 2018; Birrer et al., 2021), and lens population statistics of appearances and asymmetry in the multiple images (e.g., Sonnenfeld and Cautun, 2021; Sonnenfeld, 2021a).

We emphasize that these non-lensing observations are primarily sensitive to the total MST, the combination of LOS and internal mass density profile degeneracies (Eqn. 20). Decoupling of the different projected effects in the lensing potential is not necessary to perform an accurate cosmographic inference since the time-delay prediction only requires the combined product. However, when combining different lenses with potentially different selections, the priors and assumptions imposed in either of the two components impacting the MST can become important.

6 Estimating line-of-sight contributions

The contribution of the mass density fluctuations along the line of sight to the lensed source is generally of order few percent, and commonly lower than 10% of the total convergence of the lens. While this may appear to be small, it is not negligible when it comes to estimating the Hubble parameter to percent accuracy. A constant effective contribution of a few percents caused by the line-of-sight is equivalent to an external mass-sheet κ_{ext} (Sect. 2).

The exact impact of the line-of-sight objects depends on whether the dominant-lens approximation is valid, in which case the critical density of the line-of-sight objects is very small compared to the main deflector critical density, and on whether the tidal regime is applicable, which happens when the perturber's gravitational field is small compared to the changes of the deflection $\alpha(\theta)$ (e.g. McCully et al., 2014; Birrer et al., 2017; Fleury et al., 2021b). When one of those approximation is invalid, an explicit treatment is needed, requiring potentially to solve the multi-plane lens equation (we refer to Saha et al. (in preparation)). Conversely, when line-of-sight objects can be treated as small perturbations that only introduce convergence that is constant over the extent of the lensed system, a statistical treatment is sufficient. In practice, a hybrid scheme needs to be followed most of the time, including explicitly modelling those objects that modify differently the Fermat potential for each lensed images, and calculating the statistical contribution of the other objects that shift the Fermat potential in linear order.

From an information perspective, there is only limited direct data available of the total matter distribution on the universe at the scales relevant to constrain κ_{ext} . Hence, any method relies on some assumptions on how mass traces light. These assumptions are well motivated by large scale structure probes, but are only validated in a statistical way.

The following subsections present the various methods that have been considered to estimate κ_{ext} . Section 6.1 presents a direct modeling, Section 6.2 presents galaxy number counts statistics, Section 6.3 weak lensing measurements, and Section 6.4 a hybrid approach.

6.1 Direct modeling

The most direct approach is to collect the positions, redshifts, stellar masses and potentially even velocity dispersion measurement of the galaxies located in the field of view towards the lens and explicitly model the matter distribution of all relevant objects. A complete direct reconstruction is near-impossible. A simple approach that has been developed to estimate κ_{ext} consists in identifying which galaxies form massive galaxy groups that contribute the most significant impact along the line of sight (e.g. Fassnacht and Lubin, 2002; Momcheva et al., 2006; Wilson et al., 2016; Sluse et al., 2017). An estimate of κ_{ext} may then be derived by fitting analytical mass density profiles on those groups (Auger et al., 2007; Wilson et al., 2017). This approach generally yields estimates of κ_{ext} typically uncertain to a factor 2-4 depending on the specific assumptions one may reasonably make on the group mass density (e.g., halo associated to each individual galaxies, a common halo for all the systems), but also sometimes with low precision due to the uncertainties associated to the group identification (field of view are never complete and group finders have their own

biases). To overcome this problem, Collett et al. (2013) have proposed a simple halo model prescription to reproduce the mass along the line-of-sight from a photometric catalogue of galaxies. The convergence κ_h from each halo has then been calibrated against κ_{ext} derived from ray-tracing estimate through numerical simulations. This method does not account explicitly for the convergence due to dark structures and divergence due to voids, but those effects are included statistically owing to the calibration of κ_h against κ_{ext} .

6.2 Number counts

An alternative to the direct modeling of the line of sight consists of measuring the galaxy number density in the vicinity of the lens as a summary statistics and comparing it to reference fields, hence determining whether the LOS is over- or under-dense compared to average (Suyu et al., 2010; Fassnacht et al., 2011; Greene et al., 2013; Rusu et al., 2017). First, a detailed characterization of the line of sight towards the lens is required, using deep imaging data, complemented by spectroscopic data (see Fig. 8 for an illustration). Similar LOS are then searched for in large volume, and high resolution numerical simulations. The surface mass density of matter along these line of sight being calculated using a ray-tracing technique (Hilbert et al., 2007, 2008, 2009), it is then possible to derive a probability distribution of external convergence compatible with the observed lens matching the summary statistics.

In practice, summary statistics that deviate from pure number counts can be a better informed statistics of the underlying over- or under- density. For example, if N_{gal} galaxies are observed in the field of view of a lens, one can calculate a weighted number counts $W_q = \sum_{i=1}^{N_{\text{gal}}} q_i$ with q being a particular type of weight, such as the inverse of the distance to the lens, i.e. $1/r$. To calculate a weighted density of galaxies, ζ_q , it is necessary to perform the same measurement over an ensemble of control fields, such that for each control field (CF, j) one derives a density $\zeta_q^j = W_q / W_q^{\text{CF}, j}$. To avoid introducing any bias through this normalisation procedure, it is important to choose enough control fields but also ensure that those fields have characteristics that match closely those of the imaging data of the observed lens system. This allows one to account for sample variance and to assess that galaxy detection biases are similar for the lens and for the control fields. In particular, one should ascertain that the lens and control fields have similar depth, seeing, and pixel scale, the latter quantities being critical in the framework of source deblending and identification. It happens that some regions of the control fields are masked due to saturation of stars, cosmic rays, or camera defects. To guarantee unbiased estimates of ζ_q , it is important to apply the same mask to the weighted count of the lens field. A large variety of weighting schemes has been explored, some of them involving a proxy

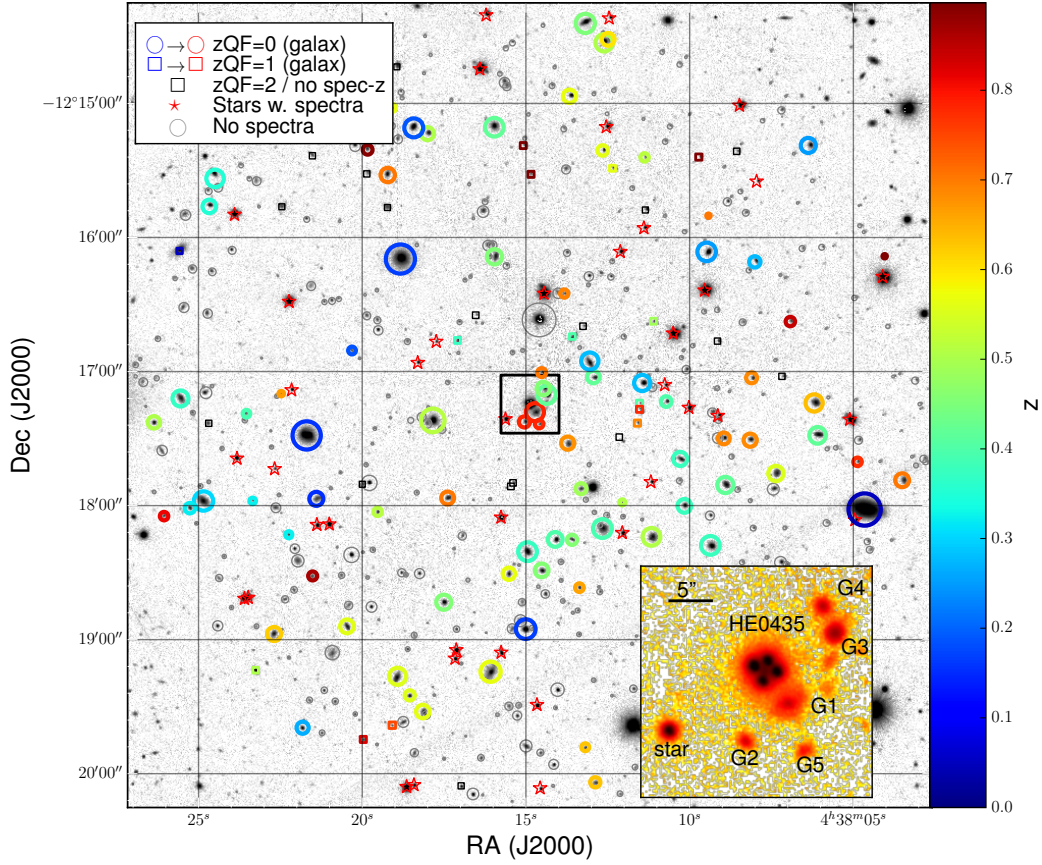


Fig. 8 Example of the result of the spectroscopic characterization of the field of view of the gravitational lens HE0435–1223. The redshifts of the objects measured in the field of view are used to identify which objects (or galaxy groups) needs to be explicitly included in the macro-model. The number counts analysis uses the galaxies located at projected distances of $<45''$ and $<120''$ from the lens to estimate $P(\kappa_{\text{ext}})$. Courtesy of Sluse et al. (2017)

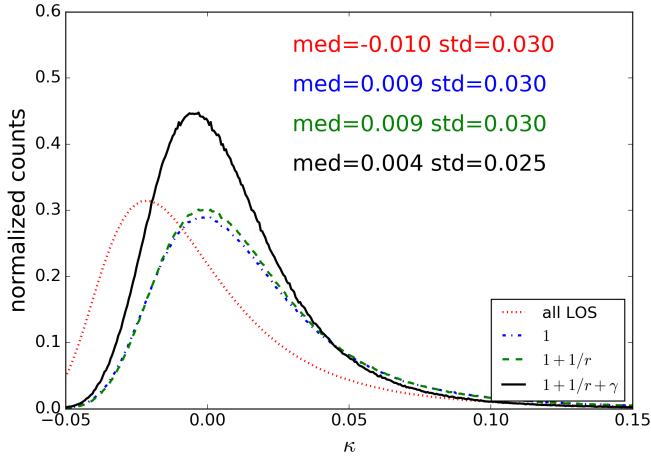


Fig. 9 Probability distribution $P(\kappa_{\text{ext}})$ for HE0435–1223 and an aperture radius of $45''$. The different curves correspond to all lines of sights (dotted red), considering only lines of sights with the same overdensity as the data (dash-dotted blue), using a weighting inversely proportional to the distance (dashed green) and the additional constraint from the shear (solid black). Courtesy of Rusu et al. (2017)

on some of the galaxy properties such as the redshift and the stellar mass. Those quantities are derived using a photometric redshift code, such as LEPHARE (Ilbert et al., 2006). This implies the availability of deep multi-band photometric data. Having a similar depth for the lens and comparison field is important to matching galaxy properties in photometric surveys. Also, similar set-up for magnitude measurements are required to minimize systematic errors caused by aperture and/or object deblending uncertainties. When spectroscopic redshift are also available, they may generally be preferred to the photometric ones.

The conversion of the probability density distribution $p(\zeta_q)$ into $p(\kappa_{\text{ext}})$ requires the use of numerical simulations for which κ_{ext} has been derived through ray-tracing. Large simulation volumes are required to minimise the impact of sample variance. The Millennium simulation (Springel et al., 2005) being dark matter only, galaxy photometric properties are inpainted using physically motivated prescriptions. A common choice has been to use the semi-analytic model of De Lucia and Blaizot (2007). Densities ζ_q can be estimated in those catalogues in similar way as for real data

except that the reference fields is now the simulation catalog itself. As explained in Rusu et al. (2017), the probability $p(\kappa_{\text{ext}} | \mathbf{d})$, where \mathbf{d} stands for the available data, is given by:

$$p(\kappa_{\text{ext}} | \mathbf{d}) = \int d\zeta_q \frac{p(\kappa_{\text{ext}}, \zeta_q) p(\zeta_q, \mathbf{d})}{p(\zeta_q) p(\mathbf{d})} = \int d\zeta_q p(\kappa_{\text{ext}} | \zeta_q) p(\zeta_q | \mathbf{d}). \quad (31)$$

Greene et al. (2013) has shown that the precision on κ_{ext} is improved by a factor 2 when using a combination of weights, the two main ones being the standard number counts ($q = 1$), and as the inverse of the projected distance to the lens ($q = 1/r$). The addition of a weight based on the modeled amplitude of the shear, γ_{ext} is also often considered, such that the general expression of $p(\kappa_{\text{ext}} | \mathbf{d})$ becomes:

$$p(\kappa_{\text{ext}} | \mathbf{d}) = \int d\zeta_1 d\zeta_{1/r} d\zeta_{q \neq 1, 1/r} d\zeta_{\gamma_{\text{ext}}} p_{\text{MS}}(\kappa_{\text{ext}} | \zeta_1, \zeta_{1/r}, \dots \zeta_{q \neq 1, 1/r}, \zeta_{\gamma_{\text{ext}}}) p(\zeta_1, \zeta_{1/r}, \zeta_{q \neq 1, 1/r}, \zeta_{\gamma_{\text{ext}}} | \mathbf{d}). \quad (32)$$

The addition of a fourth weight, $q \neq 1, 1/r$ allows one to evaluate systematic errors involved by the specific choice of equally motivated weighting schemes and explore which combination of weight yields the best precision on κ_{ext} . The first application of this technique in the framework of time-delay cosmography has been presented in Suyu et al. (2010). Subsequent time-delay cosmography analyses from H0LICOW, STRIDES and TDCOSMO have used an approach that broadly follows the strategy outlined above (see Greene et al., 2013; Rusu et al., 2017, for a more in-depth description of the method), but proposing small variations and tests in terms of weighting schemes and choices of comparison fields (Birrer et al., 2019; Sluse et al., 2019; Buckley-Geer et al., 2020). Figure 9 displays $p(\kappa_{\text{ext}})$ as derived with different weighting schemes for the lens system HE0435–1223.

A novel method for estimating κ_{ext} has recently been proposed by Park et al. (2021). They replace the weighted number count scheme by a machine learning approach. Specifically, they have trained a Bayesian Graph Neural Network on LSST DESC DC2 sky survey (LSST Dark Energy Science Collaboration (LSST DESC) et al., 2021) in order to derive a distribution of κ_{ext} for arbitrary gravitational lens sight-line.

6.3 Weak Lensing

Weak lensing, the linear shape distortion of background galaxies due to foreground structure, is a direct probe of the LOS structure. On linear scales, the cosmic shear measurements can be translated to convergence in a unique mapping (Kaiser and Squires, 1993). Hence, this technique does neither rely on priors from numerical simulations nor of a galaxy-halo connection. However, there are also several drawbacks. The

angular scale of a weak lensing measurement is limited by the number density of lensed sources, and a high S/N measurement can only be achieved at scales of arc minutes. Thus, weak lensing is an excellent observable to quantify large scale cosmic density distributions but other smaller scale density perturbations down to the scales of arc seconds are not well captured. Another limitation is that the weak lensing source population is not at the same redshift as the strongly lensed source. This requires to translate the weak lensing convergence map to a different lensing kernel, which comes with additional statistical uncertainties (e.g., Kuhn et al., 2021).

In the strong lensing context, for example, Fischer and Tyson (1997); Nakajima et al. (2009); Fadely et al. (2010) relied on the weak lensing effect produced by massive structures in the vicinity of the deflector. They constrained the external convergence by integrating the tangential weak gravitational shear in the area around the lens. More recently, Tihhonova et al. (2018, 2020) applied the weak lensing techniques to the quadruply lensed quasar systems HE0435–1223 and B1608+656 and performed a convergence map reconstruction based on HST imaging. Kuhn et al. (2021) performed a convergence map reconstruction of the COSMOS field at the position of discovered strong lenses.

6.4 Hybrid framework

Given the strengths and weaknesses of the direct modeling and summary statistics approaches, as well as weak lensing measurements, a hybrid approach can leverage the complementary methodologies. Summary statistics can be most effectively employed for objects that mostly cumulatively affect the lensing convergence while explicit modeling of LOS objects makes a difference for massive or very close by objects. The specific decision of where to split the analysis between a statistical approach and explicit modeling is primarily impacted by two factors. The first is the accuracy in the deflection properties, both in terms of higher-order lensing distortions and the need for a multi-plane lensing approach. The second is the available information and the handling of priors in the absence of sufficient information.

A method to account accurately for the line-of-sight has been proposed by McCully et al. (2014, 2017). It consists in a multi-plane lens equation where only the planes associated to important perturbing groups/clusters/galaxies are included. The other perturbers along the LOS are treated under the tidal approximation. In order to identify those objects, McCully et al. (2017) proposes to use a threshold based on the value of the flexion-shift, i.e. Δ_{3x} whose expression is given by:

$$\Delta_{3x} = f(\beta) \times \frac{(\theta_E \theta_{E,p})^2}{\theta^3}, \quad (33)$$

where θ_E and $\theta_{E,p}$ are the Einstein radius of the main lens and of the perturber, and θ is the angular separation on the sky between the lens and the perturber. The function $f(\beta) = (1-\beta)^2$ if the perturber is behind the main lens, and $f(\beta) = 1$ if the galaxy is in the foreground. In that expression, β is the pre-factor of the lens deflection in the multiplane lens equation:

$$\beta = \frac{D_{dp}D_{os}}{D_{op}D_{ds}}, \quad (34)$$

where $D_{ij} = D(z_i, z_j)$ are angular diameter distances between redshifts z_i and z_j , corresponding to the observer (o), deflector (d), perturber (p) and source (s). Missing to account for a foreground perturber may have a stronger impact on the models than missing a background one. The reason is that the background perturber will have a multiplicative effect on the source position, while the deflection from the foreground perturber enters the lens equation inside the argument of the deflection of the main lens galaxy. In other words, the foreground perturber modifies the coordinates of the lensed images positions compared to the main lens case. These non-linear effects require a multi-plane treatment to be properly accounted for. From a set of simulation of time-delay lens systems resembling real ones, and their subsequent modeling based on point-source image positions, McCully et al. (2017) suggests that a value $\Delta_3 x < 10^{-4}$ arcsec yields to a bias on H_0 of less than a percent. Since Sluse et al. (2017), this prescription is used by the H0LICOW and TDCOSMO collaborations to select the objects that they explicitly include in the lens mass modelling.

Birrer et al. (2017); Kuhn et al. (2021) combined the study of the environment using the halo-rendering approach, i.e. linking the galaxy stellar masses to the underlying mass distribution, with the external shear measurements of the strong lens system. Their combined approach yielded tighter constraints on the inferred external convergence compared to a halo-rendering approach only.

7 Cosmographic inference

Having established the necessary observations and analyses components in the previous sections, in this section we discuss how an end-to-end combined analysis leads to constraints on H_0 and other relevant cosmological parameters. First we discuss the analysis for a single lens (Section 7.1) and then state the analysis for a set of multiple lenses (Section 7.2).

7.1 Single lens cosmography

For each individual strong lens, there are preferably four data sets available: (i) imaging data of the strong lensing fea-

tures and the deflector galaxy, \mathcal{D}_{img} ; (2) time-delay measurements between the multiple images, \mathcal{D}_{td} ; (3) stellar kinematics measurement of the main deflector galaxy, $\mathcal{D}_{\text{spec}}$; (4) line-of-sight galaxy count and weak lensing statistics, \mathcal{D}_{los} . These data sets are independent and so are their likelihoods in a joint cosmographic inference. Hence, we can write the likelihood of the joint set of the data

$$\mathcal{D} = \{\mathcal{D}_{\text{img}}, \mathcal{D}_{\text{td}}, \mathcal{D}_{\text{spec}}, \mathcal{D}_{\text{los}}\} \quad (35)$$

given the cosmographic parameters $\{D_d, D_s, D_{ds}\} \equiv D_{d,s,ds}$ as

$$\begin{aligned} \mathcal{L}(\mathcal{D}|D_{d,s,ds}) &= \int \mathcal{L}(\mathcal{D}_{\text{img}}|\xi_{\text{mass}}, \xi_{\text{light}}) \\ &\times \mathcal{L}(\mathcal{D}_{\text{td}}|\xi_{\text{mass}}, \xi_{\text{light}}, \lambda, D_{\Delta t}) \\ &\times \mathcal{L}(\mathcal{D}_{\text{spec}}|\xi_{\text{mass}}, \xi_{\text{light}}, \beta_{\text{ani}}, \lambda, D_s/D_{ds}) \mathcal{L}(\mathcal{D}_{\text{los}}|\kappa_{\text{ext}}) \\ &\times p(\xi_{\text{mass}}, \xi_{\text{light}}, \lambda_{\text{int}}, \kappa_{\text{ext}}, \beta_{\text{ani}}) d\xi_{\text{mass}} d\xi_{\text{light}} d\lambda_{\text{int}} d\kappa_{\text{ext}} d\beta_{\text{ani}}. \end{aligned} \quad (36)$$

In the expression above we only included the relevant model components of the individual likelihoods. ξ_{light} formally includes the source and lens light surface brightness⁶.

The sampling of the cosmographic posterior from the joint likelihood of Equation 36 can be split in parts to simplify the problem. For example, we can first perform the imaging analysis providing constraints on ξ_{lens} and ξ_{light} without sampling the cosmological or distance parameters. In turn, simple sampling the ξ_{lens} and ξ_{light} posteriors in post-processing when evaluating the time-delay likelihood and stellar kinematic likelihood can translate the posteriors into distance posteriors in $D_{\Delta t} - D_d$ space. Marginalization over different modeling choices can also be done in the $D_{\Delta t} - D_d$ posterior space. Figure 10 provides an example of $D_{\Delta t} - D_d$ for a set of different modeling choices.

Weighting the posteriors of different models can be done with Bayesian model comparison. This weighting also allows one to combine models in a single posterior, which then includes systematics considerations. Discrete and finite choices made in the models and scatter in the sampling and BIC calculation can lead to over-constraint model selections. Procedures to take noise and finite model selection in the BIC estimate into account have been developed (Birrer et al., 2019).

7.2 Population level analysis

The overarching goal of time-delay cosmography is to provide a robust inference of cosmological parameters, π , and in particular the absolute distance scale, the Hubble constant H_0 , and possibly other parameters describing the expansion

⁶ To evaluate the time-delay likelihood, we require the time-variable image positions from the set of ξ_{light} parameters.

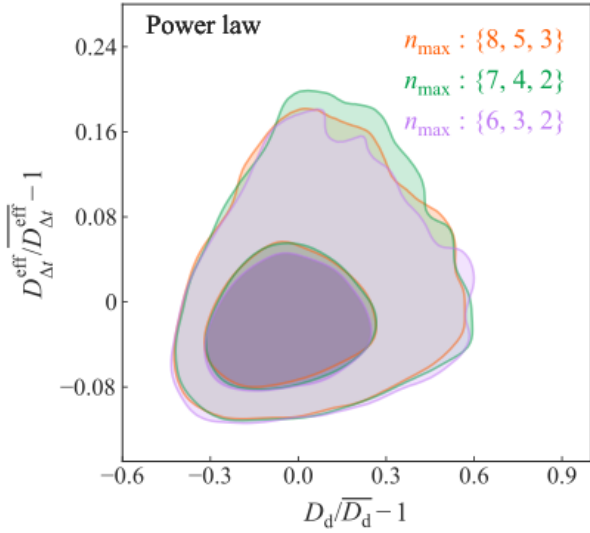


Fig. 10 Median-subtracted and mean-divided relative angular diameter distance posteriors, $D_{\Delta t}$ and D_d for a power-law mass density profile with three different source reconstruction settings. n_{max} in this figure refers to the polynomial order in the shapelets with the set of three numbers corresponding to three different sources being simultaneously modelled in the image. Figure adopted from Shajib et al. (2020).

history of the Universe (such as Ω_A or Ω_m), from a sample of gravitational lenses with measured time delays.

In Bayesian language, we want to calculate the probability of the cosmological parameters, π , given the strong lensing data set, $p(\pi | \{\mathcal{D}_i\}_N)$, where \mathcal{D}_i is the data set of an individual lens (including imaging data, time-delay measurements, kinematic observations and line-of-sight galaxy properties) and N the total number of lenses in the sample.

In addition to π , we denote ξ all the model parameters part of either a single lens analysis (Section 7.1) or present on the population level. Using Bayes rule and considering that the data of each individual lens \mathcal{D}_i is independent, we can write, following Birrer et al. (2020):

$$p(\pi | \{\mathcal{D}_i\}_N) \propto \mathcal{L}(\{\mathcal{D}_i\}_N | \pi) p(\pi) = \int \mathcal{L}(\{\mathcal{D}_i\}_N | \pi, \xi) p(\pi, \xi) d\xi \\ = \int \prod_i^N \mathcal{L}(\mathcal{D}_i | \pi, \xi) p(\pi, \xi) d\xi. \quad (37)$$

In the following, we divide the nuisance parameter, ξ , into a subset of parameters that we constrain independently per lens, ξ_i , and a set of parameters that require to be sampled across the lens sample population globally, ξ_{pop} . The parameters of each individual lens, ξ_i , include the lens model, source and lens light surface brightness and any other relevant parameter of the model to predict the data. Hence, we

can express the hierarchical inference (Eqn. 37) as

$$p(\pi | \{\mathcal{D}_i\}_N) \propto \int \prod_i [\mathcal{L}(\mathcal{D}_i | D_{d,s,ds}(\pi), \xi_i, \xi_{\text{pop}}) p(\xi_i)] \\ \times \frac{p(\pi, \{\xi_i\}_N, \xi_{\text{pop}})}{\prod_i p(\xi_i)} d\xi_i d\xi_{\text{pop}} \quad (38)$$

where $\{\xi_i\}_N = \{\xi_1, \xi_2, \dots, \xi_N\}$ is the set of the parameters applied to the individual lenses and $p(\xi_i)$ are the interim priors on the model parameters in the inference of an individual lens. The cosmological parameters π are fully encompassed in the set of angular diameter distances, $\{D_d, D_s, D_{ds}\} \equiv D_{d,s,ds}$, and thus, instead of stating π in Equation 38, we now state $D_{d,s,ds}(\pi)$. Up to this point, no approximation was applied to the full hierarchical expression (Eqn. 37).

Key differences among different inferences of H_0 from a set of lenses involve, beyond the assumptions on individual lenses, assumptions on the covariant nature and the prior on the population level of the governing hyper-parameters. For example, Wong et al. (2020) assumes full independence of the nuisance priors from one lens to another. Formally, within Bayes Theorem, this approach assumes perfect knowledge of the governing population hyper-parameter distribution prior (Eqn. 38). In this approach, the distance posteriors of individual lenses can be interpreted as measurements and the cosmographic analysis can be done in solely operating in the $D_{\Delta t} - D_d$ space with a direct independent and easy accessible likelihood description.

Millon et al. (2020b) performed an analysis exploring the difference between two different radial mass density profile families, assuming that either all lenses are of one type or another, effectively treating one modeling choice as a covariant nuisance parameter in their inference while keeping all other priors independent with an assumed population.

Denzel et al. (2021) is using a free-form approach in the modeling of individual lenses. The ensemble of models allowed by the data for an individual lens is providing the model posterior distribution. The underlying regularization scheme is the implicit prior applied on individual lenses. The identical regularization scheme is applied to all lenses assuming independence in the priors without covariances in the choice of the regularization scheme between lenses. Denzel et al. (2021) did not use any external information to break the MST. Hence, the specific choice of the regularization scheme with their underlying physical and regularization priors is responsible for the breaking of the MST on the population level.

Birrer et al. (2020) introduced the hierarchical analysis framework into time-delay cosmography and identified few key parameters, that on a per lens basis are not sufficiently well constrained and thus the population prior can significantly affect the outcome of the analysis. The parameters hierarchically sampled, beyond the cosmological ones, were

the MST population λ_{int} (Eqn. 21), and the stellar anisotropy distribution (see Section 5.3).

Park implemented a Bayesian hierarchical framework to determine the external convergence distribution on the population level for a full sample of lens systems used for time-delay cosmography and.

The required population-level description of priors, in particular of parameters that can not be constrained to high precision (overcoming the prior in the analysis) do also need to take accurately into account potential differences among subsets of the population. For example, different lens discovery channels might preferentially select a different lens and line-of-sight population.

8 Future constraints from galaxy clusters

To date, galaxy-scale lenses have dominated the literature on H_0 determination in the number of measurements and precision. Soon we may expect competitive constraints from galaxy clusters in measuring H_0 and other cosmological quantities. Massive clusters are rich in multiple images and have definite advantages over individual galaxies. The main one is that sources at multiple redshifts break the mass-sheet or steepness degeneracy (e.g., Bradač et al., 2004), which is the main degeneracy and hence source of uncertainty affecting galaxy-scale determination of H_0 (see also Section 5). Being extended on the sky, clusters are also more likely to have supernovae as background sources, whose time delays are relatively easily determined to a few percent precision, rivalling time-delay determinations from quasar sources in galaxy-scale lenses, but without the need for years of monitoring campaigns to obtain lightcurves. The drawback of clusters is that their mass distributions are more complex: they are dynamically younger than galaxies, and their multiple image regions sample a much larger fraction of the clusters' virial radius than in galaxies. Therefore the multiple image region of clusters is expected to be more abundant in substructure, and hence harder to model. These difficulties can be circumvented if there are few or several hundred multiple images, then H_0 can be estimated to a 1-few % precision (Ghosh et al., 2020). At present, in a cluster lens like MACS 1149, one can estimate H_0 to 6%, assuming a conservative 3% uncertainty on the observed time delay (Grillo et al., 2018).

The first cluster lens to produce a precise estimate of H_0 will likely be MACS 1149, where the first confirmed multiply imaged supernova was observed a few years ago (Kelly et al., 2015). The long time delay before the reappearance of the last arriving image—saddle in the arrival time surface of the cluster—allowed the lensing community to make model predictions for the time of the reappearance. Most models agreed reasonably well on 250-350 day delay (Kelly et al., 2016; Treu et al., 2016). These are encouraging findings.

9 Current status and results

The independent analysis of six lensed quasar systems (Suyu et al., 2010, 2013; Wong et al., 2017; Bonvin et al., 2017; Birrer et al., 2019; Chen et al., 2019; Rusu et al., 2020) by the H0LiCOW collaboration (Suyu et al., 2017) inferred a Hubble constant value of $H_0 = 73.3^{+1.7}_{-1.8} \text{ km s}^{-1} \text{ Mpc}^{-1}$. This measurement uses parametric forms of the mass density profile of the deflector, either described as a power-law or stars (constant mass-to-light ratio) plus dark matter halos following an NFW (Navarro et al., 1997) profile with priors on the mass and concentration of the halo reflecting the population of haloes in N-body simulations (Wong et al., 2020). The H0LiCOW result is a 2% precision measurement on H_0 , in excellent agreement with the local distance ladder measurement by the SH0ES team (Riess et al., 2019, 2021). Moreover, the H0LiCOW measurement is in more than 3σ statistical tension with early-Universe probes (e.g., Planck Collaboration et al., 2020; Aiola et al., 2020). An additional lens analyzed by the STRIDES collaboration with the same mass profile assumptions as the H0LiCOW collaboration further provided the most precise single-lens measurement of $H_0 = 74.2^{+2.7}_{-3.0} \text{ km s}^{-1} \text{ Mpc}^{-1}$ (Shajib et al., 2020). In summary, if the mass density profiles of the H0LiCOW and STRIDES lenses are well described by a power-law or a baryonic component with a constant mass-to-light ratio plus dark matter profiles from standard N-body dark matter only simulations, and under the assumption that the covariance are negligible, the tension is significant from the strong lensing measurements alone, and corroborating other measurements (e.g., Riess et al., 2021).

Given that incompatibilities between the local value of H_0 and the Λ CDM model extrapolated H_0 inference from the CMB or other early-universe physics anchored inherently break the standard model of cosmology and likely may require new physics, several groups, including H0LiCOW, STRIDES and SHARP, now TDCOSMO collaboration, are investigating potential systematics in the H_0 measurements.

The TDCOSMO collaboration found, combining six lenses from H0LiCOW, SHARP and STRIDES, that the results when assuming that all lenses are either of one or the other previously assumed forms of the mass density profile are in good agreement with each other when measuring H_0 . The good agreement in the H_0 results between power-law and composite profiles was interpreted by Millon et al. (2020b) as a consequence of the ‘bulge-halo conspiracy’ that the combined baryonic and dark matter density components form a power-law profile (e.g., Koopmans et al., 2006, 2009; van de Ven et al., 2009). Denzel et al. (2021) analyzed 8 quadruply imaged quasars with a free-form modeling approach and obtained $H_0 = 71.8^{+3.9}_{-3.3} \text{ km s}^{-1} \text{ Mpc}^{-1}$. Gilman et al. (2020) investigated the effect of unaccounted for subhalos and small undetected line-of-sight halos in the uncertainty budget and

found insignificant residual uncertainties to mitigate the tension of the measurements with the CMB and large scale structure probes. Van de Vyvere et al. (2022b,a) showed that a variety of expected azimuthal structures in the mass distribution (i.e. multipoles, twists and ellipticity gradients) should leave H_0 unaffected at the population level unless there are specific selection effect in the galaxy population.

The attention further turned to assessing and relaxing the radial profile assumption (see Section 5.2), as well as the introduction of population priors for parameters that cannot be constrained on a lens-by-lens basis for a covariant treatment of their uncertainties. Birrer et al. (2020) addressed the radial profile assumption by choosing a parametrization of the radial mass density profile that is maximally degenerate with H_0 , via the MST. This is the most explicit and direct way addressing the MST effect on the time-delay cosmographic analysis. With this more flexible parametrization, H_0 is only constrained if the measured time delays and imaging data are supplemented by stellar kinematics. Applying this extremely conservative choice to the TDCOSMO sample of 7 lenses increases the uncertainty on H_0 from 2% to 8% resulting in $H_0 = 74.5^{+5.6}_{-6.1} \text{ km s}^{-1} \text{ Mpc}^{-1}$, without changing the mean inferred value significantly.

Birrer et al. (2020) further introduced a hierarchical framework (see also Section 7.2) in which external datasets can be combined with the time-delay lenses to improve the precision, in particular on the MST parameter of the population, and hence on H_0 . They achieved a 5% precision measurement on H_0 by combining the TDCOSMO lenses with imaging modeling and stellar kinematic measurements of a sample of lenses from the Sloan Lens ACS (SLACS) survey with no time-delay information (Bolton et al., 2008; Auger et al., 2009; Shajib et al., 2021) and measured $H_0 = 67.4^{+4.1}_{-3.2} \text{ km s}^{-1} \text{ Mpc}^{-1}$. The mean of the TDCOSMO+SLACS measurement is offset with respect to the TDCOSMO-only value, effectively matching the CMB inferred value, although still statistically consistent with previous assumptions given the uncertainties in the measurement. The Birrer et al. (2020) measurements with and without the SLACS dataset added are in statistical agreement with each other and with the earlier H0LiCOW/ SHARP/ STRIDES measurements based on the radial mass profile assumptions. The result by Birrer et al. (2020) is also consistent, with the work by Shajib et al. (2021) studying more flexible mass density profiles and mass-to-light gradients. The studies by Birrer et al. (2020) and Shajib et al. (2021) share the same measurements for the SLACS lenses and the consistency is implied by construction. Shajib et al. (2021) concluded that NFW+stars, when using wider priors on mass and concentration than earlier H0LiCOW/ SHARP/ STRIDES measurements, is a sufficiently accurate description of the mass density profile of the SLACS lenses. However, a larger flexibility in the mass-concentration relation on the population level and small de-

partures from those radial forms are allowed by the data, resulting in the uncertainties reflected by the Birrer et al. (2020) analysis. The shift in the mean in H_0 when adding the SLACS lenses could be real or it could be due to an intrinsic difference between the deflector population in the TDCOSMO and SLACS samples. Differences in the deflectioners might arise from unequal selection effects. For example, the two samples are well matched in stellar velocity dispersion (total mass), but they differ in redshift. Potentially unaccounted for evolutionary trend in the mass profiles could bias the results when adding samples of lenses at different redshift. Another example is that the TDCOSMO sample is source selected, meaning the main characteristics for the data set to be discovered and selected are properties of the source as seen when lensed, and composed mostly of quadruply imaged quasars, while the SLACS sample is deflector selected, meaning the primary criteria for the selection arises from properties of the deflector irrespective of the source and its geometric lensing effect, and dominated by doubly imaged galaxies.

10 Outlook in the (near) future

The goal of time-delay cosmography is to provide a robust measurement of the Hubble constant to 1% precision to decisively tell the outcome of the currently observed tension between late and early time measurements of H_0 . In the previous Section 9 we presented current results. In this section, we discuss the potential of the time-delay method in the near future. First, we describe the data and instrumentation which enable us to push ahead (Section 10.1). Second, we will highlight avenues where continuing work is required in assessing the methodology to maintain accuracy while increasing the precision of the measurements (Section 10.2). Finally, we leave some concluding remarks about the prospects of time-delay cosmography in Section 10.3.

10.1 Future data

We expect there to be several 10'000 galaxy-galaxy lenses, several hundred quadruply lensed quasars and more than a thousand doubly lensed quasars on the full sky (e.g., Oguri and Marshall, 2010; Collett, 2015). With the upcoming large area (wide) and sensitive to faint objects (deep) ground- and space-based surveys, such as the Vera C. Rubin Observatory, Roman Observatory, and Euclid, we expect many of those lenses to be discovered within a decade. Compared to the current analyses conducted on few lenses (e.g., 7 lenses in case of current TDCOSMO results), this is an e-folding of the number of lenses possibly suitable for time-delay analyses. The sheer number of lenses will transform the measurements and new approaches are going to be required in the

domain of time-delay cosmography to efficiently and accurately make use of all the data available.

The first step in utilizing these lenses present on the sky is to discover them in the large data sets. We refer to McMahon et al. (in preparation) for an extensive review of techniques, recent successes and an outlook in the searches and discovery of strong lenses. The next step is to acquire all the necessary follow-up data products to conduct accurate and precise cosmographic analyses (see Section 3 and subsequent sections). The data products range from monitoring data for a time-delay measurements, high-resolution imaging, to spectroscopic information about the source and lens redshift as well as velocity dispersion of the deflector. This step is very resource expensive and there are going to be challenges in how to allocate these limited resources. Decisions will have to be made which lenses being excessively followed-up. We comment in Section 10.2 about developments of methodology that can deal with less constraining or incomplete data for a larger lensing data set. Some lenses might require less substantial monitoring follow-up in case where LSST light curves are good enough for a time-delay measurement (Liao et al., 2015b). Some lenses may also automatically obtain high-resolution and sufficiently high signal-to-noise ratio imaging data from wide field space surveys, such as Euclid or Roman. To what extent specific to be acquired data products impact the precision on H_0 is key to assess the need for allocating follow-up resources and on which lenses to spend it. Besides the limited resources, follow-up decisions are currently also impacted by the accessible to adaptive optics (AO) coverage for ground based large-diameter telescopes. With the next-generation AO instrumentation and their commissioning on both hemispheres, we expect a full sky accessibility that allows the community technically to target every single gravitational lens on the sky.

The dominant uncertainty in the current measurement of the Hubble constant with time-delay cosmography is attributed to uncertainties in the mass profiles of the main deflector galaxies (see e.g., Section 5.2). There are multiple independent avenues available in the near future to approach a 1% measurement of H_0 with different data sets. We will focus on these pathways with improved instrumentation and increased data sets in this section.

Spatially resolved stellar kinematics of the deflector galaxy (see Section 5.3 for details on methodology) with the next generation space (James Webb Space Telescope; JWST) and ground-based (extremely large telescopes; E-ELT, GMT, TMT) instruments provide precise measurements of the kinematics of stars. Such two-dimensional observations of the kinematics, paired with the lensing measurements, have the ability to break the mass-anisotropy degeneracy, a currently limiting systematic when interpreting and de-projecting integrated kinematic measurements to measure the three-dimensional

gravitational potential. Birrer and Treu (2021) forecasts, based on the methods and assumptions used by Birrer et al. (2020) without relying on mass-density profile assumptions to break the MST, that with 40 time-delay lenses with exquisite spatially resolved kinematics, a 1.5% precision on H_0 can be achieved (Figure 11 left graphic), and see also e.g. Yıldırım et al. (2020, 2021). Such a strategy with exquisite data on the sample of time-delay lenses is one way to make progress. Another approach is to infer the mass density profile properties from a larger set of non-time-delay lenses and apply the constraints on the mass density profile and stellar anisotropy distribution on the time-delay lenses (Birrer et al., 2020; Birrer and Treu, 2021; Gomer et al., 2022). In particular, resolved spectroscopy can also be employed on non-time delay lenses without bright and contaminating quasar images, either as prior constraints or by directly incorporating into a hierarchical analysis, to further improve the kinematic measurement precision.

Standardizable magnifications with gravitationally lensed supernovae (gLSNe) provide another promising avenue to constrain the mass density profiles and open up an avenue for a percent measurement of H_0 in the near future with the onset of LSST. Birrer et al. (2021) (Figure 11 right panel) provides a forecast with gLSNe in constraining H_0 independently of stellar kinematics. They conclude that the standardizable nature of gLSNe of type Ia enables a 1.5% H_0 measurement with a 10 years LSST survey. This forecast is contingent to a near-optimal discovery and follow-up effort of gLSNe. We refer to Suyu et al. (in preparation) for a detailed review and in-depth discussion on the discovery, expected number of gLSNe, the challenges of following them up and the caveats of micro-lensing.

Another method is to make use of the statistical distribution of images under the assumption of knowing the distribution of sources in the source plane with a statistical combination of a large sample of time-delay lenses, relying purely on strong lensing data (Sonnenfeld, 2021b).

10.2 Methodology improvements

With the expected wealth of data and the increase in the number of time-delay and non-time-delay lenses, the prospect of measuring H_0 to 1% precision can become a reality. The employed methodology and assumptions must keep up to provide the accuracy requirement. In the following we discuss methodology improvements and validations in the domain of galaxy density profiles (Section 10.2.1), assumption in the interpretation of non-lensing constraints (Section 10.2.2), selection effects (Section 10.2.3), automatization (Section 10.2.4) and general aspects of methodology verification (Section 10.2.5). These sections are not meant to be complete but to provide guidance in the near future on where focused effort is required.

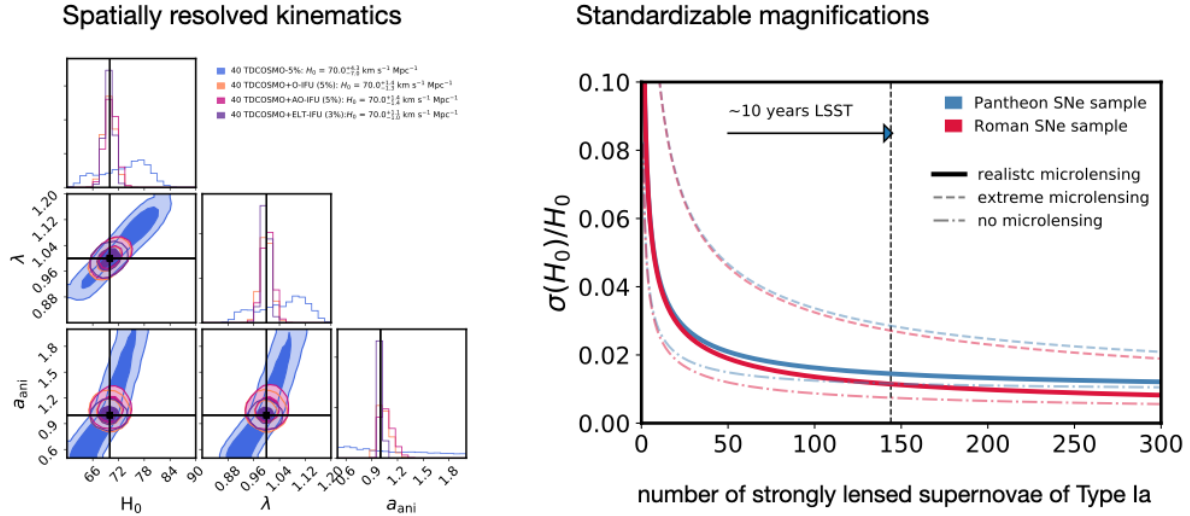


Fig. 11 Forecast for H_0 measurements in the near future with the upcoming facilities. Left: Spatially resolved kinematics measurements of a sample of 40 time-delay lenses enable a precision on H_0 of 1.5% JWST (Figure adopted from Birrer and Treu (2021)). Right: Lensed supernovae with standardizable magnification measurements. An expected yield of ~ 144 gravitationally lensed supernovae over the span of the 10 years LSST survey enable a precision on H_0 of 1.5% (Figure adopted from Birrer et al. (2021)). Both approaches, stellar kinematics and standardized magnifications, do provide independent observational constraints on the MST with different systematics.

10.2.1 Galaxy density profiles

The currently employed model mitigating the MST effect by Birrer et al. (2020) is parameterized with a pure MST parameter λ . This parameterization is foremost of mathematical nature and leaves the physical interpretation (e.g., Blum et al., 2020) ambiguous. A pure MST parameterization may in certain regimes even become unphysical, e.g. resulting in total mass profiles with negative density in the outskirts⁷. Such a one-parameter extension to previously considered more simple and rigid mass profiles may also not encompass the necessary flexibility beyond the pure MST that can affect kinematics observations (e.g., Birrer et al., 2020; Yıldırım et al., 2021), or to deal with more generalized forms of lensing degeneracies, such as the SPT. To make progress, the full degeneracy inherent in gravitational lensing needs to be folded into flexible, but physically motivated, mass profile parameters. Such an approach was explored by (Shajib et al., 2021) constraining the extended mass density profiles of the SLACS galaxy-galaxy lenses, but has not yet been employed for time-delay cosmography. Quasar microlensing studies might also help to constrain the stellar mass to light ratio in massive elliptical galaxies. Ambitious measurements below the 10% level might additionally help to constrain the mass density profiles and would allow the focus on the dark matter portion of the profile. We refer to Vernardos et al. (in prepration) for techniques and prospects of this methodology.

⁷ Projected lensing convergence can come slightly negative to the extent that the physical mass drops below the mean background density.

10.2.2 Non-lensing constraints

Significant constraints on the MST, and in general mass density profiles, are expected to come from non-lensing observables. These measurements, as well as their model interpretation, need to be tested to the percent level. For example, for the kinematic measurements, the impact of stellar template fitting needs to be further assessed and validated. For the interpretation of the measurements, de-projection assumptions, rotational structure, as well as stellar anisotropy need to be rigorously tested and assessed for covariant systematics on the population level. For upcoming magnification measurements with gISNe, micro- and milli-lensing effects need to be assessed and incorporated into the model self-consistently. Furthermore, more knowledge about the structure and size of the variable quasar accretion disc are required to determine the strength of the micro-lensing time delay effect.

10.2.3 Selection effects

The phenomena of strong gravitational lensing is inherently a very specific selection effect of an otherwise mostly weak lensing field. Quantifying the selection effect of where and in what form strong lensing phenomena occur is going to be crucial requirement to maintain accuracy when increasing precision on H_0 in the years to come. The strong lensing phenomena is impacted by both, the nature of line-of-sight structure and the main deflector. For the line-of-sight structure, the convergence either raises or lowers the lensing efficiency of an equal mass galaxy to act as a strong

lensing deflector, and the cosmic shear changes the geometry of the caustic structure, making it more likely to have quadruply imaged sources. Similarly, for the main deflector, more concentrated mass distribution, or favorable projections along the line of sight, lead to higher lensing efficiencies, and more elliptical mass profiles (also in projection) lead to a more extended inner caustic region. Including the differential selection effects among different samples of lenses, for example, quadruply lensed quasars are visible only when the source quasar lies within the diamond caustic of the lensing galaxy. This condition creates a Malmquist-like selection effect in the population of observed quadruply lensed quasars, increasing the true caustic area (Baldwin and Schechter, 2021).

Many of these effects are hard or near-impossible to quantify on a lens-by-lens basis. These selection effects need to be modeled and inferred on the population level, including making sure relative selection effects between different sub-populations are being understood. Collett and Cunningham (2016) simulated a sample of double- and quadruple-image systems and when assuming reasonable thresholds on image separation and flux, based on current lens monitoring campaigns, they found that the typical density profile slopes of monitorable lenses are significantly shallower than the input ensemble.

There are two distinct and complementary approaches to understand and mitigate selection effects in the analysis. First, one can attempt to understand the selection from first principle which then can be used to explicitly account for in the analysis procedure. This approach requires extensive simulations including all relevant aspects, starting from the full sky a priori abundance and population of phenomena and a reproducible selection function of the discovery channel and follow-up decision being made to either include a lens in the sample or not. Second, one can empirically determine a relative selection function by comparing a set of observables of a sample of lenses compared to random galaxies or sight lines on the sky. Deviations on the set of observables on the population level indicate then the level of selection bias in the sample. Observables may include, but are not restricted to, central velocity dispersion, stellar mass, size and morphology of the deflector, number of subhaloes and line-of-sight projected galaxies nearby, redshift of the deflector, among others. Deviations from established scaling relations among the galaxy properties are then indications of selection biases. We refer to Section 6 for data and approaches to quantify line of sight effects. We also stress that these techniques rely on underlying priors and model assumption on the population bias and an explicit de-biasing is required to constrain hierarchically unknown selection effects (see e.g., Park). Currently, neither of the two approaches have been successfully applied.

With the expected large number of lenses in the next few years of the mid 2020s, and the more uniform data set of large and deep surveys, both, the theoretical forward modeling and the empirical hierarchical modeling, will become feasible. We also advocate for analyses to take into account the specific discovery channel of the lenses when performing population level inferences. Understanding the selection function may or may not imply to effectively re-discover the lenses in the analysis to guarantee a uniform and reproducible selection and analysis.

10.2.4 Automatization

Current state-of-the-art analyses of single lens systems takes up more than a year of work, with the involvement of many people, as well as several hundred of thousands of CPU hours of computational cost. To utilize the upcoming larger lens samples and to achieve a high-precision H_0 measurement, the time to analyse a single system has to be reduced significantly. Automated decision-making and model choices (e.g., Schmidt et al., 2022; Ertl et al., 2022), as well as GPU assisted computations (e.g., Gu et al., 2022) hold promises in these regards. Moreover, analyses have to be able to be repeated with modifications to test for assumptions covariant among all lenses multiple times. The faster the entire analysis runs, the more explorations of potential systematics in the choices can be executed. The challenge in finding uniform analyses choices are that every lens is different from another and particularities have been noticed that needed special attention for lenses on the individual basis. The analyses conducted need to be uniform in their choices and approaches such that impacts on assumptions can be tested on the ensemble level. Uniformity of analyses can also reduce human errors and sets the analyses on quantifiable priors.

There is currently an effort in homogenizing the analysis procedure, for both time-delay lenses (Shajib et al., 2019; Schmidt et al., 2022; Ertl et al., 2022) and non-time delay lenses (Shajib et al., 2021) and further effort is underway. In parallel, alternative methodology in the modeling and posterior inference are being explored with machine learning techniques, which have the potential to speed up the analysis by orders of magnitude (e.g., Park et al., 2021)

10.2.5 Methodology verification

Guaranteeing accuracy with ever more precise measurements is a challenge throughout the cosmological community. High-precision measurements of quantities to relevance of fundamental physics is a relatively new field and we dedicate a separate subsection highlighting different strategies to verify the methodology and to perform to the necessary quality standard to maintain accuracy.

- Realistic simulations offer a validation of a methodology on a known truth (see e.g., Xu et al., 2016; Tagore et al., 2018). It is important that the complexity in the simulations are realistic to explore avenues of potential systematics and gain a deep understanding of what data products are able to constrain what aspects of the model. Simulations eventually need to encompass all aspects of the analysis, including the selection effect and the entire line-of-sight structure within the full cosmological and astrophysical context.
- Data modeling challenges, such as the Time-Delay Challenge (Liao et al., 2015a) and the Time-Delay Lens Modeling Challenge (Ding et al., 2021) offer platforms to validate currently employed methodology on mock data sets, explore new ways of analyzing the data and can provide a transparent overview of the current state of the field.
- Blind analyses prevent experimenter bias. The analysis should be guided by the assessment of uncertainties regardless of the anticipated result. Blind analyses have regularly been performed by the H0LiCOW and TD-COSMO collaborations.
- Open source accessibility of the raw data, processed data product, analysis software and entire end-to-end analysis pipelines can best guarantee reproducibility, form community trust and provides access to the community to alter and improve existing methodology.

10.3 Concluding remarks

Time-delay cosmography has an exciting time ahead. The method has come along way since its original proposal by Refsdal (1964). Current measurements of the Hubble constant with time-delay cosmography are at the few percent level, enabled by detailed analyses and precise measurements of different aspects of the analysis. With the expected increase in the lensing sample and the advances in instrumentation, the path towards a percent precision measurement of H_0 becomes in reach.

Measuring the Hubble constant to percent level precision is a challenging endeavor, regardless of the cosmological probe. In this manuscript, we aimed to provide a detailed account of the methodology and measurements to provide guidance to achieve a precise and accurate measurement of H_0 at the one-percent level. We emphasized the challenges and systematics in the different components of the analysis and strategies to mitigate them. Above all, in Carl Sagan's words: "Extraordinary claims require extraordinary evidence".

Acknowledgements We thank the International Space Science Institute in Bern (ISSI) for their hospitality and the conveners for organizing the stimulating workshop on "Strong Gravitational Lensing". We

thank Liliya Williams for contributions to Section 8 and useful comments and Paul Schechter for useful comments in the preparation of the manuscript. SB is partially supported by the Kavli Foundation. MM acknowledges support by the SNSF through grant P500PT_203114 and funding from the European Research Council (ERC) under the European Union's Horizon 2020 research and innovation programme (COSMICLENS : grant agreement No 787886). AJS is supported by NASA through the NASA Hubble Fellowship grant HST-HF2-51492 by the Space Telescope Science Institute, which is operated by the Association of Universities for Research in Astronomy, Inc., for NASA, under contract NAS5-26555. FC and DS acknowledge funding from the European Research Council (ERC) under the European Union's Horizon 2020 research and innovation programme (COSMICLENS : grant agreement No 787886). SHS thanks the Max Planck Society for support through the Max Planck Research Group. This research is supported in part by the Excellence Cluster ORIGINS which is funded by the Deutsche Forschungsgemeinschaft (DFG, German Research Foundation) under Germany's Excellence Strategy – EXC-2094 – 390783311. TT acknowledges support by the National Science Foundation through grants AST-1906976 and AST-15436, by NASA through grants HST-GO-15652, and by the Gordon and Betty Moore Foundation through grant 8548.

References

- A. Aghamousa, A. Shafieloo, Fast and Reliable Time Delay Estimation of Strong Lens Systems Using the Smoothing and Cross-correlation Methods. *Astrophys. J.* **804**(1), 39 (2015). doi:10.1088/0004-637X/804/1/39
- S. Aiola, E. Calabrese, L. Maurin, S. Naess, B.L. Schmitt, M.H. Abitbol, G.E. Addison, P.A.R. Ade, D. Alonso, M. Amiri, S. Amodeo, E. Angile, J.E. Austermann, T. Baidon, N. Battaglia, J.A. Beall, R. Bean, D.T. Becker, J.R. Bond, S.M. Bruno, V. Calafut, L.E. Campusano, F. Carrero, G.E. Chesmore, H.-m. Cho, S.K. Choi, S.E. Clark, N.F. Cothard, D. Crichton, K.T. Crowley, O. Darwish, R. Datta, E.V. Denison, M.J. Devlin, C.J. Duell, S.M. Duff, A.J. Duivenvoorden, J. Dunkley, R. Dünner, T. Essinger-Hileman, M. Fankhanel, S. Ferraro, A.E. Fox, B. Fuzia, P.A. Gallardo, V. Glusevic, J.E. Golec, E. Grace, M. Gralla, Y. Guan, K. Hall, M. Halpern, D. Han, P. Hargrave, M. Hasselfield, J.M. Helton, S. Henderson, B. Hensley, J.C. Hill, G.C. Hilton, M. Hilton, A.D. Hincks, R. Hložek, S.-P.P. Ho, J. Hubmayr, K.M. Huffenberger, J.P. Hughes, L. Infante, K. Irwin, R. Jackson, J. Klein, K. Knowles, B. Koopman, A. Kosowsky, V. Lakey, D. Li, Y. Li, Z. Li, M. Lokken, T. Louis, M. Lungu, A. MacInnis, M. Madhavacheril, F. Maldonado, M. Mallaby-Kay, D. Marsden, J. McMahon, F. Menanteau, K. Moodley, T. Morton, T. Namikawa, F. Nati, L. Newburgh, J.P. Nibarger, A. Nicola, M.D. Niemack, M.R. Nolte, J. Orłowski-Sherer, L.A. Page, C.G. Pappas, B. Partridge, P. Phakathi, G. Pisano, H. Prince, R. Puddu, F.J. Qu, J. Rivera, N. Robertson, F. Rojas, M. Salatino, E. Schaan, A. Schillaci, N. Sehgal, B.D. Sherwin, C. Sierra, J. Sievers, C. Sifon, P. Sikhosana, S. Simon, D.N. Spergel, S.T. Staggs, J. Stevens, E. Storer, D.D. Sunder,

- E.R. Switzer, B. Thorne, R. Thornton, H. Trac, J. Treu, C. Tucker, L.R. Vale, A. Van Engelen, J. Van Lanen, E.M. Vavagiakis, K. Wagoner, Y. Wang, J.T. Ward, E.J. Wollack, Z. Xu, F. Zago, N. Zhu, The Atacama Cosmology Telescope: DR4 maps and cosmological parameters. *J. of Cosm. and Astroparticle Phys.* **2020**(12), 047 (2020). doi:10.1088/1475-7516/2020/12/047
- N. Arendse, A. Agnello, R.J. Wojtak, Low-redshift measurement of the sound horizon through gravitational time-delays. *Astron. Astrophys.* **632**, 91 (2019). doi:10.1051/0004-6361/201935972
- M.W. Auger, C.D. Fassnacht, A.L. Abrahamse, L.M. Lubin, G.K. Squires, The Gravitational Lens-Galaxy Group Connection. II. Groups Associated with B2319+051 and B1600+434. *Astron. J.* **134**(2), 668–679 (2007). doi:10.1086/519238
- M.W. Auger, T. Treu, A.S. Bolton, R. Gavazzi, L.V.E. Koopmans, P.J. Marshall, K. Bundy, L.A. Moustakas, The Sloan Lens ACS Survey. IX. Colors, Lensing, and Stellar Masses of Early-Type Galaxies. *Astrophys. J.* **705**(2), 1099–1115 (2009). doi:10.1088/0004-637X/705/2/1099
- M.W. Auger, T. Treu, A.S. Bolton, R. Gavazzi, L.V.E. Koopmans, P.J. Marshall, L.A. Moustakas, S. Burles, The sloan lens acs survey. x. stellar, dynamical, and total mass correlations of massive early-type galaxies. *Astrophys. J.* **724**, 511–525 (2010). doi:10.1088/0004-637X/724/1/511
- S. Bag, A. Shafieloo, K. Liao, T. Treu, Identifying lensed quasars and measuring their time-delays from unresolved light curves. *arXiv e-prints*, 2110–15315 (2021)
- D. Baldwin, P.L. Schechter, A Malmquist-like bias in the inferred areas of diamond caustics and the resulting bias in inferred time delays for gravitationally lensed quasars. *arXiv e-prints*, 2110–06378 (2021)
- M. Barnabè, O. Czoske, L.V.E. Koopmans, T. Treu, A.S. Bolton, Two-dimensional kinematics of SLACS lenses - III. Mass structure and dynamics of early-type lens galaxies beyond $z = 0.1$. *Mon. Notices of the Royal Astron. Soc.* **415**(3), 2215–2232 (2011). doi:10.1111/j.1365-2966.2011.18842.x
- M. Barnabè, A.A. Dutton, P.J. Marshall, M.W. Auger, B.J. Brewer, T. Treu, A.S. Bolton, D.C. Koo, L.V.E. Koopmans, The SWELLS survey - IV. Precision measurements of the stellar and dark matter distributions in a spiral lens galaxy. *Mon. Notices of the Royal Astron. Soc.* **423**(2), 1073–1088 (2012). doi:10.1111/j.1365-2966.2012.20934.x
- A. Barnacka, J.-F. Glicenstein, Y. Moudden, First evidence of a gravitational lensing-induced echo in gamma rays with Fermi LAT. *Astron. Astrophys.* **528**, 3 (2011). doi:10.1051/0004-6361/201016175
- L. Biggio, A. Domi, S. Tosi, G. Vernardos, D. Ricci, L. Paganin, G. Bracco, Time delay estimation in unresolved lensed quasars. *arXiv e-prints*, 2110–01012 (2021)
- A.D. Biggs, I.W.A. Browne, P. Helbig, L.V.E. Koopmans, P.N. Wilkinson, R.A. Perley, Time delay for the gravitational lens system B0218+357. *Mon. Notices of the Royal Astron. Soc.* **304**(2), 349–358 (1999). doi:10.1046/j.1365-8711.1999.02309.x
- J. Binney, G.A. Mamon, M/L and velocity anisotropy from observations of spherical galaxies, of must M 87 have a massive black hole ? *Mon. Notices of the Royal Astron. Soc.* **200**, 361–375 (1982). doi:10.1093/mnras/200.2.361
- J. Binney, S. Tremaine, *Galactic Dynamics: Second Edition* 2008
- S. Birrer, T. Treu, C.E. Rusu, V. Bonvin, C.D. Fassnacht, J.H.H. Chan, A. Agnello, A.J. Shajib, G.C.-F. Chen, M. Auger, F. Courbin, S. Hilbert, D. Sluse, S.H. Suyu, K.C. Wong, P. Marshall, B.C. Lemaux, G. Meylan, H0LiCOW - IX. Cosmographic analysis of the doubly imaged quasar SDSS 1206+4332 and a new measurement of the Hubble constant. *Mon. Notices of the Royal Astron. Soc.* **484**(4), 4726–4753 (2019). doi:10.1093/mnras/stz200
- S. Birrer, A.J. Shajib, A. Galan, M. Millon, T. Treu, A. Agnello, M. Auger, G.C.-F. Chen, L. Christensen, T. Collett, F. Courbin, C.D. Fassnacht, L.V.E. Koopmans, P.J. Marshall, J.-W. Park, C.E. Rusu, D. Sluse, C. Spiniello, S.H. Suyu, S. Wagner-Carena, K.C. Wong, M. Barnabè, A.S. Bolton, O. Czoske, X. Ding, J.A. Frieman, L. Van de Vyvere, TDCOSMO. IV. Hierarchical time-delay cosmography – joint inference of the Hubble constant and galaxy density profiles. *Astron. Astrophys.* **643**, 165 (2020). doi:10.1051/0004-6361/202038861
- S. Birrer, Gravitational Lensing Formalism in a Curved Arc Basis: A Continuous Description of Observables and Degeneracies from the Weak to the Strong Lensing Regime. *Astrophys. J.* **919**(1), 38 (2021). doi:10.3847/1538-4357/ac1108
- S. Birrer, A. Amara, lenstronomy: Multi-purpose gravitational lens modelling software package. *Physics of the Dark Universe* **22**, 189–201 (2018). doi:10.1016/j.dark.2018.11.002
- S. Birrer, T. Treu, Astrometric requirements for strong lensing time-delay cosmography. *Mon. Notices of the Royal Astron. Soc.* **489**(2), 2097–2103 (2019). doi:10.1093/mnras/stz2254
- S. Birrer, T. Treu, TDCOSMO. V. Strategies for precise and accurate measurements of the Hubble constant with strong lensing. *Astron. Astrophys.* **649**, 61 (2021). doi:10.1051/0004-6361/202039179
- S. Birrer, A. Amara, A. Refregier, Gravitational Lens Modeling with Basis Sets. *Astrophys. J.* **813**(2), 102 (2015). doi:10.1088/0004-637X/813/2/102
- S. Birrer, A. Amara, A. Refregier, The mass-sheet degeneracy and time-delay cosmography: analysis of the strong lens RXJ1131-1231. *J. of Cosm. and Astroparticle Phys.* **2016**(8), 020 (2016). doi:10.1088/1475-

- 7516/2016/08/020
- S. Birrer, S. Dhawan, A.J. Shajib, The Hubble constant from strongly lensed supernovae with standardizable magnifications. *arXiv e-prints*, 2107–12385 (2021)
- S. Birrer, C. Welschen, A. Amara, A. Refregier, Line-of-sight effects in strong lensing: putting theory into practice. *J. of Cosm. and Astroparticle Phys.* **2017**(4), 049 (2017). doi:10.1088/1475-7516/2017/04/049
- J.A. Blackburne, C.S. Kochanek, The Effect of a Time-varying Accretion Disk Size on Quasar Microlensing Light Curves. *Astrophys. J.* **718**(2), 1079–1084 (2010). doi:10.1088/0004-637X/718/2/1079
- R. Blandford, R. Narayan, Fermat's Principle, Caustics, and the Classification of Gravitational Lens Images. *Astrophys. J.* **310**, 568 (1986). doi:10.1086/164709
- K. Blum, E. Castorina, M. Simonović, Could Quasar Lensing Time Delays Hint to a Core Component in Halos, Instead of H_0 Tension? *Astrophys. J. Letters* **892**(2), 27 (2020). doi:10.3847/2041-8213/ab8012
- A.S. Bolton, S. Burles, L.V.E. Koopmans, T. Treu, R. Gavazzi, L.A. Moustakas, R. Wayth, D.J. Schlegel, The Sloan Lens ACS Survey. V. The Full ACS Strong-Lens Sample. *Astrophys. J.* **682**(2), 964–984 (2008). doi:10.1086/589327
- V. Bonvin, M. Tewes, F. Courbin, T. Kuntzer, D. Sluse, G. Meylan, COSMOGRAIL: the COSmological MONitoring of GRAVItational Lenses. XV. Assessing the achievability and precision of time-delay measurements. *Astron. Astrophys.* **585**, 88 (2016). doi:10.1051/0004-6361/201526704
- V. Bonvin, F. Courbin, S.H. Suyu, P.J. Marshall, C.E. Rusu, D. Sluse, M. Tewes, K.C. Wong, T. Collett, C.D. Fassnacht, T. Treu, M.W. Auger, S. Hilbert, L.V.E. Koopmans, G. Meylan, N. Rumbaugh, A. Sonnenfeld, C. Spiniello, H0LiCOW - V. New COSMOGRAIL time delays of HE 0435-1223: H_0 to 3.8 per cent precision from strong lensing in a flat Λ CDM model. *Mon. Notices of the Royal Astron. Soc.* **465**(4), 4914–4930 (2017). doi:10.1093/mnras/stw3006
- V. Bonvin, M. Millon, J.H.-H. Chan, F. Courbin, C.E. Rusu, D. Sluse, S.H. Suyu, K.C. Wong, C.D. Fassnacht, P.J. Marshall, T. Treu, E. Buckley-Geer, J. Frieman, A. Hempel, S. Kim, R. Lachaume, M. Rabus, D.C.-Y. Chao, M. Chijani, D. Gilman, K. Gilmore, K. Rojas, P. Williams, T. Anguita, C.S. Kochanek, C. Morgan, V. Motta, M. Tewes, G. Meylan, COSMOGRAIL. XVIII. time delays of the quadruply lensed quasar WFI2033-4723. *Astron. Astrophys.* **629**, 97 (2019). doi:10.1051/0004-6361/201935921
- M. Bradač, M. Lombardi, P. Schneider, Mass-sheet degeneracy: Fundamental limit on the cluster mass reconstruction from statistical (weak) lensing. *Astron. Astrophys.* **424**, 13–22 (2004). doi:10.1051/0004-6361:20035744
- E.J. Buckley-Geer, H. Lin, C.E. Rusu, J. Poh, A. Palmese, A. Agnello, L. Christensen, J. Frieman, A.J. Shajib, T. Treu, T. Collett, S. Birrer, T. Anguita, C.D. Fassnacht, G. Meylan, S. Mukherjee, K.C. Wong, M. Agüena, S. Allam, S. Avila, E. Bertin, S. Bhargava, D. Brooks, A. Carnero Rosell, M. Carrasco Kind, J. Carretero, F.J. Castander, M. Costanzi, L.N. da Costa, J. De Vicente, S. Desai, H.T. Diehl, P. Doel, T.F. Eifler, S. Everett, B. Flaugher, P. Fosalba, J. García-Bellido, E. Gaztanaga, D. Gruen, R.A. Gruendl, J. Gschwend, G. Gutierrez, S.R. Hinton, K. Honscheid, D.J. James, K. Kuehn, N. Kuropatkin, M.A.G. Maia, J.L. Marshall, P. Melchior, F. Menanteau, R. Miquel, R.L.C. Ogando, F. Paz-Chinchón, A.A. Plazas, E. Sanchez, V. Scarpine, M. Schubnell, S. Serrano, I. Sevilla-Noarbe, M. Smith, M. Soares-Santos, E. Suchyta, M.E.C. Swanson, G. Tarle, D.L. Tucker, T.N. Varga, T.N. Varga, DES Collaboration, STRIDES: Spectroscopic and photometric characterization of the environment and effects of mass along the line of sight to the gravitational lenses DES J0408-5354 and WGD 2038-4008. *Mon. Notices of the Royal Astron. Soc.* **498**(3), 3241–3274 (2020). doi:10.1093/mnras/staa2563
- I. Burud, J. Hjorth, A.O. Jaunsen, M.I. Andersen, H. Korhonen, J.W. Clasen, J. Pelt, F.P. Pijpers, P. Magain, R. Østensen, An Optical Time Delay Estimate for the Double Gravitational Lens System B1600+434. *Astrophys. J.* **544**(1), 117–122 (2000). doi:10.1086/317213
- I. Burud, J. Hjorth, F. Courbin, J.G. Cohen, P. Magain, A.O. Jaunsen, A.A. Kaas, C. Faure, G. Letawe, Time delay and lens redshift for the doubly imaged BAL quasar SBS 1520+530. *Astron. Astrophys.* **391**, 481–486 (2002). doi:10.1051/0004-6361:20020856
- E.M. Cackett, K. Horne, H. Winkler, Testing thermal reprocessing in active galactic nuclei accretion discs. *Mon. Notices of the Royal Astron. Soc.* **380**(2), 669–682 (2007). doi:10.1111/j.1365-2966.2007.12098.x
- J.H.H. Chan, K. Rojas, M. Millon, F. Courbin, V. Bonvin, G. Jauffret, Measuring accretion disk sizes of lensed quasars with microlensing time delay in multi-band light curves. *Astron. Astrophys.* **647**, 115 (2021). doi:10.1051/0004-6361/202038971
- G.C.-F. Chen, S.H. Suyu, K.C. Wong, C.D. Fassnacht, T. Chiueh, A. Halkola, I.S. Hu, M.W. Auger, L.V.E. Koopmans, D.J. Lagattuta, J.P. McKean, S. Vegetti, SHARP - III. First use of adaptive-optics imaging to constrain cosmology with gravitational lens time delays. *Mon. Notices of the Royal Astron. Soc.* **462**(4), 3457–3475 (2016). doi:10.1093/mnras/stw991
- G.C.-F. Chen, J.H.H. Chan, V. Bonvin, C.D. Fassnacht, K. Rojas, M. Millon, F. Courbin, S.H. Suyu, K.C. Wong, D. Sluse, T. Treu, A.J. Shajib, J.-W. Hsueh, D.J. Lagattuta, L.V.E. Koopmans, S. Vegetti, J.P. McKean, Constraining the microlensing effect on time delays with a new time-

- delay prediction model in H_0 measurements. *Mon. Notices of the Royal Astron. Soc.* **481**(1), 1115–1125 (2018). doi:10.1093/mnras/sty2350
- G.C.-F. Chen, C.D. Fassnacht, S.H. Suyu, C.E. Rusu, J.H.H. Chan, K.C. Wong, M.W. Auger, S. Hilbert, V. Bonvin, S. Birrer, M. Millon, L.V.E. Koopmans, D.J. Lagattuta, J.P. McKean, S. Vegetti, F. Courbin, X. Ding, A. Halkola, I. Jee, A.J. Shajib, D. Sluse, A. Sonnenfeld, T. Treu, A SHARP view of H0LiCOW: H_0 from three time-delay gravitational lens systems with adaptive optics imaging. *Mon. Notices of the Royal Astron. Soc.* **490**(2), 1743–1773 (2019). doi:10.1093/mnras/stz2547
- G.C.-F. Chen, T. Treu, C.D. Fassnacht, S. Ragland, T. Schmidt, S.H. Suyu, Point-spread function reconstruction of adaptive-optics imaging: Meeting the astrometric requirements for time-delay cosmography. *arXiv e-prints*, 2106–11060 (2021a)
- G.C.-F. Chen, C.D. Fassnacht, S.H. Suyu, L.V.E. Koopmans, D.J. Lagattuta, J.P. McKean, M.W. Auger, S. Vegetti, T. Treu, SHARP VIII: J0924+0219 lens mass distribution and time-delay prediction through adaptive-optics imaging. *arXiv e-prints*, 2107–10304 (2021b)
- C.C. Cheung, S. Larsson, J.D. Scargle, M.A. Amin, R.D. Blandford, D. Bulmash, J. Chiang, S. Ciprini, R.H.D. Corbet, E.E. Falco, P.J. Marshall, D.L. Wood, M. Ajello, D. Bastieri, A. Chekhtman, F. D’Ammando, M. Giroletti, J.E. Grove, B. Lott, R. Ojha, M. Orienti, J.S. Perkins, M. Razzano, A.W. Smith, D.J. Thompson, K.S. Wood, Fermi Large Area Telescope Detection of Gravitational Lens Delayed γ -Ray Flares from Blazar B0218+357. *Astrrophys. J. Letters* **782**(2), 14 (2014). doi:10.1088/2041-8205/782/2/L14
- J.P. Coles, J.I. Read, P. Saha, Gravitational lens recovery with GLASS: measuring the mass profile and shape of a lens. *Mon. Notices of the Royal Astron. Soc.* **445**(3), 2181–2197 (2014). doi:10.1093/mnras/stu1781
- T.E. Collett, The Population of Galaxy-Galaxy Strong Lenses in Forthcoming Optical Imaging Surveys. *Astrrophys. J.* **811**(1), 20 (2015). doi:10.1088/0004-637X/811/1/20
- T.E. Collett, S.D. Cunningham, Observational selection biases in time-delay strong lensing and their impact on cosmography. *Mon. Notices of the Royal Astron. Soc.* **462**(3), 3255–3264 (2016). doi:10.1093/mnras/stw1856
- T.E. Collett, P.J. Marshall, M.W. Auger, S. Hilbert, S.H. Suyu, Z. Greene, T. Treu, C.D. Fassnacht, L.V.E. Koopmans, M. Bradač, R.D. Blandford, Reconstructing the lensing mass in the Universe from photometric catalogue data. *Mon. Notices of the Royal Astron. Soc.* **432**(1), 679–692 (2013). doi:10.1093/mnras/stt504
- W.N. Colley, R.E. Schild, C. Abajas, D. Alcalde, Z. Aslan, I. Bikmaev, V. Chavushyan, L. Chinarro, J.-P. Cournoyer, R. Crowe, V. Dudinov, A.K.D. Evans, Y.-B. Jeon, L.J. Goicoechea, O. Golbasi, I. Khamitov, K. Kjernsmo, H.J. Lee, J. Lee, K.W. Lee, M.G. Lee, O. Lopez-Cruz, E. Mediavilla, A.F.J. Moffat, R. Mujica, A. Ullan, J. Muñoz, A. Oscoz, M.-G. Park, N. Purves, O. Saanum, N. Sakhibullin, M. Serra-Ricart, I. Sinelnikov, R. Stabell, A. Stockton, J. Teuber, R. Thompson, H.-S. Woo, A. Zheleznyak, Around-the-Clock Observations of the Q0957+561A,B Gravitationally Lensed Quasar. II. Results for the Second Observing Season. *Astrrophys. J.* **587**(1), 71–79 (2003). doi:10.1086/368076
- F. Courbin, A. Eigenbrod, C. Vuissoz, G. Meylan, P. Magain, COSMOGRAIL: the COSmological MONitoring of GRAVItational Lenses, in *Gravitational Lensing Impact on Cosmology*, vol. 225, ed. by Y. Mellier, G. Meylan, 2005, pp. 297–303. doi:10.1017/S1743921305002097
- F. Courbin, V. Chantry, Y. Revaz, D. Sluse, C. Faure, M. Tewes, E. Eulaers, M. Koleva, I. Asfandiyarov, S. Dye, P. Magain, H. van Winckel, J. Coles, P. Saha, M. Ibrahimov, G. Meylan, COSMOGRAIL: the COSmological MONitoring of GRAVItational Lenses. IX. Time delays, lens dynamics and baryonic fraction in HE 0435-1223. *Astron. Astrophys.* **536**, 53 (2011). doi:10.1051/0004-6361/201015709
- F. Courbin, V. Bonvin, E. Buckley-Geer, C.D. Fassnacht, J. Frieman, H. Lin, P.J. Marshall, S.H. Suyu, T. Treu, T. Anguita, V. Motta, G. Meylan, E. Paic, M. Tewes, A. Agnello, D.C.-Y. Chao, M. Chijani, D. Gilman, K. Rojas, P. Williams, A. Hempel, S. Kim, R. Lachaume, M. Rabus, T.M.C. Abbott, S. Allam, J. Annis, M. Banerji, K. Bechtol, A. Benoit-Lévy, D. Brooks, D.L. Burke, A. Carnero Rosell, M. Carrasco Kind, J. Carretero, C.B. D’Andrea, L.N. da Costa, C. Davis, D.L. DePoy, S. Desai, B. Flaugher, P. Fosalba, J. García-Bellido, E. Gaztanaga, D.A. Goldstein, D. Gruen, R.A. Gruendl, J. Gschwend, G. Gutierrez, K. Honscheid, D.J. James, K. Kuehn, S. Kuhlmann, N. Kuropatkin, O. Lahav, M. Lima, M.A.G. Maia, M. March, J.L. Marshall, R.G. McMahon, F. Menanteau, R. Miquel, B. Nord, A.A. Plazas, E. Sanchez, V. Scarpine, R. Schindler, M. Schubnell, I. Sevilla-Noarbe, M. Smith, M. Soares-Santos, F. Sobreira, E. Suchyta, G. Tarle, D.L. Tucker, A.R. Walker, W. Wester, COSMOGRAIL: the COSmological MONitoring of GRAVItational Lenses. XVI. Time delays for the quadruply imaged quasar DES J0408-5354 with high-cadence photometric monitoring. *Astron. Astrophys.* **609**, 71 (2018). doi:10.1051/0004-6361/201731461
- G. De Lucia, J. Blaizot, The hierarchical formation of the brightest cluster galaxies. *Mon. Notices of the Royal Astron. Soc.* **375**(1), 2–14 (2007). doi:10.1111/j.1365-2966.2006.11287.x
- P. Denzel, J.P. Coles, P. Saha, L.L.R. Williams, The Hubble constant from eight time-delay galaxy lenses. *Mon. Notices of the Royal Astron. Soc.* **501**(1), 784–801 (2021).

- doi:10.1093/mnras/staa3603
- J. Dexter, E. Agol, Quasar Accretion Disks are Strongly Inhomogeneous. *Astrophys. J. Letters* **727**(1), 24 (2011). doi:10.1088/2041-8205/727/1/L24
- E. Di Valentino, O. Mena, S. Pan, L. Visinelli, W. Yang, A. Melchiorri, D.F. Mota, A.G. Riess, J. Silk, In the realm of the Hubble tension—a review of solutions. *Classical and Quantum Gravity* **38**(15), 153001 (2021). doi:10.1088/1361-6382/ac086d
- X. Ding, T. Treu, S. Birrer, G.C.-F. Chen, J. Coles, P. Denzel, M. Frigo, A. Galan, P.J. Marshall, M. Millon, A. More, A.J. Shajib, D. Sluse, H. Tak, D. Xu, M.W. Auger, V. Bonvin, H. Chand, F. Courbin, G. Despali, C.D. Fassnacht, D. Gilman, S. Hilbert, S.R. Kumar, J.Y.-Y. Lin, J.W. Park, P. Saha, S. Vegetti, L. Van de Vyvere, L.L.R. Williams, Time delay lens modelling challenge. *Mon. Notices of the Royal Astron. Soc.* **503**(1), 1096–1123 (2021). doi:10.1093/mnras/stab484
- G. Dobler, C.D. Fassnacht, T. Treu, P. Marshall, K. Liao, A. Hojjati, E. Linder, N. Rumbaugh, Strong Lens Time Delay Challenge. I. Experimental Design. *Astrophys. J.* **799**(2), 168 (2015). doi:10.1088/0004-637X/799/2/168
- F.R. Donnan, K. Horne, J.V. Hernández Santisteban, Bayesian Analysis of Quasar Lightcurves with a Running Optimal Average: New Time Delay Measurements of COSMOGRAIL Gravitationally Lensed Quasars. *arXiv e-prints*, 2107–12318 (2021)
- A. Eigenbrod, F. Courbin, C. Vuissoz, G. Meylan, P. Saha, S. Dye, COSMOGRAIL: The COSmological MONitoring of GRAvItational Lenses. I. How to sample the light curves of gravitationally lensed quasars to measure accurate time delays. *Astron. Astrophys.* **436**(1), 25–35 (2005). doi:10.1051/0004-6361:20042422
- S. Ertl, S. Schuldt, S.H. Suyu, T. Schmidt, T. Treu, S. Birrer, A.J. Shajib, D. Sluse, TDCOSMO XI. Automated Modeling of 9 Strongly Lensed Quasars and Comparison Between Lens Modeling Software. *arXiv e-prints*, 2209–03094 (2022)
- E. Eulaers, M. Tewes, P. Magain, F. Courbin, I. Asfandiyarov, S. Ehgamberdiev, S. Rathna Kumar, C.S. Stalin, T.P. Prabhu, G. Meylan, H. Van Winckel, COSMOGRAIL: the COSmological MONitoring of GRAvItational Lenses. XII. Time delays of the doubly lensed quasars SDSS J1206+4332 and HS 2209+1914. *Astron. Astrophys.* **553**, 121 (2013). doi:10.1051/0004-6361/201321140
- R. Fadel, C.R. Keeton, R. Nakajima, G.M. Bernstein, Improved Constraints on the Gravitational Lens Q0957+561. II. Strong Lensing. *Astrophys. J.* **711**(1), 246–267 (2010). doi:10.1088/0004-637X/711/1/246
- E.E. Falco, M.V. Gorenstein, I.I. Shapiro, On model-dependent bounds on H_0 from gravitational images : application to Q 0957+561 A, B. *Astrophys. J.* **289**, 1–4 (1985). doi:10.1086/184422
- C.D. Fassnacht, L.M. Lubin, The Gravitational Lens-Galaxy Group Connection. I. Discovery of a Group Coincident with CLASS B0712+472. *Astron. J.* **123**(2), 627–636 (2002). doi:10.1086/338648
- C.D. Fassnacht, L.V.E. Koopmans, K.C. Wong, Galaxy number counts and implications for strong lensing. *Mon. Notices of the Royal Astron. Soc.* **410**(4), 2167–2179 (2011). doi:10.1111/j.1365-2966.2010.17591.x
- C.D. Fassnacht, T.J. Pearson, A.C.S. Readhead, I.W.A. Browne, L.V.E. Koopmans, S.T. Myers, P.N. Wilkinson, A Determination of H_0 with the CLASS Gravitational Lens B1608+656. I. Time Delay Measurements with the VLA. *Astrophys. J.* **527**(2), 498–512 (1999). doi:10.1086/308118
- C.D. Fassnacht, E. Xanthopoulos, L.V.E. Koopmans, D. Rusin, A Determination of H_0 with the CLASS Gravitational Lens B1608+656. III. A Significant Improvement in the Precision of the Time Delay Measurements. *Astrophys. J.* **581**(2), 823–835 (2002). doi:10.1086/344368
- I. Ferreras, P. Saha, L.L.R. Williams, Stellar and Total Mass in Early-Type Lensing Galaxies. *Astrophys. J. Letters* **623**(1), 5–8 (2005). doi:10.1086/429995
- P. Fischer, J.A. Tyson, The Mass Distribution of the Most Luminous X-Ray Cluster RXJ 1347.5-1145 From Gravitational Lensing. *Astron. J.* **114**, 14–24 (1997). doi:10.1086/118447
- P. Fleury, J. Larena, J.-P. Uzan, Gravitational lenses in arbitrary space-times. *Classical and Quantum Gravity* **38**(8), 085002 (2021a). doi:10.1088/1361-6382/abea2d
- P. Fleury, J. Larena, J.-P. Uzan, Line-of-sight effects in strong gravitational lensing. *arXiv e-prints*, 2104–08883 (2021b)
- M. Foxley-Marrable, T.E. Collett, G. Varnardos, D.A. Goldstein, D. Bacon, The impact of microlensing on the standardization of strongly lensed Type Ia supernovae. *Mon. Notices of the Royal Astron. Soc.* **478**(4), 5081–5090 (2018). doi:10.1093/mnras/sty1346
- W.L. Freedman, B.F. Madore, D. Hatt, T.J. Hoyt, I.S. Jang, R.L. Beaton, C.R. Burns, M.G. Lee, A.J. Monson, J.R. Neeley, M.M. Phillips, J.A. Rich, M. Seibert, The Carnegie-Chicago Hubble Program. VIII. An Independent Determination of the Hubble Constant Based on the Tip of the Red Giant Branch. *Astrophys. J.* **882**(1), 34 (2019). doi:10.3847/1538-4357/ab2f73
- W.L. Freedman, B.F. Madore, T. Hoyt, I.S. Jang, R. Beaton, M.G. Lee, A. Monson, J. Neeley, J. Rich, Calibration of the Tip of the Red Giant Branch. *Astrophys. J.* **891**(1), 57 (2020). doi:10.3847/1538-4357/ab7339
- A. Galan, A. Peel, R. Joseph, F. Courbin, J.-L. Starck, SLITRONOMY: Towards a fully wavelet-based strong lensing inversion technique. *Astron. Astrophys.* **647**, 176 (2021). doi:10.1051/0004-6361/202039363

- A. Ghosh, L.L.R. Williams, J. Liesenborgs, Free-form grating lens inversion of galaxy clusters with up to 1000 multiple images. *Mon. Notices of the Royal Astron. Soc.* **494**(3), 3998–4014 (2020). doi:10.1093/mnras/staa962
- E. Giannini, R.W. Schmidt, J. Wambsganss, K. Alsubai, J.M. Andersen, T. Anguita, V. Bozza, D.M. Bramich, P. Browne, S. Calchi Novati, Y. Damerdj, C. Diehl, P. Dodds, M. Dominik, A. Elyiv, X. Fang, R. Figuera Jaimes, F. Finet, T. Gerner, S. Gu, S. Hardis, K. Harpsøe, T.C. Hinse, A. Hornstrup, M. Hundertmark, J. Jessen-Hansen, U.G. Jørgensen, D. Juncher, N. Kains, E. Kerins, H. Korhonen, C. Liebig, M.N. Lund, M.S. Lundkvist, G. Maier, L. Mancini, G. Masi, M. Mathiasen, M. Penny, S. Proft, M. Rabus, S. Rahvar, D. Ricci, G. Scarpetta, K. Sahu, S. Schäfer, F. Schönebeck, J. Skottfelt, C. Snodgrass, J. Southworth, J. Surdej, J. Tregloan-Reed, C. Vilela, O. Wertz, F. Zimmer, MiNDSTeP differential photometry of the gravitationally lensed quasars WFI 2033-4723 and HE 0047-1756: microlensing and a new time delay. *Astron. Astrophys.* **597**, 49 (2017). doi:10.1051/0004-6361/201527422
- D. Gilman, S. Birrer, T. Treu, TDCOSMO. III. Dark matter substructure meets dark energy. The effects of (sub)halos on strong-lensing measurements of H_0 . *Astron. Astrophys.* **642**, 194 (2020). doi:10.1051/0004-6361/202038829
- L.J. Goicoechea, V.N. Shalyapin, Gravitational lens system SDSS J1339+1310: microlensing factory and time delay. *Astron. Astrophys.* **596**, 77 (2016). doi:10.1051/0004-6361/201628790
- M. Gomer, L.L.R. Williams, Galaxy-lens determination of H_0 : constraining density slope in the context of the mass sheet degeneracy. *J. of Cosm. and Astroparticle Phys.* **2020**(11), 045 (2020). doi:10.1088/1475-7516/2020/11/045
- M.R. Gomer, L.L.R. Williams, Galaxy-lens determination of H_0 : the effect of the ellipse + shear modelling assumption. *Mon. Notices of the Royal Astron. Soc.* **504**(1), 1340–1354 (2021). doi:10.1093/mnras/stab930
- M.R. Gomer, D. Sluse, L. van de Vyvere, S. Birrer, F. Courbin, TDCOSMO X: A key test of systematics in the hierarchical method of time-delay cosmography. *arXiv e-prints*, 2209–02076 (2022)
- M.V. Gorenstein, E.E. Falco, I.I. Shapiro, Degeneracies in Parameter Estimates for Models of Gravitational Lens Systems. *Astrophys. J.* **327**, 693 (1988). doi:10.1086/166226
- Z.S. Greene, S.H. Suyu, T. Treu, S. Hilbert, M.W. Auger, T.E. Collett, P.J. Marshall, C.D. Fassnacht, R.D. Blandford, M. Bradač, L.V.E. Koopmans, Improving the Precision of Time-delay Cosmography with Observations of Galaxies along the Line of Sight. *Astrophys. J.* **768**(1), 39 (2013). doi:10.1088/0004-637X/768/1/39
- C. Grillo, P. Rosati, S.H. Suyu, I. Balestra, G.B. Caminha, A. Halkola, P.L. Kelly, M. Lombardi, A. Mercurio, S.A. Rodney, T. Treu, Measuring the Value of the Hubble Constant “à la Refsdal”. *Astrophys. J.* **860**(2), 94 (2018). doi:10.3847/1538-4357/aac2c9
- N.A. Grogan, R. Narayan, A New Model of the Gravitational Lens 0957+561 and a Limit on the Hubble Constant. *Astrophys. J.* **464**, 92 (1996). doi:10.1086/177302
- A. Gu, X. Huang, W. Sheu, G. Aldering, A.S. Bolton, K. Boone, A. Dey, A. Filipp, E. Jullo, S. Perlmutter, D. Rubin, E.F. Schlafly, D.J. Schlegel, Y. Shu, S.H. Suyu, GIGA-Lens: Fast Bayesian Inference for Strong Gravitational Lens Modeling. *Astrophys. J.* **935**(1), 49 (2022). doi:10.3847/1538-4357/ac6de4
- S. Hilbert, J. Hartlap, S.D.M. White, P. Schneider, Ray-tracing through the Millennium Simulation: Born corrections and lens-lens coupling in cosmic shear and galaxy-galaxy lensing. *Astron. Astrophys.* **499**(1), 31–43 (2009). doi:10.1051/0004-6361/200811054
- S. Hilbert, S.D.M. White, J. Hartlap, P. Schneider, Strong lensing optical depths in a Λ CDM universe. *Mon. Notices of the Royal Astron. Soc.* **382**(1), 121–132 (2007). doi:10.1111/j.1365-2966.2007.12391.x
- S. Hilbert, S.D.M. White, J. Hartlap, P. Schneider, Strong-lensing optical depths in a Λ CDM universe - II. The influence of the stellar mass in galaxies. *Mon. Notices of the Royal Astron. Soc.* **386**(4), 1845–1854 (2008). doi:10.1111/j.1365-2966.2008.13190.x
- A. Hirv, T. Eenmäe, L.J. Liivamägi, J. Pelt, Estimation of Time Delays from Two Blended Light Curves of Gravitational Lenses. *Baltic Astronomy* **16**, 241–250 (2007)
- J. Hjorth, I. Burud, A.O. Jaunsen, P.L. Schechter, J.-P. Kneib, M.I. Andersen, H. Korhonen, J.W. Clasen, A.A. Kaas, R. Østensen, J. Pelt, F.P. Pijpers, The Time Delay of the Quadruple Quasar RX J0911.4+0551. *Astrophys. J. Letters* **572**(1), 11–14 (2002). doi:10.1086/341603
- N.B. Hogg, P. Fleury, J. Larena, M. Martinelli, Measuring line-of-sight shear with Einstein rings: a proof of concept. *arXiv e-prints*, 2210–07210 (2022)
- A. Hojjati, E.V. Linder, Next generation strong lensing time delay estimation with Gaussian processes. *PRD* **90**(12), 123501 (2014). doi:10.1103/PhysRevD.90.123501
- A. Hojjati, A.G. Kim, E.V. Linder, Robust strong lensing time delay estimation. *PRD* **87**(12), 123512 (2013). doi:10.1103/PhysRevD.87.123512
- O. Ilbert, S. Arnouts, H.J. McCracken, M. Bolzonella, E. Bertin, O. Le Fèvre, Y. Mellier, G. Zamorani, R. Pellò, A. Iovino, L. Tresse, V. Le Brun, D. Bottini, B. Garilli, D. Maccagni, J.P. Picat, R. Scaramella, M. Scodeggio, G. Vettolani, A. Zanichelli, C. Adami, S. Bardelli, A. Cappi, S. Charlot, P. Ciliegi, T. Contini, O. Cucciati, S. Foucaud, P. Franzetti, I. Gavignaud, L. Guzzo, B. Marano, C. Marinoni, A. Mazure, B. Meneux, R. Merighi, S. Paltani, A.

- Pollo, L. Pozzetti, M. Radovich, E. Zucca, M. Bondi, A. Bongiorno, G. Busarello, S. de La Torre, L. Gregorini, F. Lamareille, G. Mathez, P. Merluzzi, V. Ripepi, D. Rizzo, D. Vergani, Accurate photometric redshifts for the CFHT legacy survey calibrated using the VIMOS VLT deep survey. *Astron. Astrophys.* **457**(3), 841–856 (2006). doi:10.1051/0004-6361:20065138
- I. Jee, E. Komatsu, S.H. Suyu, Measuring angular diameter distances of strong gravitational lenses. *J. of Cosm. and Astroparticle Phys.* **2015**(11), 033 (2015). doi:10.1088/1475-7516/2015/11/033
- R. Joseph, F. Courbin, J.-L. Starck, S. Birrer, Sparse Lens Inversion Technique (SLIT): lens and source separability from linear inversion of the source reconstruction problem. *Astron. Astrophys.* **623**, 14 (2019). doi:10.1051/0004-6361/201731042
- N. Kaiser, G. Squires, Mapping the Dark Matter with Weak Gravitational Lensing. *Astrophys. J.* **404**, 441 (1993). doi:10.1086/172297
- C.R. Keeton, L.A. Moustakas, A New Channel for Detecting Dark Matter Substructure in Galaxies: Gravitational Lens Time Delays. *Astrophys. J.* **699**(2), 1720–1731 (2009). doi:10.1088/0004-637X/699/2/1720
- P.L. Kelly, S.A. Rodney, T. Treu, L.-G. Strolger, R.J. Foley, S.W. Jha, J. Selsing, G. Brammer, M. Bradač, S.B. Cenko, O. Graur, A.V. Filippenko, J. Hjorth, C. McCully, A. Molino, M. Nonino, A.G. Riess, K.B. Schmidt, B. Tucker, A. von der Linden, B.J. Weiner, A. Zitrin, Deja Vu All Over Again: The Reappearance of Supernova Refsdal. *Astrophys. J. Letters* **819**(1), 8 (2016). doi:10.3847/2041-8205/819/1/L8
- P.L. Kelly, S.A. Rodney, T. Treu, R.J. Foley, G. Brammer, K.B. Schmidt, A. Zitrin, A. Sonnenfeld, L.-G. Strolger, O. Graur, A.V. Filippenko, S.W. Jha, A.G. Riess, M. Bradač, B.J. Weiner, D. Scolnic, M.A. Malkan, A. von der Linden, M. Trenti, J. Hjorth, R. Gavazzi, A. Fontana, J.C. Merten, C. McCully, T. Jones, M. Postman, A. Dressler, B. Patel, S.B. Cenko, M.L. Graham, B.E. Tucker, Multiple images of a highly magnified supernova formed by an early-type cluster galaxy lens. *Science* **347**(6226), 1123–1126 (2015). doi:10.1126/science.aaa3350
- L. Knox, M. Millea, Hubble constant hunter’s guide. *PRD* **101**(4), 043533 (2020). doi:10.1103/PhysRevD.101.043533
- C.S. Kochanek, What Do Gravitational Lens Time Delays Measure? *Astrophys. J.* **578**(1), 25–32 (2002). doi:10.1086/342476
- C.S. Kochanek, Overconstrained gravitational lens models and the Hubble constant. *Mon. Notices of the Royal Astron. Soc.* **493**(2), 1725–1735 (2020). doi:10.1093/mnras/staa344
- C.S. Kochanek, Overconstrained models of time delay lenses redux: how the angular tail wags the radial dog. *Mon. Notices of the Royal Astron. Soc.* **501**(4), 5021–5028 (2021). doi:10.1093/mnras/staa4033
- C.S. Kochanek, N.D. Morgan, E.E. Falco, B.A. McLeod, J.N. Winn, J. Dembicky, B. Ketzeback, The Time Delays of Gravitational Lens HE 0435-1223: An Early-Type Galaxy with a Rising Rotation Curve. *Astrophys. J.* **640**(1), 47–61 (2006). doi:10.1086/499766
- T.S. Kolatt, M. Bartelmann, Gravitational lensing of type IA supernovae by galaxy clusters. *Mon. Notices of the Royal Astron. Soc.* **296**(3), 763–772 (1998). doi:10.1046/j.1365-8711.1998.01466.x
- L.V.E. Koopmans, Gravitational Lensing & Stellar Dynamics: Dark-Matter and Baryons in Early-type Galaxies to $z=1$. arXiv e-prints, 0412596 (2004)
- L.V.E. Koopmans, Gravitational imaging of cold dark matter substructures. *Mon. Notices of the Royal Astron. Soc.* **363**(4), 1136–1144 (2005). doi:10.1111/j.1365-2966.2005.09523.x
- L.V.E. Koopmans, A.G. de Bruyn, E. Xanthopoulos, C.D. Fassnacht, A time-delay determination from VLA light curves of the CLASS gravitational lens B1600+434. *Astron. Astrophys.* **356**, 391–402 (2000)
- L.V.E. Koopmans, T. Treu, C.D. Fassnacht, R.D. Blandford, G. Surpi, The Hubble Constant from the Gravitational Lens B1608+656. *Astrophys. J.* **599**(1), 70–85 (2003). doi:10.1086/379226
- L.V.E. Koopmans, A. Bolton, T. Treu, O. Czoske, M.W. Auger, M. Barnabè, S. Vegetti, R. Gavazzi, L.A. Moustakas, S. Burles, The Structure and Dynamics of Massive Early-Type Galaxies: On Homology, Isothermality, and Isotropy Inside One Effective Radius. *Astrophys. J. Letters* **703**(1), 51–54 (2009). doi:10.1088/0004-637X/703/1/L51
- L.V.E. Koopmans, T. Treu, A.S. Bolton, S. Burles, L.A. Moustakas, The Sloan Lens ACS Survey. III. The Structure and Formation of Early-Type Galaxies and Their Evolution since $z \sim 1$. *Astrophys. J.* **649**(2), 599–615 (2006). doi:10.1086/505696
- F.A. Kuhn, S. Birrer, C. Bruderer, A. Amara, A. Refregier, Combining strong and weak lensing estimates in the Cosmos field. *J. of Cosm. and Astroparticle Phys.* **2021**(4), 010 (2021). doi:10.1088/1475-7516/2021/04/010
- T. Kundić, E.L. Turner, W.N. Colley, I. Gott J. Richard, J.E. Rhoads, Y. Wang, L.E. Bergeron, K.A. Gloria, D.C. Long, S. Malhotra, J. Wambsganss, A Robust Determination of the Time Delay in 0957+561A, B and a Measurement of the Global Value of Hubble’s Constant. *Astrophys. J.* **482**(1), 75–82 (1997a). doi:10.1086/304147
- T. Kundić, E.L. Turner, W.N. Colley, I. Gott J. Richard, J.E. Rhoads, Y. Wang, L.E. Bergeron, K.A. Gloria, D.C. Long, S. Malhotra, J. Wambsganss, A Robust Determination of the Time Delay in 0957+561A, B and a Measurement of the Global Value of Hubble’s Constant. *Astrophys. J.*

- 482**(1), 75–82 (1997b). doi:10.1086/304147
- C. Lemon, T. Anguita, M. Auger, F. Courbin, A. Galan, R. McMahon, F. Neira, M. Oguri, P. Schechter, A. Shajib, T. Treu, Gravitationally lensed quasars in Gaia – IV. 150 new lenses, quasar pairs, and projected quasars. arXiv e-prints, 2206–07714 (2022)
- K. Liao, T. Treu, P. Marshall, C.D. Fassnacht, N. Rumbaugh, G. Dobler, A. Aghamousa, V. Bonvin, F. Courbin, A. Hogg, N. Jackson, V. Kashyap, S. Rathna Kumar, E. Linder, K. Mandel, X.-L. Meng, G. Meylan, L.A. Moustakas, T.P. Prabhu, A. Romero-Wolf, A. Shafieloo, A. Siemiginowska, C.S. Stalin, H. Tak, M. Tewes, D. van Dyk, Strong Lens Time Delay Challenge. II. Results of TDC1. *Astrophys. J.* **800**(1), 11 (2015a). doi:10.1088/0004-637X/800/1/11
- K. Liao, T. Treu, P. Marshall, C.D. Fassnacht, N. Rumbaugh, G. Dobler, A. Aghamousa, V. Bonvin, F. Courbin, A. Hogg, N. Jackson, V. Kashyap, S. Rathna Kumar, E. Linder, K. Mandel, X.-L. Meng, G. Meylan, L.A. Moustakas, T.P. Prabhu, A. Romero-Wolf, A. Shafieloo, A. Siemiginowska, C.S. Stalin, H. Tak, M. Tewes, D. van Dyk, Strong Lens Time Delay Challenge. II. Results of TDC1. *Astrophys. J.* **800**(1), 11 (2015b). doi:10.1088/0004-637X/800/1/11
- K. Liao, A. Shafieloo, R.E. Keeley, E.V. Linder, A Model-independent Determination of the Hubble Constant from Lensed Quasars and Supernovae Using Gaussian Process Regression. *Astrophys. J. Letters* **886**(1), 23 (2019). doi:10.3847/2041-8213/ab5308
- K. Liao, A. Shafieloo, R.E. Keeley, E.V. Linder, Determining Model-independent H_0 and Consistency Tests. *Astrophys. J. Letters* **895**(2), 29 (2020). doi:10.3847/2041-8213/ab8dbb
- LSST Dark Energy Science Collaboration (LSST DESC), B. Abolfathi, D. Alonso, R. Armstrong, É. Aubourg, H. Awan, Y.N. Babuji, F.E. Bauer, R. Bean, G. Beckett, R. Biswas, J.R. Bogart, D. Boutigny, K. Chard, J. Chiang, C.F. Claver, J. Cohen-Tanugi, C. Combet, A.J. Connolly, S.F. Daniel, S.W. Digel, A. Drlica-Wagner, R. Dubois, E. Gangler, E. Gawiser, T. Glanzman, P. Gris, S. Habib, A.P. Hearin, K. Heitmann, F. Hernandez, R. Hložek, J. Hollowed, M. Ishak, Ž. Ivezić, M. Jarvis, S.W. Jha, S.M. Kahn, J.B. Kalmbach, H.M. Kelly, E. Kovacs, D. Korytov, K.S. Krughoff, C.S. Lage, F. Lanusse, P. Larsen, L. Le Guillou, N. Li, E.P. Longley, R.H. Lupton, R. Mandelbaum, Y.-Y. Mao, P. Marshall, J.E. Meyers, M. Moniez, C.B. Morrison, A. Nomerotski, P. O’Connor, H. Park, J.W. Park, J. Peloton, D. Perrefort, J. Perry, S. Plaszczyński, A. Pope, A. Rasmussen, K. Reil, A.J. Roodman, E.S. Rykoff, F.J. Sánchez, S.J. Schmidt, D. Scolnic, C.W. Stubbs, J.A. Tyson, T.D. Uram, A. Villarreal, C.W. Walter, M.P. Wiesner, W.M. Wood-Vasey, J. Zuntz, The LSST DESC DC2 Simulated Sky Survey. *Astrophys. J. Supplement* **253**(1), 31 (2021). doi:10.3847/1538-4365/abd62c
- C. McCully, C.R. Keeton, K.C. Wong, A.I. Zabludoff, A new hybrid framework to efficiently model lines of sight to gravitational lenses. *Mon. Notices of the Royal Astron. Soc.* **443**(4), 3631–3642 (2014). doi:10.1093/mnras/stu1316
- C. McCully, C.R. Keeton, K.C. Wong, A.I. Zabludoff, Quantifying Environmental and Line-of-sight Effects in Models of Strong Gravitational Lens Systems. *Astrophys. J.* **836**(1), 141 (2017). doi:10.3847/1538-4357/836/1/141
- D. Merritt, Distribution functions for spherical galaxies. *Mon. Notices of the Royal Astron. Soc.* **214**, 25–28 (1985a). doi:10.1093/mnras/214.1.25P
- D. Merritt, Spherical stellar systems with spheroidal velocity distributions. *Astron. J.* **90**, 1027–1037 (1985b). doi:10.1086/113810
- A.D. Meyer, D.A. van Dyk, H. Tak, A. Siemiginowska, TDCARMA: Painless, accurate, and scalable estimates of gravitational-lens time delays with flexible CARMA processes. arXiv e-prints, 2207–09327 (2022)
- M. Millon, F. Courbin, V. Bonvin, E. Paic, G. Meylan, M. Tewes, D. Sluse, P. Magain, J.H.H. Chan, A. Galan, R. Joseph, C. Lemon, O. Tikhonova, R.I. Anderson, M. Marmier, B. Chazelas, M. Lendl, A.H.M.J. Triaud, A. Wyttenbach, COSMOGRAIL. XIX. Time delays in 18 strongly lensed quasars from 15 years of optical monitoring. *Astron. Astrophys.* **640**, 105 (2020a). doi:10.1051/0004-6361/202037740
- M. Millon, A. Galan, F. Courbin, T. Treu, S.H. Suyu, X. Ding, S. Birrer, G.C.-F. Chen, A.J. Shajib, D. Sluse, K.C. Wong, A. Agnello, M.W. Auger, E.J. Buckley-Geer, J.H.H. Chan, T. Collett, C.D. Fassnacht, S. Hilbert, L.V.E. Koopmans, V. Motta, S. Mukherjee, C.E. Rusu, A. Sonnenfeld, C. Spiniello, L. Van de Vyvere, TDCOSMO. I. An exploration of systematic uncertainties in the inference of H_0 from time-delay cosmography. *Astron. Astrophys.* **639**, 101 (2020b). doi:10.1051/0004-6361/201937351
- M. Millon, F. Courbin, V. Bonvin, E. Buckley-Geer, C.D. Fassnacht, J. Frieman, P.J. Marshall, S.H. Suyu, T. Treu, T. Anguita, V. Motta, A. Agnello, J.H.H. Chan, D.C.-Y. Chao, M. Chijani, D. Gilman, K. Gilmore, C. Lemon, J.R. Lucey, A. Melo, E. Paic, K. Rojas, D. Sluse, P.R. Williams, A. Hempel, S. Kim, R. Lachaume, M. Rabus, TDCOSMO. II. Six new time delays in lensed quasars from high-cadence monitoring at the MPIA 2.2 m telescope. *Astron. Astrophys.* **642**, 193 (2020c). doi:10.1051/0004-6361/202038698
- I. Momcheva, K. Williams, C. Keeton, A. Zabludoff, A Spectroscopic Study of the Environments of Gravitational Lens Galaxies. *Astrophys. J.* **641**(1), 169–189 (2006). doi:10.1086/500382
- M. Moresco, L. Amati, L. Amendola, S. Birrer, J.P.

- Blakeslee, M. Cantiello, A. Cimatti, J. Darling, M. Della Valle, M. Fishbach, C. Grillo, N. Hamaus, D. Holz, L. Izzo, R. Jimenez, E. Lusso, M. Meneghetti, E. Piedipalumbo, A. Pisani, A. Pourtsidou, L. Pozzetti, M. Quartin, G. Risaliti, P. Rosati, L. Verde, Unveiling the Universe with Emerging Cosmological Probes. arXiv e-prints, 2201–07241 (2022)
- E. Mortsell, A. Goobar, J. Johansson, S. Dhawan, The Hubble Tension Bites the Dust: Sensitivity of the Hubble Constant Determination to Cepheid Color Calibration. arXiv e-prints, 2105–11461 (2021)
- R. Nakajima, G.M. Bernstein, R. Fadely, C.R. Keeton, T. Schrabback, Improved Constraints on the Gravitational Lens Q0957+561. I. Weak Lensing. *Astrophys. J.* **697**(2), 1793–1804 (2009). doi:10.1088/0004-637X/697/2/1793
- J.F. Navarro, C.S. Frenk, S.D.M. White, A Universal Density Profile from Hierarchical Clustering. *Astrophys. J.* **490**(2), 493–508 (1997). doi:10.1086/304888
- M. Oguri, Gravitational Lens Time Delays: A Statistical Assessment of Lens Model Dependences and Implications for the Global Hubble Constant. *Astrophys. J.* **660**(1), 1–15 (2007). doi:10.1086/513093
- M. Oguri, Strong gravitational lensing of explosive transients. *Reports on Progress in Physics* **82**(12), 126901 (2019). doi:10.1088/1361-6633/ab4fc5
- M. Oguri, Y. Kawano, Gravitational lens time delays for distant supernovae: breaking the degeneracy between radial mass profiles and the Hubble constant. *Mon. Notices of the Royal Astron. Soc.* **338**(4), 25–29 (2003). doi:10.1046/j.1365-8711.2003.06290.x
- M. Oguri, P.J. Marshall, Gravitationally lensed quasars and supernovae in future wide-field optical imaging surveys. *Mon. Notices of the Royal Astron. Soc.* **405**(4), 2579–2593 (2010). doi:10.1111/j.1365-2966.2010.16639.x
- L.P. Osipkov, Spherical systems of gravitating bodies with an ellipsoidal velocity distribution. *Pisma v Astronomicheskii Zhurnal* **5**, 77–80 (1979). <http://adsabs.harvard.edu/abs/1979PAZh....5...77O>
- D. Paraficz, J. Hjorth, Gravitational lenses as cosmic rulers: Ω_m , Ω_Λ from time delays and velocity dispersions. *Astron. Astrophys.* **507**(3), 49–52 (2009). doi:10.1051/0004-6361/200913307
- J.W. Park, In prep. in prep
- J.W. Park, S. Wagner-Carena, S. Birrer, P.J. Marshall, J.Y.-Y. Lin, A. Roodman, LSST Dark Energy Science Collaboration, Large-scale Gravitational Lens Modeling with Bayesian Neural Networks for Accurate and Precise Inference of the Hubble Constant. *Astrophys. J.* **910**(1), 39 (2021). doi:10.3847/1538-4357/abdfc4
- J. Pelt, R. Kayser, S. Refsdal, T. Schramm, The light curve and the time delay of QSO 0957+561. *Astron. Astrophys.* **305**, 97 (1996)
- Planck Collaboration, N. Aghanim, Y. Akrami, M. Ashdown, J. Aumont, C. Baccigalupi, M. Ballardini, A.J. Banday, R.B. Barreiro, N. Bartolo, S. Basak, R. Battye, K. Benabed, J.-P. Bernard, M. Bersanelli, P. Bielewicz, J.J. Bock, J.R. Bond, J. Borrill, F.R. Bouchet, F. Boulanger, M. Bucher, C. Burigana, R.C. Butler, E. Calabrese, J.-F. Cardoso, J. Carron, A. Challinor, H.C. Chiang, J. Chluba, L.P.L. Colombo, C. Combet, D. Contreras, B.P. Crill, F. Cuttaia, P. de Bernardis, G. de Zotti, J. Delabrouille, J.-M. Delouis, E. Di Valentino, J.M. Diego, O. Doré, M. Douspis, A. Ducout, X. Dupac, S. Dusini, G. Efstathiou, F. Elsner, T.A. Enßlin, H.K. Eriksen, Y. Fantaye, M. Farhang, J. Fergusson, R. Fernandez-Cobos, F. Finelli, F. Forastieri, M. Frailis, A.A. Fraisse, E. Franceschi, A. Frolov, S. Galeotta, S. Galli, K. Ganga, R.T. Génova-Santos, M. Gerbino, T. Ghosh, J. González-Nuevo, K.M. Górski, S. Gratton, A. Gruppuso, J.E. Gudmundsson, J. Hamann, W. Handley, F.K. Hansen, D. Herranz, S.R. Hildebrandt, E. Hivon, Z. Huang, A.H. Jaffe, W.C. Jones, A. Karakci, E. Keihänen, R. Keskitalo, K. Kiiveri, J. Kim, T.S. Kisner, L. Knox, N. Krachmalnicoff, M. Kunz, H. Kurki-Suonio, G. Lagache, J.-M. Lamarre, A. Lasenby, M. Lattanzi, C.R. Lawrence, M. Le Jeune, P. Lemos, J. Lesgourgues, F. Levrier, A. Lewis, M. Liguori, P.B. Lilje, M. Lilley, V. Lindholm, M. López-Caniego, P.M. Lubin, Y.-Z. Ma, J.F. Macías-Pérez, G. Maggio, D. Maino, N. Mandolesi, A. Mangilli, A. Marcos-Caballero, M. Maris, P.G. Martin, M. Martinelli, E. Martínez-González, S. Matarrese, N. Mauri, J.D. McEwen, P.R. Meinhold, A. Melchiorri, A. Mennella, M. Migliaccio, M. Millea, S. Mitra, M.-A. Miville-Deschênes, D. Molinari, L. Montier, G. Morgante, A. Moss, P. Natoli, H.U. Nørgaard-Nielsen, L. Pagano, D. Paoletti, B. Partridge, G. Patanchon, H.V. Peiris, F. Perrotta, V. Pettorino, F. Piacentini, L. Polastri, G. Polenta, J.-L. Puget, J.P. Rachen, M. Reinecke, M. Remazeilles, A. Renzi, G. Rocha, C. Rosset, G. Roudier, J.A. Rubiño-Martín, B. Ruiz-Granados, L. Salvati, M. Sandri, M. Savelainen, D. Scott, E.P.S. Shellard, C. Sirignano, G. Sirri, L.D. Spencer, R. Sunyaev, A.-S. Suur-Uski, J.A. Tauber, D. Tavagnacco, M. Tenti, L. Toffolatti, M. Tomasi, T. Trombetti, L. Valenziano, J. Valiviita, B. Van Tent, L. Vibert, P. Vielva, F. Villa, N. Vittorio, B.D. Wandelt, I.K. Wehus, M. White, S.D.M. White, A. Zacchei, A. Zonca, Planck 2018 results. VI. Cosmological parameters. *Astron. Astrophys.* **641**, 6 (2020). doi:10.1051/0004-6361/201833910
- S. Poindexter, N. Morgan, C.S. Kochanek, E.E. Falco, Mid-IR Observations and a Revised Time Delay for the Gravitational Lens System Quasar HE 1104-1805. *Astrophys. J.* **660**(1), 146–151 (2007). doi:10.1086/512773
- S. Rathna Kumar, M. Tewes, C.S. Stalin, F. Courbin, I. Asfandiyarov, G. Meylan, E. Eulaers, T.P. Prabhu, P. Magain, H. Van Winckel, S. Ehgamberdiev, COSMOGRAIL: the COSmological MONitoring of GRAVita-

- tional Lenses. XIV. Time delay of the doubly lensed quasar SDSS J1001+5027. *Astron. Astrophys.* **557**, 44 (2013). doi:10.1051/0004-6361/201322116
- J.I. Read, P. Saha, A.V. Macciò, Radial Density Profiles of Time-Delay Lensing Galaxies. *Astrophys. J.* **667**(2), 645–654 (2007). doi:10.1086/520714
- S. Refsdal, On the possibility of determining Hubble’s parameter and the masses of galaxies from the gravitational lens effect. *Mon. Notices of the Royal Astron. Soc.* **128**, 307 (1964). doi:10.1093/mnras/128.4.307
- A.G. Riess, S. Casertano, W. Yuan, L.M. Macri, D. Scolnic, Large Magellanic Cloud Cepheid Standards Provide a 1% Foundation for the Determination of the Hubble Constant and Stronger Evidence for Physics beyond Λ CDM. *Astrophys. J.* **876**(1), 85 (2019). doi:10.3847/1538-4357/ab1422
- A.G. Riess, S. Casertano, W. Yuan, J.B. Bowers, L. Macri, J.C. Zinn, D. Scolnic, Cosmic Distances Calibrated to 1% Precision with Gaia EDR3 Parallaxes and Hubble Space Telescope Photometry of 75 Milky Way Cepheids Confirm Tension with Λ CDM. *Astrophys. J. Letters* **908**(1), 6 (2021). doi:10.3847/2041-8213/abdbaf
- A.J. Romanowsky, C.S. Kochanek, Constraints on H_0 from the Central Velocity Dispersions of Lens Galaxies. *Astrophys. J.* **516**(1), 18–26 (1999). doi:10.1086/307077
- C.E. Rusu, C.D. Fassnacht, D. Sluse, S. Hilbert, K.C. Wong, K.-H. Huang, S.H. Suyu, T.E. Collett, P.J. Marshall, T. Treu, L.V.E. Koopmans, H0LiCOW - III. Quantifying the effect of mass along the line of sight to the gravitational lens HE 0435-1223 through weighted galaxy counts. *Mon. Notices of the Royal Astron. Soc.* **467**(4), 4220–4242 (2017). doi:10.1093/mnras/stx285
- C.E. Rusu, K.C. Wong, V. Bonvin, D. Sluse, S.H. Suyu, C.D. Fassnacht, J.H.H. Chan, S. Hilbert, M.W. Auger, A. Sonnenfeld, S. Birrer, F. Courbin, T. Treu, G.C.-F. Chen, A. Halkola, L.V.E. Koopmans, P.J. Marshall, A.J. Shajib, H0LiCOW XII. Lens mass model of WFI2033-4723 and blind measurement of its time-delay distance and H_0 . *Mon. Notices of the Royal Astron. Soc.* **498**(1), 1440–1468 (2020). doi:10.1093/mnras/stz3451
- P. Saha, L.L.R. Williams, A Portable Modeler of Lensed Quasars. *Astron. J.* **127**(5), 2604–2616 (2004). doi:10.1086/383544
- P. Saha, L.L.R. Williams, Gravitational Lensing Model Degeneracies: Is Steepness All-Important? *Astrophys. J.* **653**(2), 936–941 (2006). doi:10.1086/508798
- P.L. Schechter, C.D. Bailyn, R. Barr, R. Barvainis, C.M. Becker, G.M. Bernstein, J.P. Blakeslee, S.J. Bus, A. Dressler, E.E. Falco, R.A. Fesen, P. Fischer, K. Gebhardt, D. Harmer, J.N. Hewitt, J. Hjorth, T. Hurt, A.O. Jaunsen, M. Mateo, D. Mehlert, D.O. Richstone, L.S. Sparke, J.R. Thorstensen, J.L. Tonry, G. Wegner, D.W. Willmarth, G. Worthey, The Quadruple Gravitational Lens PG 1115+080: Time Delays and Models. *Astrophys. J. Letters* **475**(2), 85–88 (1997). doi:10.1086/310478
- P.L. Schechter, A. Udalski, M. Szymański, M. Kubiak, G. Pietrzyński, I. Soszyński, P. Woźniak, K. Żebruń, O. Szewczyk, Ł. Wyrzykowski, Microlensing of Relativistic Knots in the Quasar HE 1104-1805 AB. *Astrophys. J.* **584**(2), 657–663 (2003). doi:10.1086/345716
- T. Schmidt, T. Treu, S. Birrer, A.J. Shajib, C. Lemon, M. Millon, D. Sluse, A. Agnello, T. Anguita, M.W. Auger-Williams, R.G. McMahon, V. Motta, P. Schechter, C. Spiniello, I. Kayo, F. Courbin, S. Ertl, C.D. Fassnacht, J.A. Frieman, A. More, S. Schuldt, S.H. Suyu, M. Agüena, F. Andrade-Oliveira, J. Annis, D. Bacon, E. Bertin, D. Brooks, D.L. Burke, A. Carnero Rosell, M. Carrasco Kind, J. Carretero, C. Conselice, M. Costanzi, L.N. da Costa, M.E.S. Pereira, J. De Vicente, S. Desai, P. Doel, S. Everett, I. Ferrero, D. Friedel, J. García-Bellido, E. Gaztanaga, D. Gruen, R.A. Gruendl, J. Gschwend, G. Gutierrez, S.R. Hinton, D.L. Hollowood, K. Honscheid, D.J. James, K. Kuehn, O. Lahav, F. Menanteau, R. Miquel, A. Palmese, F. Paz-Chinchón, A. Pieres, A.A. Plazas Malagón, J. Prat, M. Rodríguez-Monroy, A.K. Romer, E. Sanchez, V. Scarpine, I. Sevilla-Noarbe, M. Smith, E. Suchyta, G. Tarle, C. To, T.N. Varga, STRIDES: Automated uniform models for 30 quadruply imaged quasars. *arXiv e-prints*, 2206–04696 (2022)
- P. Schneider, A new formulation of gravitational lens theory, time-delay, and Fermat’s principle. *Astron. Astrophys.* **143**(2), 413–420 (1985)
- P. Schneider, D. Sluse, Mass-sheet degeneracy, power-law models and external convergence: Impact on the determination of the Hubble constant from gravitational lensing. *Astron. Astrophys.* **559**, 37 (2013). doi:10.1051/0004-6361/201321882
- P. Schneider, D. Sluse, Source-position transformation: an approximate invariance in strong gravitational lensing. *Astron. Astrophys.* **564**, 103 (2014). doi:10.1051/0004-6361/201322106
- P. Schneider, J. Ehlers, E.E. Falco, *Gravitational Lenses* 1992. doi:10.1007/978-3-662-03758-4
- N. Schöneberg, G.F. Abellán, A. Pérez Sánchez, S.J. Witte, V. Poulin, J. Lesgourgues, The H_0 Olympics: A fair ranking of proposed models. *arXiv e-prints*, 2107–10291 (2021)
- M. Schwarzschild, A numerical model for a triaxial stellar system in dynamical equilibrium. *Astrophys. J.* **232**, 236–247 (1979). doi:10.1086/157282
- P. Shah, P. Lemos, O. Lahav, A buyer’s guide to the Hubble Constant. *arXiv e-prints*, 2109–01161 (2021)
- A.J. Shajib, T. Treu, A. Agnello, Improving time-delay cosmography with spatially resolved kinematics. *Mon. Notices of the Royal Astron. Soc.* **473**, 210–226 (2018). doi:10.1093/mnras/stx2302

- A.J. Shajib, S. Birrer, T. Treu, M.W. Auger, A. Agnello, T. Anguita, E.J. Buckley-Geer, J.H.H. Chan, T.E. Collett, F. Courbin, C.D. Fassnacht, J. Frieman, I. Kayo, C. Lemon, H. Lin, P.J. Marshall, R. McMahon, A. More, N.D. Morgan, V. Motta, M. Oguri, F. Ostrovski, C.E. Rusu, P.L. Schechter, T. Shanks, S.H. Suyu, G. Meylan, T.M.C. Abbott, S. Allam, J. Annis, S. Avila, E. Bertin, D. Brooks, A. Carnero Rosell, M. Carrasco Kind, J. Carretero, C.E. Cunha, L.N. da Costa, J. De Vicente, S. Desai, P. Doel, B. Flaugher, P. Fosalba, J. García-Bellido, D.W. Gerdes, D. Gruen, R.A. Gruendl, G. Gutierrez, W.G. Hartley, D.L. Hollowood, B. Hoyle, D.J. James, K. Kuehn, N. Kuropatkin, O. Lahav, M. Lima, M.A.G. Maia, M. March, J.L. Marshall, P. Melchior, F. Menanteau, R. Miquel, A.A. Plazas, E. Sanchez, V. Scarpine, I. Sevilla-Noarbe, M. Smith, M. Soares-Santos, F. Sobreira, E. Suchyta, M.E.C. Swanson, G. Tarle, A.R. Walker, Is every strong lens model unhappy in its own way? Uniform modelling of a sample of 13 quadruply+ imaged quasars. *Mon. Notices of the Royal Astron. Soc.* **483**(4), 5649–5671 (2019). doi:10.1093/mnras/sty3397
- A.J. Shajib, S. Birrer, T. Treu, A. Agnello, E.J. Buckley-Geer, J.H.H. Chan, L. Christensen, C. Lemon, H. Lin, M. Millon, J. Poh, C.E. Rusu, D. Sluse, C. Spiniello, G.C.-F. Chen, T. Collett, F. Courbin, C.D. Fassnacht, J. Frieman, A. Galan, D. Gilman, A. More, T. Anguita, M.W. Auger, V. Bonvin, R. McMahon, G. Meylan, K.C. Wong, T.M.C. Abbott, J. Annis, S. Avila, K. Bechtol, D. Brooks, D. Brout, D.L. Burke, A. Carnero Rosell, M. Carrasco Kind, J. Carretero, F.J. Castander, M. Costanzi, L.N. da Costa, J. De Vicente, S. Desai, J.P. Dietrich, P. Doel, A. Drlica-Wagner, A.E. Evrard, D.A. Finley, B. Flaugher, P. Fosalba, J. García-Bellido, D.W. Gerdes, D. Gruen, R.A. Gruendl, J. Gschwend, G. Gutierrez, D.L. Hollowood, K. Honscheid, D. Huterer, D.J. James, T. Jeltema, E. Krause, N. Kuropatkin, T.S. Li, M. Lima, N. MacCrann, M.A.G. Maia, J.L. Marshall, P. Melchior, R. Miquel, R.L.C. Ogando, A. Palmese, F. Paz-Chinchón, A.A. Plazas, A.K. Romer, A. Roodman, M. Sako, E. Sanchez, B. Santiago, V. Scarpine, M. Schubnell, D. Scolnic, S. Serrano, I. Sevilla-Noarbe, M. Smith, M. Soares-Santos, E. Suchyta, G. Tarle, D. Thomas, A.R. Walker, Y. Zhang, STRIDES: a 3.9 per cent measurement of the Hubble constant from the strong lens system DES J0408-5354. *Mon. Notices of the Royal Astron. Soc.* **494**(4), 6072–6102 (2020). doi:10.1093/mnras/staa828
- A.J. Shajib, T. Treu, S. Birrer, A. Sonnenfeld, Dark matter haloes of massive elliptical galaxies at $z \sim 0.2$ are well described by the Navarro-Frenk-White profile. *Mon. Notices of the Royal Astron. Soc.* **503**(2), 2380–2405 (2021). doi:10.1093/mnras/stab536
- V.N. Shalyapin, L.J. Goicoechea, Gravitationally Lensed Quasar SDSS J1442+4055: Redshifts of Lensing Galaxies, Time Delay, Microlensing Variability, and Intervening Metal System at $z \sim 2$. *Astrophys. J.* **873**(2), 117 (2019). doi:10.3847/1538-4357/ab08f0
- Y. Shu, V. Belokurov, N.W. Evans, Discovering strongly lensed QSOs from unresolved light curves. *Mon. Notices of the Royal Astron. Soc.* **502**(2), 2912–2921 (2021). doi:10.1093/mnras/stab241
- D. Sluse, M. Tewes, Imprints of the quasar structure in time-delay light curves: Microlensing-aided reverberation mapping. *Astron. Astrophys.* **571**, 60 (2014). doi:10.1051/0004-6361/201424776
- D. Sluse, A. Sonnenfeld, N. Rumbaugh, C.E. Rusu, C.D. Fassnacht, T. Treu, S.H. Suyu, K.C. Wong, M.W. Auger, V. Bonvin, T. Collett, F. Courbin, S. Hilbert, L.V.E. Koopmans, P.J. Marshall, G. Meylan, C. Spiniello, M. Tewes, H0LiCOW - II. Spectroscopic survey and galaxy-group identification of the strong gravitational lens system HE 0435-1223. *Mon. Notices of the Royal Astron. Soc.* **470**(4), 4838–4857 (2017). doi:10.1093/mnras/stx1484
- D. Sluse, C.E. Rusu, C.D. Fassnacht, A. Sonnenfeld, J. Richard, M.W. Auger, L. Coccato, K.C. Wong, S.H. Suyu, T. Treu, A. Agnello, S. Birrer, V. Bonvin, T. Collett, F. Courbin, S. Hilbert, L.V.E. Koopmans, O. Tihhanova, P.J. Marshall, G. Meylan, A.J. Shajib, J. Annis, S. Avila, E. Bertin, D. Brooks, E. Buckley-Geer, D.L. Burke, A. Carnero Rosell, M. Carrasco Kind, J. Carretero, F.J. Castander, L.N. da Costa, J. De Vicente, S. Desai, P. Doel, A.E. Evrard, B. Flaugher, J. Frieman, J. García-Bellido, D.W. Gerdes, D.A. Goldstein, R.A. Gruendl, J. Gschwend, W.G. Hartley, D.L. Hollowood, K. Honscheid, D.J. James, A.G. Kim, E. Krause, K. Kuehn, N. Kuropatkin, M. Lima, H. Lin, M.A.G. Maia, J.L. Marshall, P. Melchior, F. Menanteau, R. Miquel, A.A. Plazas, E. Sanchez, S. Serrano, I. Sevilla-Noarbe, M. Smith, M. Soares-Santos, F. Sobreira, E. Suchyta, M.E.C. Swanson, G. Tarle, H0LiCOW - X. Spectroscopic/imaging survey and galaxy-group identification around the strong gravitational lens system WFI 2033-4723. *Mon. Notices of the Royal Astron. Soc.* **490**(1), 613–633 (2019). doi:10.1093/mnras/stz2483
- A. Sonnenfeld, On the choice of lens density profile in time delay cosmography. *Mon. Notices of the Royal Astron. Soc.* **474**(4), 4648–4659 (2018). doi:10.1093/mnras/stx3105
- A. Sonnenfeld, Statistical strong lensing. II. Cosmology and galaxy structure with time-delay lenses. *arXiv e-prints*, 2109–00009 (2021a)
- A. Sonnenfeld, Statistical strong lensing. II. Cosmology and galaxy structure with time-delay lenses. *arXiv e-prints*, 2109–00009 (2021b)
- A. Sonnenfeld, M. Cautun, Statistical strong lensing. I. Constraints on the inner structure of galaxies from samples of a thousand lenses. *Astron. Astrophys.* **651**, 18 (2021).

- doi:10.1051/0004-6361/202140549
- V. Springel, S.D.M. White, A. Jenkins, C.S. Frenk, N. Yoshida, L. Gao, J. Navarro, R. Thacker, D. Croton, J. Helly, J.A. Peacock, S. Cole, P. Thomas, H. Couchman, A. Evrard, J. Colberg, F. Pearce, Simulations of the formation, evolution and clustering of galaxies and quasars. *Nature* **435**(7042), 629–636 (2005). doi:10.1038/nature03597
- O.M. Springer, E.O. Ofek, Measuring time delays - I. Using a flux time series that is a linear combination of time-shifted light curves. *Mon. Notices of the Royal Astron. Soc.* **506**(1), 864–876 (2021). doi:10.1093/mnras/stab1600
- D. Starkey, K. Horne, M.M. Fausnaugh, B.M. Peterson, M.C. Bentz, C.S. Kochanek, K.D. Denney, R. Edelson, M.R. Goad, G. De Rosa, M.D. Anderson, P. Arévalo, A.J. Barth, C. Bazhaw, G.A. Borman, T.A. Boroson, M.C. Bottorff, W.N. Brandt, A.A. Breeveld, E.M. Cackett, M.T. Carini, K.V. Croxall, D.M. Crenshaw, E. Dalla Bontà, A. De Lorenzo-Cáceres, M. Dietrich, N.V. Efimova, J. Ely, P.A. Evans, A.V. Filippenko, K. Flatland, N. Gehrels, S. Geier, J.M. Gelbord, L. Gonzalez, V. Gorjian, C.J. Grier, D. Grupe, P.B. Hall, S. Hicks, D. Horenstein, T. Hutchison, M. Im, J.J. Jensen, M.D. Joner, J. Jones, J. Kaasstra, S. Kaspi, B.C. Kelly, J.A. Kennea, S.C. Kim, M. Kim, S.A. Klimanov, K.T. Korista, G.A. Kriss, J.C. Lee, D.C. Leonard, P. Lira, F. MacInnis, E.R. Manne-Nicholas, S. Mathur, I.M. McHardy, C. Montouri, R. Musso, S.V. Nazarov, R.P. Norris, J.A. Nousek, D.N. Okhmat, A. Pancoast, J.R. Parks, L. Pei, R.W. Pogge, J.-U. Pott, S.E. Rafter, H.-W. Rix, D.A. Saylor, J.S. Schimoia, K. Schnülle, S.G. Sergeev, M.H. Siegel, M. Spencer, H.-I. Sung, K.G. Teems, C.S. Turner, P. Uttley, M. Vestergaard, C. Villforth, Y. Weiss, J.-H. Woo, H. Yan, S. Young, W. Zheng, Y. Zu, Space Telescope and Optical Reverberation Mapping Project.VI. Reverberating Disk Models for NGC 5548. *Astrophys. J.* **835**(1), 65 (2017). doi:10.3847/1538-4357/835/1/65
- S.H. Suyu, P.J. Marshall, M.P. Hobson, R.D. Blandford, A Bayesian analysis of regularized source inversions in gravitational lensing. *Mon. Notices of the Royal Astron. Soc.* **371**(2), 983–998 (2006). doi:10.1111/j.1365-2966.2006.10733.x
- S.H. Suyu, P.J. Marshall, R.D. Blandford, C.D. Fassnacht, L.V.E. Koopmans, J.P. McKean, T. Treu, Dissecting the Gravitational Lens B1608+656. I. Lens Potential Reconstruction. *Astrophys. J.* **691**(1), 277–298 (2009). doi:10.1088/0004-637X/691/1/277
- S.H. Suyu, P.J. Marshall, M.W. Auger, S. Hilbert, R.D. Blandford, L.V.E. Koopmans, C.D. Fassnacht, T. Treu, Dissecting the Gravitational lens B1608+656. II. Precision Measurements of the Hubble Constant, Spatial Curvature, and the Dark Energy Equation of State. *Astrophys. J.* **711**(1), 201–221 (2010). doi:10.1088/0004-637X/711/1/201
- S.H. Suyu, M.W. Auger, S. Hilbert, P.J. Marshall, M. Tewes, T. Treu, C.D. Fassnacht, L.V.E. Koopmans, D. Sluse, R.D. Blandford, F. Courbin, G. Meylan, Two Accurate Time-delay Distances from Strong Lensing: Implications for Cosmology. *Astrophys. J.* **766**(2), 70 (2013). doi:10.1088/0004-637X/766/2/70
- S.H. Suyu, V. Bonvin, F. Courbin, C.D. Fassnacht, C.E. Rusu, D. Sluse, T. Treu, K.C. Wong, M.W. Auger, X. Ding, S. Hilbert, P.J. Marshall, N. Rumbaugh, A. Sonnenfeld, M. Tewes, O. Tihhonova, A. Agnello, R.D. Blandford, G.C.-F. Chen, T. Collett, L.V.E. Koopmans, K. Liao, G. Meylan, C. Spiniello, H0LiCOW - I. H₀ Lenses in COSMOGRAIL's Wellspring: program overview. *Mon. Notices of the Royal Astron. Soc.* **468**(3), 2590–2604 (2017). doi:10.1093/mnras/stx483
- S.H. Suyu, T.-C. Chang, F. Courbin, T. Okumura, Cosmological Distance Indicators. *Space Science Reviews* **214**(5), 91 (2018). doi:10.1007/s11214-018-0524-3
- A.S. Tagore, D.J. Barnes, N. Jackson, S.T. Kay, M. Schaller, J. Schaye, T. Theuns, Reducing biases on H₀ measurements using strong lensing and galaxy dynamics: results from the EAGLE simulation. *Mon. Notices of the Royal Astron. Soc.* **474**(3), 3403–3422 (2018). doi:10.1093/mnras/stx2965
- H. Tak, K. Mandel, D.A. van Dyk, V.L. Kashyap, X.-L. Meng, A. Siemiginowska, Bayesian Estimates of Astronomical Time Delays between Gravitationally Lensed Stochastic Light Curves. *arXiv e-prints*, 1602–01462 (2016)
- S. Taubenberger, S.H. Suyu, E. Komatsu, I. Jee, S. Birrer, V. Bonvin, F. Courbin, C.E. Rusu, A.J. Shajib, K.C. Wong, The Hubble constant determined through an inverse distance ladder including quasar time delays and Type Ia supernovae. *Astron. Astrophys.* **628**, 7 (2019). doi:10.1051/0004-6361/201935980
- L. Teodori, K. Blum, E. Castorina, M. Simonović, Y. Soreq, Comments on the mass sheet degeneracy in cosmography analyses. *arXiv e-prints*, 2201–05111 (2022)
- M. Tewes, F. Courbin, G. Meylan, COSMOGRAIL: the COSmological MONitoring of GRAvitational Lenses. XI. Techniques for time delay measurement in presence of microlensing. *Astron. Astrophys.* **553**, 120 (2013a). doi:10.1051/0004-6361/201220123
- M. Tewes, F. Courbin, G. Meylan, C.S. Kochanek, E. Eu-laers, N. Cantale, A.M. Mosquera, P. Magain, H. Van Winckel, D. Sluse, G. Cataldi, D. Vörös, S. Dye, COSMOGRAIL: the COSmological MONitoring of GRAvitational Lenses. XIII. Time delays and 9-yr optical monitoring of the lensed quasar RX J1131-1231. *Astron. Astrophys.* **556**, 22 (2013b). doi:10.1051/0004-6361/201220352

- S.S. Tie, C.S. Kochanek, Microlensing makes lensed quasar time delays significantly time variable. *Mon. Notices of the Royal Astron. Soc.* **473**(1), 80–90 (2018). doi:10.1093/mnras/stx2348
- O. Tihhonova, F. Courbin, D. Harvey, S. Hilbert, C.E. Rusu, C.D. Fassnacht, V. Bonvin, P.J. Marshall, G. Meylan, D. Sluse, S.H. Suyu, T. Treu, K.C. Wong, H0LiCOW VIII. A weak-lensing measurement of the external convergence in the field of the lensed quasar HE 0435-1223. *Mon. Notices of the Royal Astron. Soc.* **477**(4), 5657–5669 (2018). doi:10.1093/mnras/sty1040
- O. Tihhonova, F. Courbin, D. Harvey, S. Hilbert, A. Peel, C.E. Rusu, C.D. Fassnacht, V. Bonvin, P.J. Marshall, G. Meylan, D. Sluse, S.H. Suyu, T. Treu, K.C. Wong, H0LiCOW - XI. A weak lensing measurement of the external convergence in the field of the lensed quasar B1608+656 using HST and Subaru deep imaging. *Mon. Notices of the Royal Astron. Soc.* **498**(1), 1406–1419 (2020). doi:10.1093/mnras/staa1436
- T. Treu, L.V.E. Koopmans, The internal structure of the lens PG1115+080: breaking degeneracies in the value of the Hubble constant. *Mon. Notices of the Royal Astron. Soc.* **337**(2), 6–10 (2002). doi:10.1046/j.1365-8711.2002.06107.x
- T. Treu, G. Brammer, J.M. Diego, C. Grillo, P.L. Kelly, M. Oguri, S.A. Rodney, P. Rosati, K. Sharon, A. Zitrin, I. Balestra, M. Bradač, T. Broadhurst, G.B. Caminha, A. Halkola, A. Hoag, M. Ishigaki, T.L. Johnson, W. Karman, R. Kawamata, A. Mercurio, K.B. Schmidt, L.-G. Strolger, S.H. Suyu, A.V. Filippenko, R.J. Foley, S.W. Jha, B. Patel, “Refsdal” Meets Popper: Comparing Predictions of the Re-appearance of the Multiply Imaged Supernova Behind MACSJ1149.5+2223. *Astrophys. J.* **817**(1), 60 (2016). doi:10.3847/0004-637X/817/1/60
- T. Treu, L.V.E. Koopmans, Massive Dark Matter Halos and Evolution of Early-Type Galaxies to $z \sim 1$. *Astrophys. J.* **611**(2), 739–760 (2004). doi:10.1086/422245
- T. Treu, P.J. Marshall, Time delay cosmography. *Astron. Astrophys. Review* **24**(1), 11 (2016). doi:10.1007/s00159-016-0096-8
- S. Unruh, P. Schneider, D. Sluse, Ambiguities in gravitational lens models: the density field from the source position transformation. *Astron. Astrophys.* **601**, 77 (2017). doi:10.1051/0004-6361/201629048
- G. van de Ven, R. Mandelbaum, C.R. Keeton, Galaxy density profiles and shapes - I. Simulation pipeline for lensing by realistic galaxy models. *Mon. Notices of the Royal Astron. Soc.* **398**(2), 607–634 (2009). doi:10.1111/j.1365-2966.2009.15167.x
- L. Van de Vyvere, D. Sluse, M.R. Gomer, S. Mukherjee, Consequences of the lack of azimuthal freedom in the modeling of lensing galaxies. *arXiv e-prints*, 2206–00022 (2022a)
- L. Van de Vyvere, M.R. Gomer, D. Sluse, D. Xu, S. Birrer, A. Galan, G. Vernardos, TDCOSMO. VII. Boxyness/discyness in lensing galaxies: Detectability and impact on H_0 . *Astron. Astrophys.* **659**, 127 (2022b). doi:10.1051/0004-6361/202141551
- C. Vanderriest, J. Schneider, G. Herpe, M. Chevreton, M. Moles, G. Wlerick, The value of the time delay ΔT (A,B) for the ‘double’ quasar 0957+561 from optical photometric monitoring. *Astron. Astrophys.* **215**, 1–13 (1989)
- S. Vegetti, L.V.E. Koopmans, Bayesian strong gravitational-lens modelling on adaptive grids: objective detection of mass substructure in Galaxies. *Mon. Notices of the Royal Astron. Soc.* **392**(3), 945–963 (2009). doi:10.1111/j.1365-2966.2008.14005.x
- L. Verde, T. Treu, A.G. Riess, Tensions between the early and late Universe. *Nature Astronomy* **3**, 891–895 (2019). doi:10.1038/s41550-019-0902-0
- C. Vuissoz, F. Courbin, D. Sluse, G. Meylan, M. Ibrahimov, I. Asfandiyarov, E. Stoops, A. Eigenbrod, L. Le Guillou, H. van Winckel, P. Magain, COSMOGRAIL: the COSmological MONitoring of GRAvItational Lenses. V. The time delay in SDSS J1650+4251. *Astron. Astrophys.* **464**(3), 845–851 (2007). doi:10.1051/0004-6361:20065823
- C. Vuissoz, F. Courbin, D. Sluse, G. Meylan, V. Chantry, E. Eulaers, C. Morgan, M.E. Eyler, C.S. Kochanek, J. Coles, P. Saha, P. Magain, E.E. Falco, COSMOGRAIL: the COSmological MONitoring of GRAvItational Lenses. VII. Time delays and the Hubble constant from WFI J2033-4723. *Astron. Astrophys.* **488**(2), 481–490 (2008). doi:10.1051/0004-6361:200809866
- S. Wagner-Carena, J.W. Park, S. Birrer, P.J. Marshall, A. Roodman, R.H. Wechsler, LSST Dark Energy Science Collaboration, Hierarchical Inference with Bayesian Neural Networks: An Application to Strong Gravitational Lensing. *Astrophys. J.* **909**(2), 187 (2021). doi:10.3847/1538-4357/abdf59
- S.J. Warren, S. Dye, Semilinear Gravitational Lens Inversion. *Astrophys. J.* **590**(2), 673–682 (2003). doi:10.1086/375132
- M.L. Wilson, A.I. Zabludoff, S.M. Ammons, I.G. Momcheva, K.A. Williams, C.R. Keeton, A Spectroscopic Survey of the Fields of 28 Strong Gravitational Lenses: the Group Catalog. *Astrophys. J.* **833**(2), 194 (2016). doi:10.3847/1538-4357/833/2/194
- M.L. Wilson, A.I. Zabludoff, C.R. Keeton, K.C. Wong, K.A. Williams, K.D. French, I.G. Momcheva, A Spectroscopic Survey of the Fields of 28 Strong Gravitational Lenses: Implications for H_0 . *Astrophys. J.* **850**(1), 94 (2017). doi:10.3847/1538-4357/aa9653
- K.C. Wong, S.H. Suyu, M.W. Auger, V. Bonvin, F. Courbin, C.D. Fassnacht, A. Halkola, C.E. Rusu, D. Sluse, A. Son-

- nenfeld, T. Treu, T.E. Collett, S. Hilbert, L.V.E. Koopmans, P.J. Marshall, N. Rumbaugh, H0LiCOW - IV. Lens mass model of HE 0435-1223 and blind measurement of its time-delay distance for cosmology. *Mon. Notices of the Royal Astron. Soc.* **465**(4), 4895–4913 (2017). doi:10.1093/mnras/stw3077
- K.C. Wong, S.H. Suyu, G.C.-F. Chen, C.E. Rusu, M. Milion, D. Sluse, V. Bonvin, C.D. Fassnacht, S. Taubenberger, M.W. Auger, S. Birrer, J.H.H. Chan, F. Courbin, S. Hilbert, O. Tihhonova, T. Treu, A. Agnello, X. Ding, I. Jee, E. Komatsu, A.J. Shajib, A. Sonnenfeld, R.D. Blandford, L.V.E. Koopmans, P.J. Marshall, G. Meylan, H0LiCOW - XIII. A 2.4 per cent measurement of H_0 from lensed quasars: 5.3σ tension between early- and late-Universe probes. *Mon. Notices of the Royal Astron. Soc.* **498**(1), 1420–1439 (2020). doi:10.1093/mnras/stz3094
- D. Xu, D. Sluse, P. Schneider, V. Springel, M. Vogelsberger, D. Nelson, L. Hernquist, Lens galaxies in the Illustris simulation: power-law models and the bias of the Hubble constant from time delays. *Mon. Notices of the Royal Astron. Soc.* **456**(1), 739–755 (2016). doi:10.1093/mnras/stv2708
- A. Yıldırım, S.H. Suyu, G.C.-F. Chen, E. Komatsu, TD-COSMO VIII: Cosmological distance measurements in light of the mass-sheet degeneracy – forecasts from strong lensing and IFU stellar kinematics. *arXiv e-prints*, 2109–14615 (2021)
- A. Yıldırım, S.H. Suyu, A. Halkola, Time-delay cosmographic forecasts with strong lensing and JWST stellar kinematics. *Mon. Notices of the Royal Astron. Soc.* **493**(4), 4783–4807 (2020). doi:10.1093/mnras/staa498